E-glass fiber reinforced composite as an oral implant abutment material

In vitro bacterial adhesion assay and biomechanical tests

Marina Etxeberria Urra

Marina Etxeberria Urra

E-GLASS FIBER REINFORCED COMPOSITE AS AN ORAL IMPLANT ABUTMENT MATERIAL

2015

UNIVERSITAT DE BARCELONA

PHD THESIS

E-GLASS FIBER REINFORCED COMPOSITE AS AN ORAL IMPLANT ABUTMENT MATERIAL

In vitro bacterial adhesion assay and biomechanical tests

DOCTORAL PROGRAM IN ODONTOLOGICAL SCIENCES

by

Marina Etxeberria Urra

UNIVERSITY OF BARCELONA
Barcelona 2015

UNIVERSITAT DE BARCELONA

E-GLASS FIBER REINFORCED COMPOSITE AS AN ORAL IMPLANT ABUTMENT MATERIAL

In vitro bacterial adhesion assay and biomechanical tests

by

Marina Etxeberria Urra

UNIVERSITY OF BARCELONA
Barcelona 2015

From the Department of Prosthetic Dentistry, Dental School and the Department of Pathology and Experimental Therapeutics, Medicine School, Doctoral Program in "Odontological Sciences" University of Barcelona, Barcelona, Spain.

Directors:

Dr. Tomas Escuin
Department of Odontoestomatology,
Dental School,
University of Barcelona
Barcelona, Spain

and

Dr. Miquel Viñas
Department of Pathology and Experimental Therapeutics,
Medicine School,
University of Barcelona
Barcelona, Spain

“Keep Ithaka always in your mind.
Arriving there is what you're destined for.
But don't hurry the journey at all.
Better if it lasts for years,
So you're old by the time you reach the island,
whealty with all you've gained on the way,
Not expecting Ithaka to make you rich.

Ithaka gave you the marvellous journey,
without her you wouldn't have set out.
She has nothing left to give you now.
And if you find her poor, Ithaka won't have fooled you.
Wise as you will have become, so full of experience,
You'll have understood by then what these Ithakas mean**.”**

Cavafy, Collected Poems.

“Txoria txori**”**

Mikel Laboa

To my family and friends

UNIVERSITAT DE BARCELONA

Departament d'Odontoestomatologia
Departament de Patologia i
Terapèutica Experimental

Facultats d'Odontologia i de Medicina
Campus de Bellvitge
Pavelló de Govern, 4ª planta

HUBC Health Universitat de Barcelona Campus

Tomás Escuin Henar Professor titular del departament d'odontoestomatologia i Miquel Viñas Ciordia Catedràtic del Departament de Patologia i Terapèutica experimental

F A N C O N S T A R,

Que la tesi doctoral presentada per la Llicenciada **Marina Etxeberria Urra** titulada "E-GLASS FIBER REINFORCED COMPOSITE AS AN ORAL IMPLANT ABUTMENT MATERIAL bacterial adhesion and biomechanics" ha estat desenvolupada sota la nostra direcció en els laboratoris d'aquest Campus in en els de la Universitat de Turku (Finlandia)

Que la memòria compleix al nostre criteri els requisits necessaris perquè sigui defensada davant del tribunal corresponent.

I per a que consti signen el present a l'Hospitalet de Llobregat el dia 20 de abril de 2015

Tomas Escuin Miquel Viñas

TABLE OF CONTENTS

ABSTRACT

E-glass fiber-reinforced composites (FRC) have become popular in dental and medical applications for load-bearing applications. This is due to their enhanced biomechanical matching with living tissues compared to traditional materials, as well as additional biocompatible properties. Recently, it has been shown that FRC enhances gingival soft tissue integration. Besides, satisfactory results have been observed after undergoing five years of simulated oral fatigue on unidirectionally reinforced FRC abutments. These studies make FRC promising materials for implant abutment applications. Nonetheless, there is a lack of studies regarding bacterial adhesion of FRC when compared with those published on traditional implant abutment materials. Furthermore, the effect of different fiber orientation on the load-bearing capacity of FRC abutments has yet to be determined. Therefore, this work aimed to evaluate E-glass FRC in terms of biological and mechanical aspects in order to explore a new alternative metal-free abutment material. A further aim has been to develop a standard set of surface analysis methods.

Surface topography characterization was performed by using atomic force microscopy and white light interferometry. Wettability was determined by using the sessile drop method. Additionally, a novel standard set of surface parameters to characterize biomaterial surfaces was proposed taking into account their correlation values and sensitivity in material discrimination (Study I). The attachment (bacterial adhesion) of *Escherichia coli* and *Staphylococcus aureus* was determined and discussed (Study II). Finally, the mechanical properties were assessed by three-point bending tests and the load-bearing capacity examined using static loading following ISO 10477 and ISO 14801 standards (Study III).

The results of the FRC surface characterization showed that they exhibited rough surfaces with hydrophobic characteristics. This increased roughness enhanced the early bacterial adhesion on FRC surfaces nevertheless, on the later, mature biofilm compensated these differences. The following parameters were best in biomaterials discrimination: S_a, S_{ku}, and S_{mid} at the nanoscale, S_a and S_z at the microscale and one contact angle. Bidirectionally reinforced FRC rods showed a greater breakage capacity compared to unidireccional rods. Bidirectionally reinforced FRC abutments showed statistically higher load-bearing capacities compared to unidirectionally reinforced abutments. Hence, owing to its comparable bacterial response to current implant abutment materials in addition to the adequate mechanical properties of bidirectional FRC abutments, it can be concluded that FRC is a promising alternative material in implant prosthetic dentistry.

Keywords: fiber-reinforced composite, implant abutment, roughness, nanoroughness, wettability, load-bearing capacity, static load.

RESUMEN

Los materiales compuestos de resina reforzados con fibras de vidrio E (FRC) están aumentando su uso en aplicaciones dentales y ortopédicas como materiales de soporte de carga. Esto es debido a que exhiben una mejor adaptación biomecánica con los tejidos vivos en comparación con los materiales tradicionales, así como por sus propiedades biocompatibles. Recientemente, se ha observado que mejora la formación del tejido gingival peri-implantario. Además, pilares de FRC reforzados unidireccionalmente han soportado satisfactoriamente 5 años de fatiga oral simulada. Estos estudios hacen que los FRC sean materiales prometedores para pilares de prótesis sobre implantes. Sin embargo, hay una falta de estudios que comparen la adhesión bacteriana de FRC a los materiales actuales para prótesis sobre implantes. Además, el efecto de la diferente orientación de las fibras en la capacidad de carga de los FRC como pilar implantario está aún por determinar. Por lo tanto, este estudio tuvo como objetivo evaluar los aspectos bacterianos y mecánicos de los FRC en con el fin de investigar un nuevo material alternativo libre de metal como pilar para prótesis sobre implante.

La caracterización de la rugosidad superficial se realizó mediante microscopía de fuerza atómica e interferometría de luz blanca, y la humectabilidad se determinó utilizando el método de la gota sésil. Se analizaron los parámetros de superficie obtenidos en función de su eficacia en discriminar materiales y se propuso un conjunto de parámetros con el mayor poder discriminatorio (Estudio I). Posteriormente se cuantificó y analizó la adhesión bacteriana de *Escherichia coli* y *Staphylococcus aureus* (Estudio II). Por último, se evaluaron las propiedades mecánicas mediante ensayos de flexión de tres puntos y la capacidad de carga estática siguiendo las normas ISO 10477 e ISO 14801 respectivamente (Estudio III).

Los resultados de la caracterización de superficie mostraron que los FRC presentan superficies rugosas con características hidrofóbicas. Esta rugosidad aumentó la adhesión bacteriana temprana aunque si nos atenemos al biofilm maduro no se observaron diferencias. Los parámetros S_a, S_{ku} y S_{mid} en la nanoescala, S_a y S_z en la microescala y un ángulo de contacto resultaron ser los más eficaces en la discriminación de biomateriales. Las barras reforzadas bidireccionalmente mostraron una mayor capacidad de fractura en comparación con las unidireccionales. Los pilares de FRC reforzados bidireccionalmente mostraron estadísticamente una mayor capacidad de carga en comparación con pilares reforzados unidireccionalmente. Por lo tanto, debido a su similar respuesta bacteriana con los actuales materiales así como de las adecuadas propiedades mecánicas de los pilares de FRC reforzados bidireccionalmente, se puede concluir que los FRC son materiales alternativos prometedores para su aplicación en prótesis sobre implante.

Palabras clave: compuestos reforzados con fibras, pilar sobre implante, rugosidad, nanorugosidad, humectabilidad, capacidad de carga, carga estática.

LIST OF ABBREVIATIONS

AFM	Atomic Force Microscopy
ANOVA	Analysis of variance
ATCC	American type culture collection
BAG	Bioactive glass
Bis-GMA	Bisphenol-A-glycidyl dimethacrylate
CAD-CAM	Computer-aided-design/Computer-aided-manufacturing
CD	Degree of conversion
CDD	Charged-double-device
DMLS	Direct laser metal soldering
E-glass	Electrical glass
FRC	Fiber-reinforced composite
HEMA	Hydroxyethylmethacrylate
ISO	International Organization for Standardization
kHz	Kilohertz
mm	Milimeter
mW/cm^2	Milliwatt per square centimeter
Mpa	Megapascal
n	Sample size
nm	Nanometer
N	Newtons
N/m	Newton per metro
OD	Optical density
PEEK	Polyetheretherketone
SD	Standart Deviation
SEM	Scanning electron microscopy
SPSS	Statistical package for the social sciences
STL	Standard stereolithography
TEGDMA	Triethyleneglycoldimethacrylate
UCLA	University of California, Los Angeles
UDMA	Urethane dimethacrylate
WLI	White light interferometry
rpm	Revolutions per minute
Vol. %	Volume percentage
Y-TZP	Yttria-stabilized tetragonal zirconia polycrystal

DEFINITIONS

Anisotropic is the property of being directionally dependent or non-uniform (e.g. unidirectional FRC, natural bone).

Biomaterial is a material intended to interact with biological systems to evaluate, treat, augment, or replace any tissue, organ of function of a body (Williams, 1999).

Bioactive glass is any glass or glass ceramic that displays the characteristics of bioactivity (Williams, 1999).

Bioactivity is a phenomenon in which a biomaterial elicits or modulates a biological response at the interface of the material that results in the formation of bond between the tissue and the material (Williams, 1999).

Biocompatibility is an ability of a material used in a medical device to perform with an appropiate host response in a specific application (Williams, 1999).

Cross-link is a bond that links a polymer chain to other polymer chains by covalent bonds (e.g. BisGMA-TEGDMA help in the stablishment of cross-linked chains).

Elastic modulus or modulus of elasticity (*E*) is the ratio of the stress applied to a body or substance to the resulting strain within the elastic elastic deformation region. It describes the rigidity of the material.

Flexural modulus or **bending modulus** is the stress to strain ratio in flexural deformation. It describes the tendency for a material to bend.

Flexural strength is defined as a material's ability to resist deformation under load. It represents the highest stress (force per unit area) experienced at the instant within the material at its moment of rupture subjected to flexural loading.

Toughness (K) is the ability of a material to absorb energy and plastically deform without fracturing. It is represented by the total area of the stress-strain curve.

Isotropic is the property of being uniform in all orientations (e.g. short fiber composite, particulate filler composite).

Load-bearing capacity or Fracture strength is the maximum stress a material withstands before failure when subjected to load.

Osteoinductive is the ability to induce bone growth in nonosseous tissues.

Osteointegration is the direct structural and functional connection between living bone and the surface of a load-bearing implant.

Strain is the change in length per unit of the original length uppon applied stress.

Stress/Load is the force applied to produce a deformation is a specimen.

Thermoset is a physical property of a material that when heated polymer chains attach to each other by cross-linking. Therefore, it irreversibly cures (e.g. BisGMA, epoxy resin).

Thermoplastic is a physical property of a material that when heated does not cross-link, instead, the polymer chain becomes fluid and moldable and sodifies upon cooling (e.g. denture base resin).

Orthotropic materials are a subset of anisotropic materials that show two axes of elastic symmetry with independent properties in this orthotropic direction (e.g. bidirectional FRC).

LIST OF ORIGINAL PUBLICATIONS

This thesis has originated the following original articles:

I. **Etxeberria M,** Escuin T, Vinas M, Ascaso C. (2015) Useful surface roughness parameters for biomaterial discrimination. Scanning, in press.

II. **Etxeberria M,** López-Jiménez L, Merlos A, Escuín T, Viñas M. (2013) Bacterial adhesion efficiency on implant abutments: a comparative study. International Microbiology 16:235-242.

III. **Etxeberria M,** Abdulmajeed AA, Escuin T, Vinas M, Lassila L, Närhi TO. (2015) Load-bearing capacity of fiber-reinforced composite abutments and one-piece implants. European Journal of Prosthodontics and Restorative Dentistry, in press.

This thesis has originated the following congress contribution:

I. **Etxeberria M,** Escuin T, Lassila L, Abdulmajeed AA, Vinas M, Närhi TO. (2014) Fracture resistance of fiber reinforced composite implant abutments. Dental Materials. 30: e2-e3.

1 INTRODUCTION

Current implant systems cannot reproduce the functional semi-elastic attachment to the peri-implant bone like the one that exists between the natural tooth and a sound periodontal ligament. Therefore, occlusal forces are transmitted directly to the bone. In addition to this, in severe bone resorption conditions, the difference in stiffness of traditional implant materials´ with human living tissues can generate stresses that may lead to treatment failure (Lemons, 1998). Hence, interest in implant dentistry has shifted towards achieving implant materials that could provide better biomechanical properties to match those of natural bone in order to facilitate the transmission of physiological stress levels to the peri-implant tissues (Adbulmajeed *et al.,* 2011a; Ballo *et al.,* 2014a; Ballo *et al.,* 2014b; Moritz *et al.,* 2014).

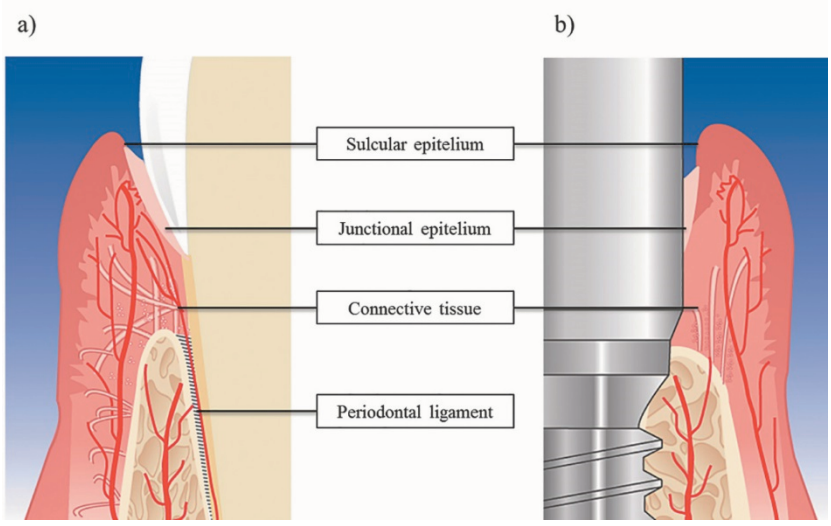

Figure 1: Soft tissue interface differences between teeth and implants. (Source: Fombellida F & Martos F (2004). Cirugía mucogingival. Team Work Media España. 12;371-428). In the natural tooth (a) there is a direct connective tissue attachment to the tooth while in an implant (b) this is inexistent. In addition, implants lack a periodontal ligament to act as a shock-absorber.

Fiber-reinforced resin composite materials have become popular owing to the fact that their mechanical properties can be tailored to match those of the living tissues (Ballo *et al.,* 2009; Zhao *et al.,* 2009; Adbulmajeed *et al*., 2011a; Ballo *et al.,* 2014b; Moritz *et al*., 2014). One of such materials is fiber-reinforced composite (FRC) made of bisphenol-A-glycidyl dimethacrylate (BisGMA) and triethyleneglycoldimethacrylate (TEGDMA) light-polymerizable biopolymers reinforced with unidirectional silanized E-glass fiber rovings. FRCs are durable materials characterized by a low elastic modulus which is similar to the dentin and bone tissues and exhibits high fracture resistance and tensile strength (Vallittu, 1999; Abdulmajeed *et al.,* 2011a).

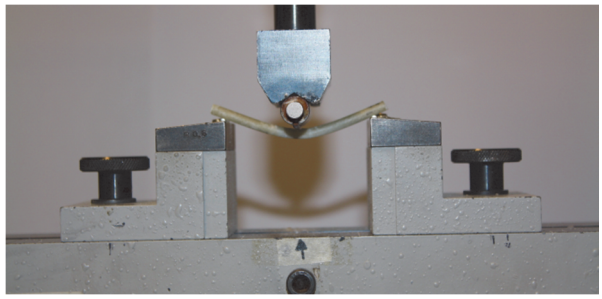

Figure 2: Three-point bending test of FRC rod showing high flexural strength and toughness. The unidirectional E-glass fibers maintain the structural integrity of the FRC after failure.

Fiber-reinforced composite materials have been used in restorative and prosthetic dentistry for years. The use of FRC has increased in many disciplines such as fixed and removable prosthodontics (Vallittu, 2004; Dyer *et al.,* 2005; Perea *et al.,* 2014), periodontal splints (Meiers *et al.,* 1998), root canal posts (Lassila *et al.,* 2004; Manocci *et al.,* 2005), orthodontic treatment (Ohtonen *et al.,* 2013), and in restorative composite resins (Garoushi *et al.,* 2013).

In recent years, FRC implants have been developed for head-and-neck, maxillofacial and orthopedic applications which also makes them a promising materials for occlusal load-bearing appliances (Zhao *et al.,* 2009; Aitasalo *et al.,* 2014). Furthermore, FRC surfaces have shown adequate oral bacterial response (Tanner *et al*., 2005; Lassila *et al*., 2009), favorable fibroblast response (Adbulmajeed *et al*., 2014; Adbulmajeed *et al*., 2015), as well as osteoinductive properties after adding bioactive glass particles (BAG) (Ballo *et al.,* 2009; Ballo *et al.,* 2014a; Ballo *et al.,* 2014b).

Although there is a lack of scientific data on using FRC as an oral implant abutment, the material shows promising potential for further research. This study is a part of a group of studies that attempt to use FRC as a potential alternative implant abutment material. The aim of this project was to evaluate the biocompatibility (by means of surface characteristics and oral microbial adhesion on FRC surfaces) and the mechanical properties of FRC as a potential implant abutment material.

Figure 3: Image of a unidirectional FRC abutment.

2 REVIEW OF THE LITERATURE. STATE OF THE ART

2.1 Implant abutment materials

2.1.1 Historical perspective

2.1.1.1 From 1985 to 1990

Per-Ingvar Brånemark´s research group was first to develop the restorative treatment called "tissue integrated prostheses" in 1985 (Zarb *et al.,* 1985). This approach consisted of full-arch prostheses anchored to osseointegrated implants to restore function on a totally edentulous mandible. One of the main goals was the fabrication of a strong metal gold framework to splint multiple implants. These prostheses were made out of long titanium transepithelial abutments, cast gold cylinders with small gold screws and a cast noble alloy framework that was later processed using acrylic resin. Nevertheless, these transmucosal components (between the abutment and the implant) were visible, which were highly unaesthetic.

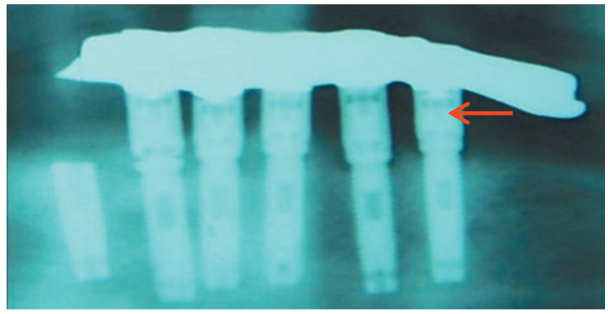

Figure 4: A full-arch prostheses attached to implants with long transepithelial abutments according to the Brånemark´s principles.

At the same time single tooth restorations were developed and they consisted of prefabricated machined titanium abutments veneered primarily with acrylic resin, resulting in a one-piece abutment-crown restoration (Jemt, 1986).

The next relevant step was the development of the UCLA abutment which consisted of a machined plastic pattern fully castable, allowing the direct connection between the implant supported restoration and the upper part of the implant fixture (Lewis *et al.,* 1988). This system avoided transmucosal metal components thereby improving the aesthetic outcome. Moreover, the bigger screw reduced loosening of the screw and at the same time made it feasible to create cement-retained reconstructions. Subsequently, UCLA abutments with a pre-machined metal base were developed to avoid fit

imperfections of casting techniques. This abutment continues to be used today for both screw and cement-retained restorations.

Figure 5: UCLA abutment prototypes.

At that time, the principles of implant prosthodontics were based on basic prosthethic procedures that included intraoral impressions, jaw relation registrations, waxing, casting noble alloys by the lost wax technique, metal framework try-in and delivery. Although casting errors could be corrected using various soldering techniques, high incidence of prosthodontics complications were observed (Zarb & Schmitt, 1990).

2.1.1.2 From 1990 to 2000

During the nineties, prosthetic techniques improved with the goal to minimize problems associated with manufacturing techniques; these were mainly screw fractures and esthetic considerations. The need for improved aesthetics was solved by the design of abutments where the crown margins could be placed below the margin of the mucosa in a controlled manner. NobelPharma (now Nobel Biocare, Göteborg, Sweden) developed the CeraOne concept in 1990. This approach was based on the use of aluminum oxide machined caps or standard gold alloy caps (used for crown fabrication) which were cemented to the CeraOne abutment. With this development, the emphasis moved from screw-retained to cemented restorations. In 1993, Prestipino & Ingberg (Prestipino & Ingberg, 1993) introduced the ceramic CerAdapt alumina abutment (Nobel Biocare, Göteborg, Sweden) that offered more esthetically favorable characteristics. In addition to this, these pioneer ceramic abutments offered good surface properties such as low corrosion, high biocompatibility, and low thermal conductivity. However, these restorations made out of ceramic cores were weaker when compared to metal-ceramic restorations.

An important breakthrough was the introduction of computer-aid-designing and computer-aid-manufacturing (CAD-CAM) technique in the late nineties. The Procera technique was introduced to create custom implant abutments by CAD-CAM to improve the precision of fit of gold cast frameworks.

2.1.1.3 From 2000 to today

At the beginning of the 21th century, the gold prices increased dramatically and a new generation of metals such as cobalt-chromium alloys started to gain interest. These base metals became a popular replacement to noble alloys because of their higher fracture strength, elastic modulus, hardness and lower cost. However, these metals are difficult to cast and inaccuracies may occur (Anusavice & Phillips 2012; Oyagüe *et al.,* 2012; Castillo-Oyagüe *et al.,* 2013).

Therefore, in 2008, direct metal laser sintering (DMLS) method was first introduced in dentistry (Quante *et al.,* 2008) to overcome the potential distortions inherent in casting of dental alloys. This technique is based on a high-power laser beam (e.g., a carbon dioxide laser) that fuses metal alloy powder particles into a mass to fabricate the projected frame. Structures are built up in layers from the occlusal surface to the margins by scanning cross-sections following a 3D CAD design.

2.1.2 Current implant abutments

Nowadays metals, ceramics, polymers and composites are used for fabrication of implant abutments. FRC will be introduced in this thesis as a potential implant abutment.

2.1.2.1 Metals

Metal implant abutments and frameworks can be made out of titanium or cast metal alloys which can be noble, high noble or base metal.

Ti_6 Al_4 V (titanium grade V) is preferable for implant abutments over the commercially pure titanium (grades I to IV) due to its higher strength (Elias *et al.,* 2008). On the other hand, commercially pure titanium is preferred for endosseous dental implants.

Among cast metal alloys, noble metals are superior to base metals due to their lower corrosion. However, as previously mentioned, because of their high cost, noble metals were replaced by base metal alloys. Among them, alloys of cobalt-chromium (Co-Cr) have been widely used due to their favorable combination of excellent biocompatibility and mechanical properties compared to noble metal alloys (Hultherstrom *et al.,* 1994; Roach, 2007). The properties of the cobalt-chrome alloy Wirobond® C (BEGO Bremer Goldschlägerei Wilh. Herbst GmbH & Co, Bremen, Germany) are considered excellent due to the adherent layer of chrome-based oxides on the surface that creates a passivating effect improving the corrosion resistance (McCabe 1990; Zupancic *et al.,* 2006).

Nonetheless, metal implant abutments show some potential shortcomings. The increasing esthetic demands justify the search for other materials with better optical properties (Jung *et al.,* 2008). Their possible cytotoxicity is still considered a major concern of debate. Reactive metals may exhibit alloy corrosion and hence, may release metal ions into the oral environment being a potential cause of health damage (Sicilia *et*

al., 2008; Siddiqi *et al.,* 2011). In addition to this, they show a high biomechanical mismatch with the living tissues due to their higher stiffness. For instance, titanium alloy shows a modulus of elasticity which is ten times higher compared to that of dentin and cortical bone (Lemons, 1998).

2.1.2.2 Ceramics

A demand for more esthetic restorations lead to the introduction of several ceramic materials such as alumina, lithium disilicate glass-ceramic and zirconia. A recent systematic review showed that the yttria-stabilized tetragonal zirconia polycrystal (Y-TZP) is the "material of choice" for implant abutments (Bidra & Rungruanganunt, 2013). In that study, among the all-ceramic dental materials, zirconia abutments showed superior fracture strength. Nevertheless, ceramic abutments may show some limitations. Their major drawback is their brittleness, and thus, they show low tensile strength and fracture toughness. Besides, they are difficult to repair (Belser *et al.,* 2004; Sailer *et al.,* 2009). Jung et al. found encouraging five-year survival rates of implant supported all-ceramic single crowns (91.2%) compared to metal-ceramic crowns (95.4%) (Jung *et al*., 2008). However, long-term clinical evaluations are needed in order to support their application (Bidra & Rungruanganunt, 2013). Thus, their use is recommended in aesthetically compromised areas (Gomes & Montero, 2011).

2.1.2.3 Polymers: Polyetheretherketone

Polyetheretherketone (PEEK) is a newly developed high performance thermoplastic polymer that shows good biocompatibility, mechanical strength, ductility, and low density (Kurtz & Devine, 2007). However, Peek implant abutments show some potential shortcomings in the field of restorative and prosthetic dentistry. These are related to their high resistance to surface modification by chemical treatments (e.g., acid-etching) that makes bonding to composite resin materials difficult (Ohl *et al.,* 1999; Noiset *et al.,* 2000). Thereby, their use is currently limited to temporary (for a period of 6 months) restorations (Tetelman & Babbush, 2008). Being a novel implant abutment material more research is needed to justify and evaluate these aspects and other eventual applications.

2.1.2.4 Fiber-reinforced composites

In the last few years, the search for new metal-free materials has increased the development of composites. Between them, E-glass and carbon/graphite fiber-reinforced frameworks have been presented as alternatives to metallic frameworks (Björk *et al.,* 1985; Bergendal *et al.,* 1995; Duncan *et al.,* 2000; Behr *et al.,* 2001; Freilich *et al.,* 2002). Rationale for using composite materials is that they can be engineered to fit physiologic requirements of the application site and closely match the modulus of the dentin and bone. In addition to this, they show low weight and high load-bearing capacity.

The use of FRCs in dentistry started in the beginning of 1960 as a denture base reinforcement (Smith, 1961). However limitations related to the high viscosity of the resin systems of that time made it difficult to preimpregnate the fibers on the resin and thus decreased the final strength of the composite. Nevertheless, Vallittu (Vallitu, 1999) developed a technique that allowed a more effective impregnation of the fibers within the matrix obtaining major improvements in the mechanical properties of the materials in 1999. This consisted in preimpregnation of reinforcing fibers with highly porous polymer Stick (S) and Stick Net (GC, Japan). The use of light-curing dimethacrylate monomer instead of porous polymer can also serve for the same purpose (Vallitu, 1999).

FRC is a material composed of a resin matrix and reinforcing fibers.

Thermoset resins are preferred over thermoplastics for fiber reinforced systems due to their lower viscosity that enables an adequate impregnation of reinforcing fibers. For this reason, first thermoplastic composites were reinforced with chopped (discontinuous) fibers, however, on the other hand, they showed inferior strength compared to continuous FRC (Brown *et al.,* 1990). Among thermosets, the bisphenol-A-glycidyl dimethacrylate (BisGMA) has been extensively used as a matrix in composite formulations since 1960s (Bowen, 1963). BisGMA was first developed by Bowen to improve the polymerization shrinkage, strength and adhesiveness of resin restorations by attaching methyl methacrylate groups to epoxy resins, thereby converting epoxy resins to dimethacrylate resins. This resin showed cross-linking abilities (stronger than linear polymers) during polymerization. However, its high viscosity led to the addition of diluent monomers with lower viscosities such as triethyleneglycol dimethacrylate (TEGDMA) (Darvell, 2006).

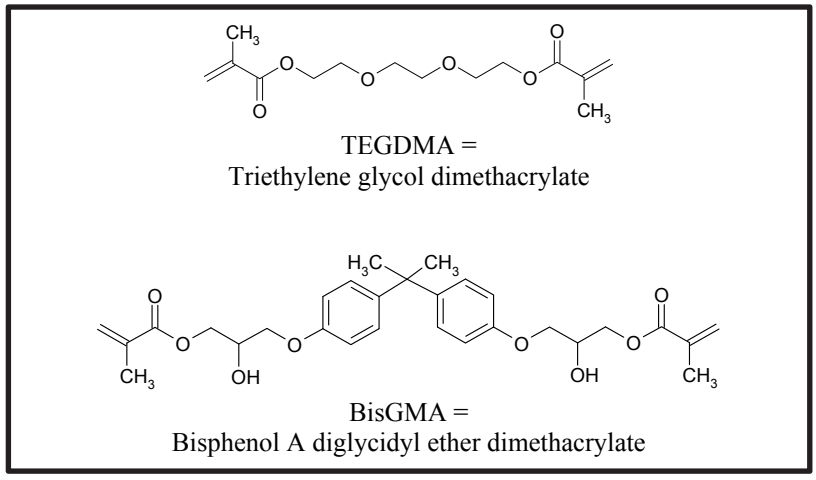

Figure 6: Chemical structure of Bis-GMA and TEGDMA monomers.

Nowadays, dimethacrylate-based resins (e.g. BisGMA or urethane dimethacrylate (UDMA) diluted with TEGDMA or hydroxyethylmethacrylate (HEMA)) and silorane-

based epoxy resins are reinforced with inorganic fillers (commercial dental composites) or fibers (fiber-reinforced composites). The specific characteristics of the silorane-based matrix and the epoxy-functional silane agent restrict the use of particular fillers, resulting in a formulation with a reduced filler content (Leprince *et al.,* 2010).

Among dimethacrylate-based resins the fully cured biostable 50/50 BisGMA-TEGDMA (equal parts of the monomers) in addition to CQ (0.7 wt%) and DMDA (0.7 wt%) resin did not show any cytotoxic effects in animal experimentation (Zhao *et al.,* 2009; Adbulmajeed *et al.,* 2015). This resin mixture showed a degree of monomer conversion (DC) above 60%; resulting in a minimal release of residual monomer (Imazato *et al.,* 2001; Uctasli *et al.,* 2005). Additionally, it can be autoclaved at 121º at 0.1MPa pressure (Zhao *et al.,* 2009; Adbulmajeed *et al.,* 2015).

When a load is applied to FRC, fibers reinforce the resin carrying the load. Various types of fibers can be used for reinforcement of resins such as carbon, polyethylene, and glass fibers. E-Glass fibers (silica-based fibers) can bond to BIS-GMA-TEGDMA through silane coupling agents rendering them excellent mechanical properties for load-bearing devices in dental (Abdulmajeed *et al.,* 2011a) and orthopedic applications (Zhao *et al.,* 2009, Aitasalo *et al.,* 2014; Ballo *et al.,* 2014a). In addition, they show favorable aesthetic properties compared to carbon fibers.

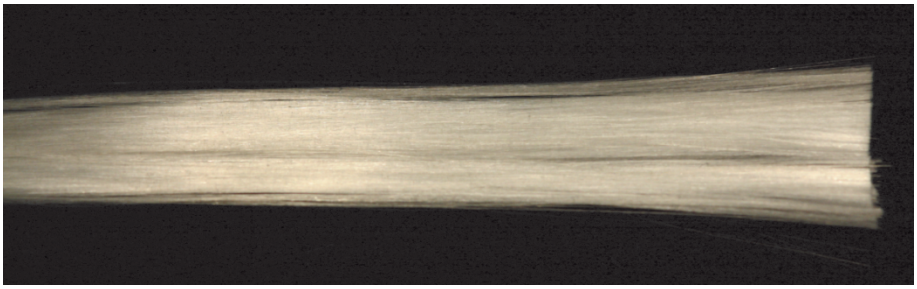

Figure 7: E-glass bundle formed by 2.400 continuous unidirectional silanized E-glass fibers (diameter 15 μm).

Continuous glass fibers have been widely used in various dental applications. Depending upon the orientation on the resin matrix, they are classified into unidirectional (fiber bundle), bidirectional (fiber weave) or randomly oriented (mat). Unidirectional fibers provide anisotropic mechanical properties being therefore best to the direction of the stress; bidirectional fibers provide orthotropic characteristics suitable in two-dimensional stresses and multidirectional fibers show isotropic properties being adequate for three-dimensional stresses (Vallittu *et al.,* 1998).

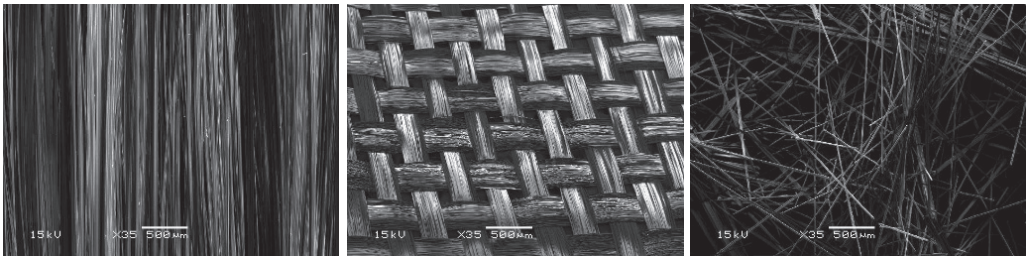

Figure 8: SEM images of different fiber orientations. Left to right unidirectional; bidirectional plain-weave; and randomly oriented E-glass fibers.

FRC materials possess several advantages such as computer-aid-designing and computer-aid-manufacturing (CAD-CAM) fabrication and permit intraoral adjustments without heat transfer to the bone. Besides, they also show adequate esthetic properties and high fracture strength. Thereby, FRC implant abutments have been introduced as promising alternatives to traditional abutment materials (Behr *et al.,* 2001; Kim *et al* 2009; Erkmen *et al.,* 2011).

2.2 Surface characterization of implant abutments

Surface characteristics of implant abutments govern major aspects of biological interactions such as the bacterial attachment. Subsequently, surface properties of implant abutments are key factors in the implant treatment outcome (Park *et al.,* 2012; Gittens *et al.,* 2013). In other words, bacterial attachment depends not only upon the bacterial abilities but also on the material properties. Among them there are three main characteristics modulating bacterial adhesion: roughness, wettability and surface chemistry (Subramani *et al.,* 2009).

2.2.1 Surface roughness

A considerable attention is devoted to surface roughness since it plays an important role in the bacterial adhesion to biomaterials. It is stated that there is a threshold roughness value of 0.2 µm, suggesting that lower values may not affect the biofilm formation (Bollen *et al.,* 1997; Teughels *et al.,* 2006). Amoroso et al. claimed that since most bacteria are larger than 0.2 µm, roughness values inferior to this size may not promote bacterial adherence (Amoroso *et al.,* 2006). Thus, surface roughness modification strategies have been performed to modulate the surface properties of biomaterials in order to act on bacteria-substrate interactions and improve the overall biological response (Ivanova *et al.,* 2010). Nevertheless, to accomplish this, a detailed characterization of surface roughness must be performed.

2.2.1.1 Roughness analysis methods

Previous studies have measured the surface roughness of biomaterials using scanning electron microscopy (SEM), contact surface profilometer, atomic force microscopy

(AFM) and white light interferometry (WLI) (Hove *et al.,* 2008; Teté *et al.,* 2008; Pegueroles *et al*., 2010; Gittens *et al* 2011; Rosa *et al.,* 2012; Park *et al.,* 2012; Pereira *et al.,* 2013; Luangruangrong *et al.,* 2014). Among these techniques, only, profilometry, AFM and WLI provide quantitative topographical data. To overcome the surface damage created by the traditional profilometry techniques a non-destructive 3D surface profilometer has been developed. Nevertheless there are only a few reports using this newly developed roughness analysis method (Liu *et al.,* 2013; Uppal *et al.,* 2013).

2.2.1.1.1 Atomic force microscopy

Atomic force microscopy has become a powerful tool in imaging the surface topography of biomaterials and bacteria being up today, the most used tool for topographical characterization at the nanoscale. Hence, AFM is widely used in the life sciences providing high-resolution images in mapping surface topography of biomolecules, membranes and cells (Binnig *et al.,* 1986; Dorobantu & Gray, 2010; Dorobantu *et al.,* 2012). Another highlighting characteristic of AFM is its usefulness in analyzing living or dead cells directly in their natural medium without sample preparation.

The mechanisms of the AFM is based on capturing the forces of interaction between a sharp tip (connected to a flexible spring) and the atoms, molecules or nanostructures of the sample surface being analysed. The AFM tip is tipically silica or silicon nitride (Si_3N_4, or SiO_2) with a radius of curvature on the order of nanometers and supported on a flexible cantilever. As the tip passes through the sample surface, it oscillates (due to the action of e.g. interatomic van der Waals forces) deflecting the cantilever following Hooke´s law. This law states that the force (F) needed to elongate or compress a spring by some distance (x) is proportional to that distance within the elastic limit (Binnig *et al.,* 1986).

$F = kx$ where k is is a constant factor characteristic of the spring, its stiffness

The deflection of the cantilever is then measured by a laser spot reflected from the surface of the cantilever and registered by photodiodes (photodetectors that transform light into current or voltage) and seen on the computer as the tip scans the surface.

There is a wide variety of imaging modes that are generally divided into static (contact) of dynamic (non-contact or "tapping") modes.

The acquired data during the surface scanning is converted into 4 types of images: topography, signal, amplitude, and phase. In topography images it is possible to observe the shape, structure and texture of the sample surface while the phase images emphasizes the variations in the chemical composition of the sample in addition to the relative softness/hardness of the sample (Dorobantu & Gray, 2010).

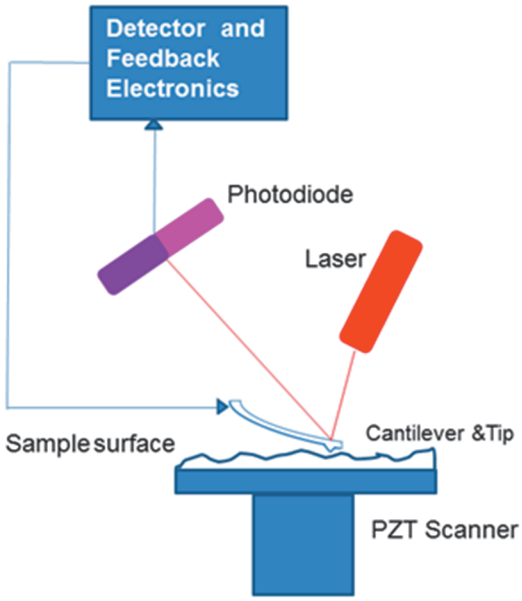

Figure 9: Schematic representation of the principle of the measurement of an AFM.

2.2.1.1.2 White light interferometry

WLI is a non-contact computerized optical interference microscopy. Its use has rapidly spread as a quality control of microscale engineering processes. WLI topography measurements are simpler, faster and more accurate than other optical methods and can cover a larger image area than atomic force microscopy. This method has been demonstrated to be fast, non-destructive and accurate (Hove *et al.,* 2008; Stenhagen *et al.,* 2010).

The topography measurement is based on a non-contact interferometric computerized optical interference microscope operating in vertical scanning interferometry mode producing a 3D topographic image. The basic principle of a white light interferometer follows Michelson´s Interferometer that consists of an incident light source that splits into two paths, one of which goes to a reference surface which is completely smooth and the other is directed to the sample surface. Both beams, are reflected and recombined inside the interferometer generating the so-called constructive and destructive interference phenomena. Subsequently, an interferometer pattern or interferogram with white and dark fringes is created (Jackson, 2008). Taking into account that the vertical movement of the reference surface can be easily tracked, it is possible to create a 3D map by measuring the position of the lens to create the brightest image at each point of the charged-double-device (CCD).

The intensity of each point of light is then digitally registered on the CDD. Each pixel of the CDD array acts as an effective interferometer, creating an accurate 3D map image point by point of the sample surface (de Groot & Deck, 1995).

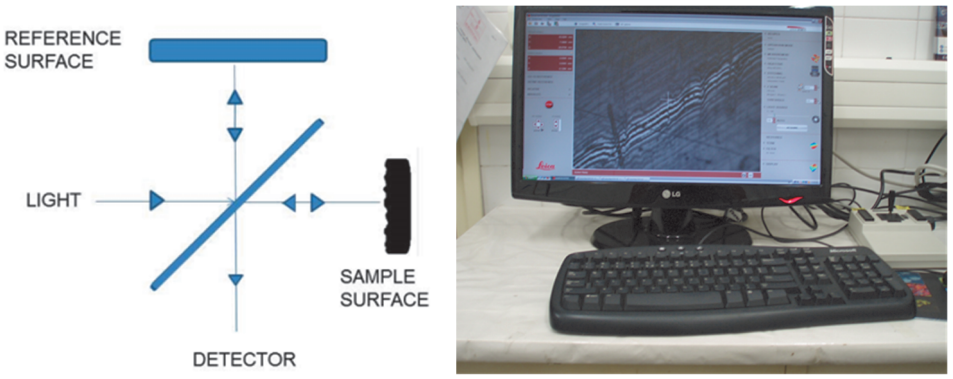

Figure 10: Schematic representation of the principle of the measurement of a WLI. Image of a constructive interference pattern.

2.2.1.2 Surface parameters

In dentistry a multi-parameter representation method has been suggested in order to provide an accurate description of a surface. Hence, a wide variety of surface roughness parameters have been developed and termed as "the parameter rash" by Whitehouse (Whitehouse, 1982). Despite of this, inconsistencies have been reported when describing a surface topography (Dong *et al.*, 1994; Gadelmawla *et al.,* 2002). This fact may be explained by the lack of standardized techniques (Wennerberg & Albrektsson 2000; Crawford *et al.,* 2012). To evercome this situation a possible solution is the reduction in the number of parameters for general standardization in order to facilitate data comparisons.

Among the surface parameters, amplitudinal parameters are calculated according to the height (vertical) values of a given profile or surface, and therefore considered the most relevant surface morphology characteristic. Surface roughness parameters are denoted with the letter S, followed by an identifying subscript, e.g. S_a. Likewise, profile roughness parameters are denoted with the letter R. The arithmetical mean deviation of surface roughness S_a (or its counterpart R_a) is so far the most cited surface parameter for the description of the topography of biomaterials (Whitehead *et al.,* 2005; Mitik-Dineva *et al.,* 2009; Truong *et al.,* 2010).

Recent studies focused on this topic suggest including spatial (horizontal) parameters in order to obtain the best overall surface description. Nevertheless, "the parameter rash" should be avoided; Dong et al. claimed that the selection of the surface should be based on sound statistical principles (Dong *et al,.* 1994). In contrast, the statistical dependence or independence of the surface parameters is rarely studied in the literature (Radford *et al.,* 1998; Wang *et al.,* 2004).

2.2.1.2.1 The parameter reduction method

Many attempts to achieve a parameter selection method have been developed for years (Thomas 1981; Nowicki 1985; Kaiser & Brinkmann, 2006). Among them, the parameter reduction method is effective in selecting which roughness parameters should be addressed (Nowicki 1985; Rosen *et al.,* 2008; Ham & Powers, 2014). As stated by Nowicki, the parameters least correlated are best for discriminating between materials whereas among the highly correlated parameters, one can represent the whole group (Nowicki, 1985).

In brief, the correlation coefficient (r) is related to the covariance coefficient and the standard deviation of two data sets. Thus, when the value of (r) approaches to one, the two data sets show a strong correlation and are therefore interchangeable. In contrast, when it approaches zero the two data sets are not related and therefore both give complementary and thus relevant information.

2.2.1.3 Surface roughness of implant abutments

For implant abutments, average roughness values ranged between 0.088 and 0.2 μm for titanium (Rimondini *et al.,* 1997; Bollen *et al.,* 1997; Sawase *et al.,* 2000; Hanel *et al.,* 2014); and between 0.15 to 0.39 μm for cobalt-chrome (Hjalmarsson, 2009; Herbst *et al.,* 2013; Kim *et al.,* 2015). Values ranged between 0.08 to 0.22 μm for zirconia surfaces (Bollen *et al.,* 1996; Rimondini *et al.,* 2002; Rosenttrit *et al.,* 2009; Yang *et al.,* 2015), and <0.1 to 1.25 μm for FRC surfaces (Tanner *et al.,* 2003; Lassila *et al.,* 2009; Adbulmajeed *et al.,* 2014). Finally for PEEK surfaces values varied from 0.084 to 0.536 μm (Rochford *et al.,* 2014).

2.2.2 Surface wettability

Hydrophobicity of a surface is a major factor in the regulation of bacterial attachment and therefore, is considered a predictive index of cytocompatibility (Lim & Oshida, 2001). The direct correlation shown by previous studies explains that the higher capacity of a surface to interact within a liquid, the higher bacterial attachment rate is expected. Many techniques can be used for measuring wettability. Among them, the sessile drop technique is the most commonly used one (Ivanova *et al.,* 2010; Gittens *et al.,* 2011; de Oliveira *et al.,* 2012). This method measures the internal (intersection of the line tangent to the liquid and the sample surface) or the external angle which is supplementary to the former. Internal high contact angles indicate poor wettability while low contact angles indicate good wettability. This angle can be modified by certain properties such as surface roughness and surface chemistry (Wenzel, 1949).

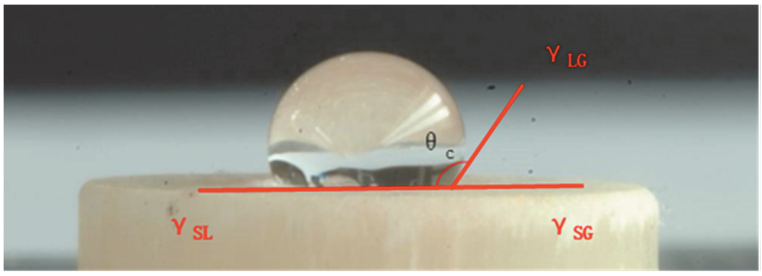

Figure 11: An example of the sessile drop technique. Equilibrium contact angle θ_c

2.2.2.1 Surface wettability of implant abutments

For implant abutments, wettability values in degrees ranged between: 76.3 to 81.4 for titanium (Ivanova *et al*., 2010; Kim *et al.,* 2015); 90.2 for cobalt-chrome (Kim *et al.,* 2015); 51.98 to 63.87µm for zirconia surfaces (Yang *et al*., 2015; Kim *et al.,* 2015); 54.3 to 69 for FRC surfaces (Adbulmajeed *et al*., 2011b); and 60 to 80 for PEEK surfaces (Ourahmoune *et al.,* 2014).

2.2.3 Surface chemistry

Surface chemical composition influences bacterial adhesion and proliferation (Subramani *et al.,* 2009, Yamane *et al.,* 2013; Nascimento *et al.,* 2014). Several studies have demonstrated differences in biofilm formation between alloys and ceramics showing that alloys feature thicker biofilms compared to ceramic materials (Ausschill *et al.,* 2002; Busscher *et al.,* 2010). This may be explained by the fact that the electron transfer of reactive free electrons of metallic surfaces can contribute to bacterial adhesion (Poortinga *et al.,* 1999; Poortinga *et al.,* 2001). Meanwhile, ceramics, are bio-inert and thus non-reactive materials. Nevertheless, further investigations are needed to confirm this assumption due to the fact that its clinical repercussion remains unclear. To date, there is almost no scientific evidence available regarding the formation of biofilms on the surface of polymers. One *in vitro* study showed that PEEK gathered similar bacterial count to that of titanium (Gorth *et al.,* 2012). Regarding FRCs, only a few studies have observed the bacterial adhesion onto FRC surfaces but the results are encouraging. FRC gathered similar bacterial adhesion *in vivo* and *in vitro* when compared to conventional restorative materials (Tanner *et al.,* 2005; Lassila *et al.,* 2009). However, we lack studies comparing bacterial adhesion of FRC with traditional implant abutment materials.

2.3 Bacterial adhesion on implant abutments

Bacterial contamination and the subsequent biofilm growth on implant abutments is a major concern in oral implantology. Since the vast majority of peri-implantitis start with the bacterial contamination of the peri-implant soft tissues in contact with the surface of abutments (Lindhe *et al.,* 1992; Groessner-Schreiber *et al.,* 2004), these prosthetic

devices are of utmost relevance in the maintenance of implant health. However, current implant abutments cannot fully prevent the bacterial adhesion. Thus one of the major aims of oral prosthetic dentistry is to prevent or at least reduce oral biofilm formation on the implant abutment surfaces.

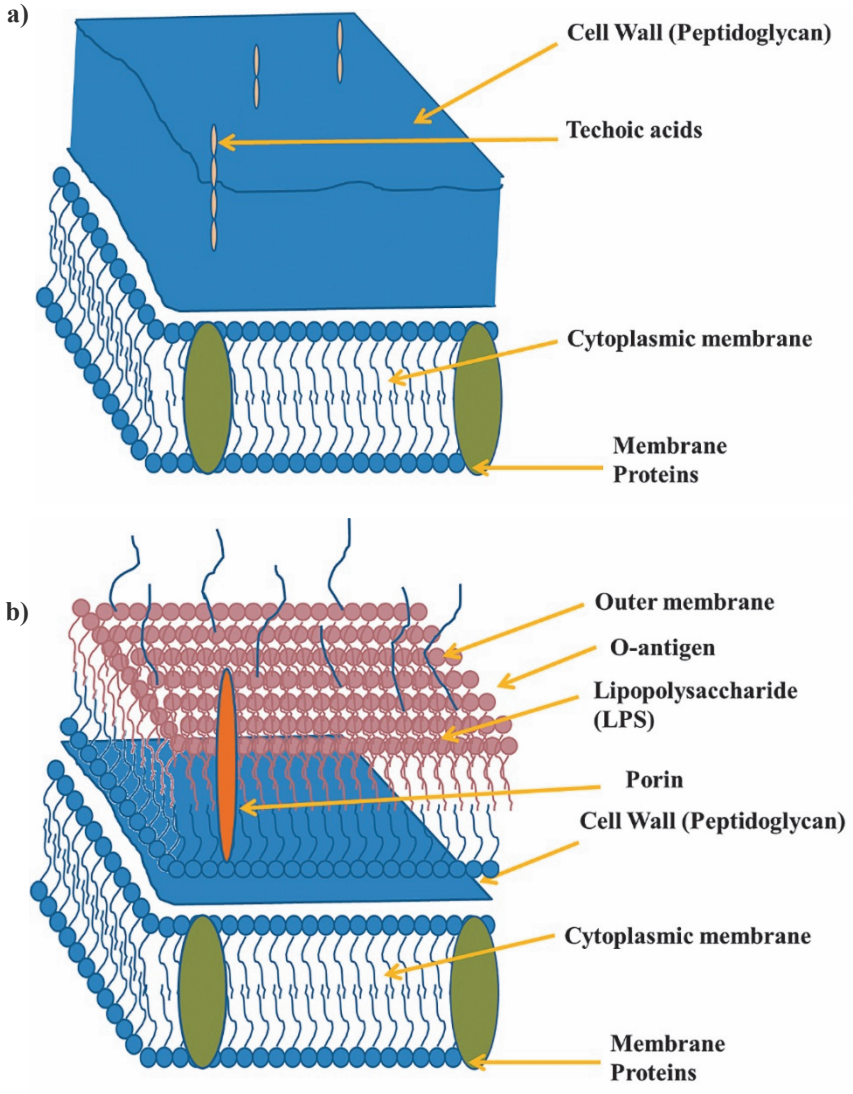

Figure 12: Schematic representation of a Gram-positive bacterium **a)** and a Gram-negative bacterium **b)**. Gram-positive bacteria do not contain lipopolysaccharide on their outer membrane, they possess a thick external layer of peptidoglycan instead.

Bacteria are prokaryotic organisms, measuring nanometers in size (< 1µm in length), which show a wide variety of shapes. From a morphological point of view, bacteria can be cocci (spherical), bacili (rod-shaped) and spirochaetes (helicoidal). According to the

staining characteristics of their cell envelopes they are divided into two subgroups: Gram-positive and Gram-negative. Gram-positive bacterial envelopes consist of the cytoplasmic membranes in addition to a peptidoglycan wall, whereas Gram-negative bacteria possess a cytoplasmic membrane covered by a thin layer of peptidoglycan and an additional membrane called the outer membrane or endotoxin (Salton, 1953; Gregersen, 1978). Depending on their metabolic requirement, bacteria can require oxygen (aerobes) or oxygen-free environment (anerobes). Obligate aerobes require oxygen to grow because their ATP-generating system is dependent on oxygen as the final electron acceptor (aerobic respiration).

In the oral cavity, bacterial adhesion to a dental or prosthetic material surface is considered to be a two-stage process comprising of an initial immediate and reversible stage (the salivary acquired pellicle) followed by a time-related and irreversible phase (biofilm formation) (An & Friedman, 1998). The pioneer bacteria (mostly streptococci and related bacteria) once adhered, constitute the basis for the attachment of other microbes. These are termed late colonizers which include both Gram-negative and Gram-positive bacteria and finally after 48 hours when mature, anaerobes become predominant (Viñas *et al.,* 1991; Subramani *et al.,* 2009). Oral biofilm formation is a highly sophisticated ecological succession able to originate a relatively stable community, so-called climax community or mature biofilm. When mature, a biofilm is formed by a wide variety of Gram-positive, Gram-negative bacteria and extracellular components extremely resistant to host defense mechanisms and antibiotic treatment leading to implant treatment failure. Mature oral biofilm is found to have a significant impact on the pathogenesis of peri-implantitis and implant loss (Scarano *et al.,* 2004).

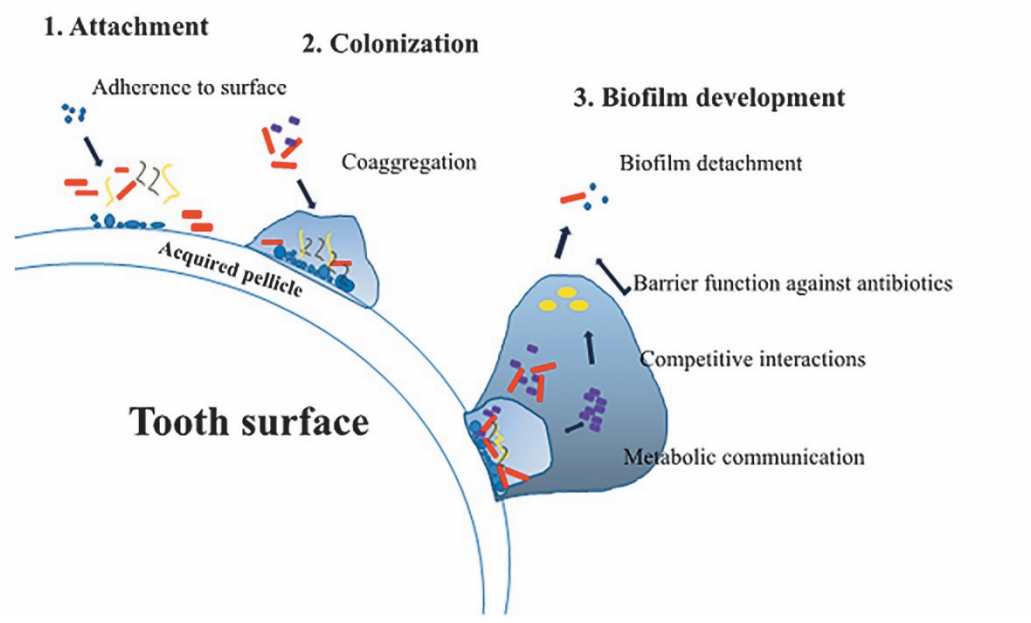

Figure 13: Schematic model of the phases involved in biofilm formation.

Thereby, in the past decades, many strategies have been developed to prevent or reduce bacterial colonization of the surface of implant devices. Such strategies include: surface modification approach on the chemical and physical properties of the implant abutments, mechanical removal with curettes, and the application of antimicrobial agents like disinfectants. Microorganisms found in oral biofilm have shown an increased resistance to host defenses and most conventional antimicrobial therapies, which may result in more intense and persistent infections (Ramage *et al.,* 2006; Tsang *et al.,* 2007). This has increased the administration of broad-spectrum antibiotics (due to differences in antibiotic-resistance depending on bacteria) that can result in imbalances in the oral flora which promotes the emergence of opportunistic bacterial infections. In general the Gram-positive bacteria are more susceptible to antibiotics than the Gram-negative ones since their outer membrane is a permeable barrier which prevents or reduces the antibiotic penetration (Viñas *et al.,* 1991). Detailed knowledge of these substrate-cell interactions may constitute the conceptual basis to develop the research and production of "intelligent surfaces" featuring enhanced performance for a specific application site (Variola *et al.,* 2011).

Considering the aforementioned, it is wishful that implant abutment materials feature low biofilm formation on their surface. However, little evidence is available regarding bacterial adhesion to FRC materials.

2.4 Load-bearing capacity of implant abutments

Dental implants do not have periodontal ligaments but rather ankylosis, thereby transmitting loads directly to the bone. This load transmission can be influenced by the material and the design of the restorative material.Traditional materials for implant restorations show a high modulus of elasticity displaying a great stiffness mismatch compared to living tissues. Therefore, increased interest has been devoted in implant prosthetic dentistry towards achieving materials that could provide better biomechanical matching in order to allow a physiological load transmission (Adbulmajeed *et al.,* 2011a; Ballo et *al.,* 2014; Moritz *et al*., 2014).

2.4.1 Mechanical properties

Mechanical properties relevant to dentistry include, among others, elastic modulus, fracture toughness, flexural strength and load-bearing capacity. All of them are measures of resistance of a material to deformation, crack propagation, or fracture under an applied force.

Flexural tests are widely used to obtain the mechanical properties of dental materials (Vallittu *et al.,* 1994; Vallittu, 1999). One of these, the three-point bending test (Figure 3) applies a load perpendicular to the longitudinal axis of a specimen generating

compressive and tensile stresses in the specimens (Vishu, 2007). As the axial load is gradually applied, the strain for a given stress is always the same and the two are related by Hooke´s Law (stress is directly proportional to strain). Knowing the cross-sectional area and length of the specimen, stress–strain curves (Figure 14) can be obtained to categorize materials as ductile and brittle materials.

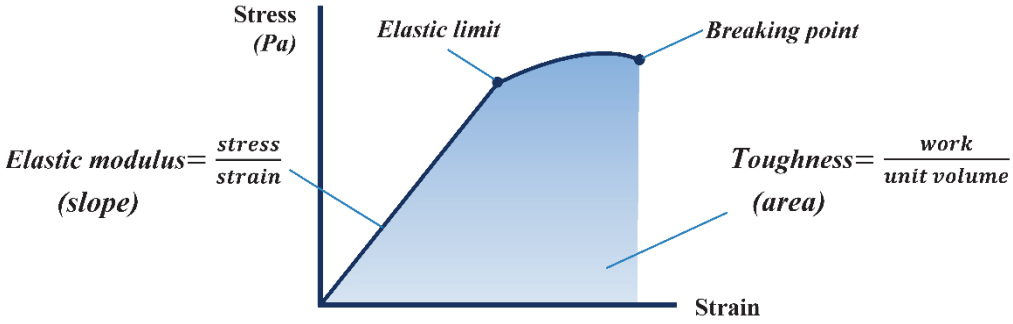

Figure 14: Curve Stress vs Strain describing the mechanical deformation of a solid.

The strength of FRC relies on the failure mechanisms i.e. toughness is associated with the capacity of the composite to absorb energy. Several damage modes including: fiber de-bonding, fiber pull-out, delamination, fiber breakage and matrix cracking have been described as energy absorbing mechanisms (Scheirs, 2000). Glass fibers are brittle thus they poorly contribute to energy absorption in failure while highly organized polymer fibers show the ability to absorb higher amounts of energy during loading.

2.4.2 Load-bearing capacity

Abutments should withstand functional masticatory loads. Static load testing until material fracture to measure the load-bearing capacity is the most commonly used test in preclinical assessment of newly developed material. For this purpose, a standardized guideline for dental implants by the International Organization for Standardization (ISO 14801) has been established. Maximum masticatory loads in anterior region have been reported to range between 40 and 370 N (Papanghoraki *et al.,* 1997; Ferrario *et al.,* 2004). However, higher possible loads (i.e. bruxism) should be considered when selecting appropriate materials.

Current abutments have shown adequate mechanical properties. Among ceramics, zirconia abutments are being increasingly accepted due to their higher fracture resistance compared to alumina. Alumina shows a poor fracture resistance (280 N) compared to zirconia (738 N) or titanium (944 N) (Yildirim *et al;* 2003; Dittmer *et al*., 2012). Regarding PEEK abutments, despite showing values of 329.4 N, (Agustín-Panadero *et al.,* 2015), they are still considered provisional abutments (Tetelman & Babbush, 2008; Agustín-Panadero *et al.,* 2015). This is partly explained by their inherent difficulty in

achieving adequate bond strength to the veneering composite resin (Ohl *et al.,* 1999; Noiset *et al.,* 2000). In contrast, FRCs are promising materials for implant abutments. A study by Behr *et al*. describes a mean fracture resistance of 321N after undergoing five years of simulated oral stress (Behr *et al.,* 2001). These promising results encourage further research due to the fact that in their study only unidirectional fibers were analyzed.

FRC structures may fulfill clinical performance criteria. The strength of FRC is related to the fiber orientation. Dyer et al. showed that reinforcement with unidirectional glass fiber occurred when fibers were located perpendicular to the compression side of the specimen (Dyer *et al*. 2005). However, this anisotropic behavior of unidirectional FRC structures contributed to the failure of FRC (delamination) during clinical function (Freilich *et al*., 2002; Behr *et al*. 2003; Gohring & Roos, 2005). Thereby, to overcome this, design strategies may include reinforcement in several directions to reduce the anisotropicity of unidirectional FRC. On the other hand, this multidirectional reinforcement occurs at the expense of a decrease in the fracture strength (Krenchel, 1963; Dyer *et al.,* 2004).

Potential concerns of these prostheses are decrease of strength due to water absorption and subsequently a reduction in the long-term stability. Water can break the bond between the polymer and fiber (Lassila *et al.,* 2002). Moreover, the release of residual monomers in the oral environment can potentially cause mucosal irritation or allergic reactions (Ruyter, 1995).

3 AIMS OF THE THESIS

This study was based on the working hypothesis that the E glass-FRC features biocompatible bacteria culture conditions and satisfactory mechanical properties comparable to current implant abutments aimed to be used for oral clinical application. Therefore, the following specific aims were set to:

1. Characterize FRC surfaces. Evaluate the role of the surface roughness and wettability parameters in biomaterials discrimination (Study I).

2. Determine bacterial adhesion to FRC (Study II).

3. Evaluate the load-bearing capacity of FRC implants and abutments (Study III).

4 MATERIALS AND METHODS

4.1 Surface characterization and bacterial adhesion to implant abutments

4.1.1 Fabrication of the substrates

Disks, ten mm in diameter and two mm thick (Figure 15), were manufactured (n = 16) from six different implant abutment materials. The materials are presented in Table 1.

Table 1: Materials used in the bacterial adhesion tests.

Materials	Description	Manufacturer
Cast Co-Cr	Cast and polished Co-Cr alloy	Bego
DLMS Co-Cr	Direct laser metal soldered and polished Co-Cr alloy	Bego
Titanium	Titanium grade V machined and polished	Klockner
Zirconia	Y-TZP disks	Dentisel
FRC	E-glass FRC	Bioloren
PEEK	Polyetheretherketone	Tekniimplant

4.1.1.1 Cast cobalt-chromium disks

Acrylic resin (pattern resin® LS, GC Corp.) disks of the desired final shape were fabricated and casted by induction (Ducatron Série 3 UGIN'Dentaire. Seyssins. France) using Co-Cr (Wirobond C® alloy, BEGO, Bremer Goldschlägerei Wilh. Herbst GmbH & Co. KG, Bremen, Germany). After casting, the sprues were eliminated with the aid of carbide discs at low speed. The castings were sandblasted with 110-μm aluminum oxide particles (Korox®, Bego, Bremen, Germany) under 3 bar pressure to remove oxide films and residual investment. Care was taken not to damage the disks' surfaces.

4.1.1.2 DLMS cobalt-chromium disks

The disk shaped specimens were designed in a 3D software package and saved in an industry standard stereolithography (STL) format. The standard DLMS (direct laser metal soldering) manufacturing method by EOSINT M 270 (EOSINT 270 GmbH Electro Optical Systems, Munich,Germany) was used to fabricate the disks.

Both the cast and the DLMS Co-Cr disks were polished in three stages: (a) using a hard rubber disk at 15,000 rpm; (b) then with a soft rubber disk at 15,000 rpm, and finally (c) using a soft brush with a polishing paste at 1400 rpm. Each polishing phase lasted 90 seconds.

4.1.1.3 Titanium disks

Machined and polished titanium grade V disks were provided by Klockner® (Klockner-Soadco S.L., Andorra).

4.1.1.4 Zirconia disks

Zirconia (Y-TZP) disks were supplied by Dentisel (Dentisel S.L., Barcelona, Spain).

4.1.1.5 FRC disks

E-glass FRC disks, prepared from rods, were provided by Bioloren® (Bioloren, S.r.L, Saronno, Varese, Italy).

4.1.1.6 PEEK disks

Polyetheretherketone (PEEK) disks were obtained from rods and were supplied by Tekniimplant® (Tekniimplant S.L., Barcelona, Spain).

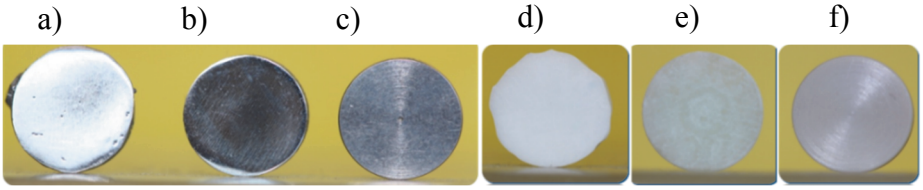

Figure 15: Representative images of the tested materials: a) cast Co-Cr; b) DLMS Co-Cr; c)titanium; d) zirconia; e) FRC and f) PEEK.

4.1.2 Surface characterization

4.1.2.1 Atomic Force Microscopy

Atomic Force Microscope XE-70 (Park Systems, Korea) imaging was carried out in a non-contact mode. The rectangular-shaped silicon cantilever tip (ACTA Si-cantilevers, Park Systems, Korea) with a force constant of 40 of ± N/m, a resonance frequency of ± 300 kHz, and a tip radius with a curvature of < 10 nm was used. Images were simultaneously acquired with scan areas of 5 × 5 μm², at a scan rate of 0.6 Hz. and a resolution of 256 × 256 pixels. The acquired data during the surface scanning were converted into 4 types of images: topography, signal, amplitude and phase (4 images of each type thus, 16 images in total for each disc) and analysed using XEI software (Park Systems, Korea). Topography images were levelled to order 1 and representative roughness parameters S_{min}, S_{max}, S_{mid}, S_{mean}, S_{pv}, S_q, S_a, S_z, S_{sk} and S_{ku} (Dong *et al.,* 1994) described in Table 2 were obtained.

4.1.2.2 White light interferometry

Specimens were scanned on a white light interferometer microscope (LeicaSCAN DCM3D, Leica Microsystems, Switzerland), with a Mirau-interferometer objective lens (Leica N Plan H 50×/0.50) and an image resolution of 250.64 × 190.90 μm². The Leica map DCM 3D, version 6.2.6561 image processor (Leica Microsystems, Switzerland) was used to analyze the images with a the threshold value of 1.0% and a Gaussian filter of 25 μm. Images and R_p ,R_v, R_z, R_t, R_a, R_q S_a, S_z, S_q (Dong *et al.,* 1994) roughness parameters (Table 2) were acquired.

4.1.2.3 Contact angle measurements

Surface wettability measurements were conducted by measuring the equilibrium contact angles using the sessile drop method (Truong *et al.,* 2010; Gittens *et al.,* 2013). A drop of 10 μl of MilliQ water quality was dropped onto the centre of each specimen using an injector and digital photographs were taken (Nikon D70). Afterwards, the images were analyzed using IMAT software (CCIT, Barcelona, Spain) and external contact angle values θ_{left} and θ_{right} (Table 2) were obtained.

Table 2: List of parameters analyzed in the present study (Dong et al., 1994).

Technique	Parameter	Symbol	Definition
AFM	Surface	S_{min}	Minimum height
		S_{max}	Maximum height
		S_{mid}	Median height
		S_{mean}	Mean height
		S_{pv}	Peak to valley height
		S_a	Arithmetic mean
		S_q	Ten point height
		S_z	Maximum height
		S_{sk}	Skeweness
		S_{ku}	Kurtosis
WLI	Surface	S_a	Arithmetic mean heigh
		S_z	Ten point height
		S_q	Root-mean-square deviation
	Profile	R_p	Maximum peak height
		R_v	Maximum valley depth
		R_z	Ten point height
		R_t	Total height
		R_a	Arithmetic mean deviation
		R_q	Root-mean-square
Sessile drop	Contact angle	θ_{left}	Left contact angle
		θ_{right}	Right contact angle

4.1.3 Surface parameter selection

The nanoroughness parameters acquired by AFM, microroughness parameters obtained by WLI and water angle contact values obtained by the sessile drop method were statistically correlated compared in order to assess which parameter provides the best optimum surface characterization method. SPSS 21.0 (Version 21.0; SPSS. Inc, Chicago, Illinois) was utilized for data analysis.

4.1.3.1 Descriptive analysis

The median, maximum and minimum were computed for each surface parameter and represented in Box-plot Figures.

4.1.3.2 Statistical analysis

Statistical analysis was performed with Statistical Package for the Social Sciences (Version 21.0; SPSS. Inc, Chicago, Illinois). First the Kruskall-Wallis adjustment was applied in order to evaluate the effects of surface parameters among the different samples of pairs of materials. Subsequently, in order to identify how many or where did the differences occur, the Mann–Whitney U-test tests was performed with the Bonferroni correction according to the number of tests performed.

In addition, for each roughness parameter, Spearman´s correlation coefficient with every other roughness parameter was calculated. To seek the correlations and the effective parameters, correlations among nanoroughness parameters, microroughness parameters and wettability data were performed. Coefficient values of "0.80-1.0" were considered as highly correlated for data interpretation. A 5% of alfa error with an interval estimate of 95% confidence level was considered for contrasting hypothesis.

4.1.4 Bacterial adhesion tests

The adhesion of two bacterial strains was tested on the six different substrates (n=16). The tested materials (substrates) were: Cast Co-Cr, DLMS Co-Cr, titanium grade V, zirconia, FRC and PEEK.

4.1.4.1 Adhesion experiments

Prior to bacterial tests, disks were sterilized in an autoclave for 15 min at 121ºC at 0.1 MPa pressure. A Gram-negative bacterium *Escherichia coli* ATCC 25922 and a Gram-positive bacterium *Staphylococcus aureus* ATCC 28213 were used in adhesion experiments. They were obtained from the American Type Culture Collection (ATCC, USA). First fresh bacterial suspensions were prepared for each strain, grown overnight in 100 mL of Triptic Soy Broth and incubated at 37ºC with shaking (120 rpm). The cell density of each strain was adjusted to $OD_{600nm} = 0.3$ (Ivanova *et al*., 2010; Truong *et al*., 2010) by using a spectrophotomer to obtain suspensions with a similar number of cells.

Incubation of the bacterial cultures was carried out as follows: aliquots of 100 mL of a bacterial suspension of 1×10^6 colony forming units/ml (CFU/ml) were used to submerge the discs and incubated for 2 and 24 hours. After incubation, the discs were washed four times in Ringer's ¼ to remove unattached bacteria and then placed in test tubes containing 1 ml of Ringer ¼. In order to detach the surface-attached bacteria, tubes were ultrasonically treated for 3 min, vigorously vortexed for 1 min, and then sonicated again for 3 min. Serial dilutions (10^0 - 10^{-7}) of these suspensions were used to inoculate agar plates, which were incubated for 48 hours. Colonies were then scored and counted.

4.1.4.2 AFM imaging

Following incubation discs were washed four-fold by using Ringer ¼ and allowed to dry in air at room temperature. Samples were imaged in air by using a non-contact mode Atomic Force Microscope XE-70 (Park Systems, Korea) using rectangular-shaped silicon cantilevers with a spring constant of ± 40 N/m and a resonance frequency of ± 300 kHz. The images were simultaneously acquired with scan size of 25 μm^2 at a scan rate of 0.6 Hz. The acquired data during the surface scanning were converted into images of topography, signal, amplitude, and phase; and analysed by using XEP and XEI software (Park Systems, Korea).

4.2 Mechanical tests

The materials used for the mechanical loading test are listed in Table 3.

Table 3: Materials used in the mechanical tests.

Product	Description	Manufacture	Lot no.	Composition
***E-glass fiber**	Unidirectional fiber bundle	Ahlstrom, Karhula, Finland	11372313	55% SiO_2, 15% Al_2O_3, 22% CaO, 6% B_2O_3, 0.5%MgO, and >1.0% Fe + Na + K
	Bidirectional weave plane fiber		240299	
Stick Resin	Light curing resin	Stick Tech, Turku, Finland	54031672	BisGMA-** TEGDMA*** (50-50%)

* E-glass, electrical glass
** Bis-GMA, bisphenol A-glycidyl- dimethacrylate
*** TEGDMA, triethylenglycol-dimethacrylate

4.2.1 Flexural test

4.2.1.1 Experimental groups

Unidirectional and bidirectional (4mm Ø, 66mm length) FRC rods (n = 9) were prepared for three-point bending tests.

4.2.1.1.1 Preparation of the unidirectional rods

The specimens were manufactured by collecting 8 bundles. Each bundle consisted of 2.400 continuous unidirectional silanized E-glass fibers of 15 µm diameter approximately. The final fiber bundle was manually pre-impregnated for 48h in light by light-polymerizable BisGMA-TEGDMA (50-50%) resin in an incubator at 37ºC (D 06062, Modell600, Memmert GmbH + Co.KG, Schwabach, Deutschland). Cylindrical unidirectional rods (n = 9) were fabricated by pulling the fiber bundles through a special cylindrical mold with an opening diameter of 4.2 mm (Adbulmajeed *et al*., 2011a).

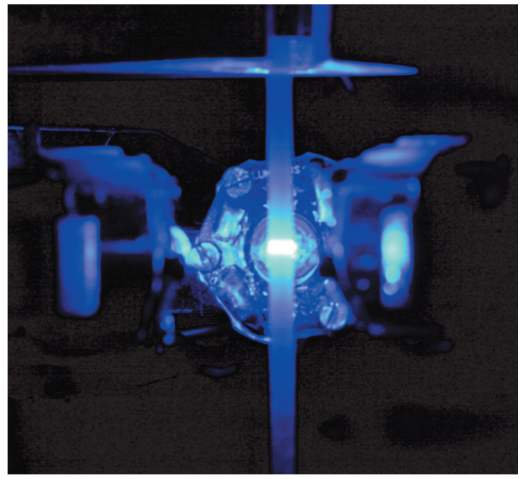

Figure 16: Fabrication of the unidirectional FRC specimens.

4.2.1.1.2 Preparation of the bidirectional rods

Bidirectional weave plane fiber FRC net (130 mm) was pre-impregnated with light-polymerizable BisGMA-TEGDMA (50-50%) resin and incubated for 48h in an incubator at 37ºC before polymerization (D 06062, Modell 600, Memmert GmbH + Co.KG, Schwabach, Deutschland). Cylindrical bidirectional rods concentrically orientated (n = 9) were manually prepared by a rolling technique.

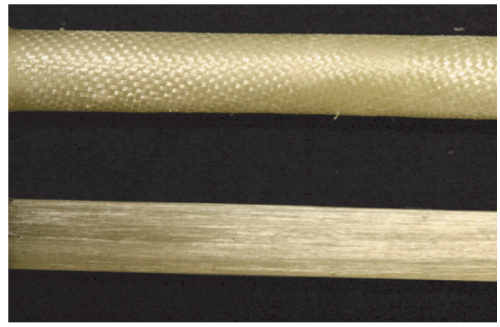

Figure 17: Rod-shaped bidirectional and unidirectional FRC specimens.

4.2.1.1.3 Polymerization condition

The substrates were photopolimerized for 2 min per side (Elipar S10, 3M Espe, Seefeld, Germany). The irradiance was 950 mW/cm^2 measured using a curing radiometer. Consequently, the polymerization was pursued for 25 min in a light curing oven (Targis Power, Ivoclar, Schann, Liechtenstein), whereby the temperature was increased up to 90ºC. In order to optimize the degree of monomer conversion (CD%) the substrates were post-polymerized for 24 hours in hot-air oven at 120ºC (Adbulmajeed *et al*., 2011a).

4.2.1.2 Three-point bending test

The cantilever bending test was performed to measure the flexural properties of the specimens. Specimens were tested with a universal testing device (LR 30K plus, Lloyd, Sussex, UK) adapted to ISO 10477:92 standards (test span 5 0mm, crosshead speed 5.0 mm/min, indenter 2 mm diameter). Thus, specimens were placed 50 mm apart and the force applying tip in the middle of the two supports. The device was set at a crosshead speed of 5.0 mm/min., and the stress-strain curves were recorded and analyzed with a PC-computer program (Nexygen, Lloyd Instruments Ltd., Fareham, England). The flexural modulus, fracture toughness, flexural strength and load-bearing capacity were determined.

4.2.2 Load-bearing capacity under static load

4.2.2.1 Experimental groups

The materials used for the fabrication of FRC specimens are listed in Table 3. Four different experimental FRC groups of one-piece implants and abutments in addition to two control groups were included (n = 6), as follows:

- **one-piece unidirectional FRC implant** obtained from unidirectional rods (as described previously) and prepared by CAD-CAM.
- **one-piece bidirectional FRC implant** obtained from bidirectional rods (as described previously) and prepared by CAD-CAM.
- **unidirectional FRC abutment** obtained from bidirectional rods (as described previously), prepared by CAD-CAM and screwed onto MIS implants (size 3.75/11.5 Lance, MIS™, Israel).
- **bidirectional FRC abutment** obtained from bidirectional rods (as described previously) , prepared by CAD-CAM and screwed onto MIS implants (size 3.75/11.5 Lance, MIS™, Israel).
- **custom-made zirconia abutment (control group)** Custom-made zirconia abutments (ICE Zircon translucent, Zirkonzahn GmbH, Gais, Italy) were prepared

using CAD/CAM technology (Zirkonzahn GmbH, Gais, Italy), and screwed onto to MIS implants (size 3.75/11.5 Lance, MIS™, Israel).

- **commercially available titanium abutment (control group).** External hexagonal commercially available titanium (Teknimplant, Barcelona, Spain) were screwed onto MIS implants (3.75/11.5 Lance, MIS™, Israel).

4.2.2.2 Fabrication of the abutments and one-piece implants

A commercially available titanium hexagonal abutment was shaped to a length of 7.2 mm to simulate a central incisor abutment and served as the master abutment. The master abutment was scanned (Zirkonzahn, GmbH, Gays, Italy), and 6 identical abutments of each FRC group and zirconia group were manufactured.

An external hexagonal implant (size 3.75/11.5 Lance, MIS™, Tel Aviv, Israel) was screwed onto the master abutment. This implant and abutment were scanned (Zirkonzahn, GmbH, Gays, Italy), and 6 identical one-piece unidirectional and bidirectional FRC implants were manufactured.

Table 4: Description of the implant abutment systems.

Type of connection	Abutment Material	Manufacture	Implant/Abutment interface
Screw-retained	Unidirectional FRC	CAD / CAM	FRC / Ti
	Bidirectional FRC	CAD / CAM	FRC / Ti
	Zirconia	CAD / CAM	Zr / Ti
	Titanium	Milling	Ti / Ti
One-piece	Unidirectional FRC	CAD / CAM	FRC / FRC
	Bidirectional FRC	CAD / CAM	FRC / FRC

Figure 18: Representative images of the one-piece experimental groups: left to right one-piece unidirectional FRC implant and one-piece bidirectional FRC implant.

Figure 19: Representative images of the abutments. Left to right: unidirectional FRC abutment; bidirectional FRC abutment; zirconia, and titanium.

4.2.2.3 Preparation of specimens for static loading

36 standardized acrylic holders were custom made and filled with cold curing resin (Vertex™, Vertex-Dental, B.V. Headquarters, The Netherlands). FRC and Titanium implants were placed in the holders and fixed to the resin using dual-polymerizing resin composite cement (RelyX™ Ultimate, 3M ESPE Dental, Seefeld, Germany). Following ISO 14801, the resin had a modulus of elasticity beyond 3 GPa and 3mm of implant shoulder were left uncovered to simulate bone resorption in order to replicate the worst clinical case-scenario. The abutments were fixed on their respective implants according to the manufacturer's instructions. The access holes were cleaned with ethanol (95%) and then conditioned with Scothbond™ Universal adhesive (3M, Gmbh, Neuss, Germany). Afterwards, the access holes were closed by a cotton pellet (cotton pellets, ∅ 2 mm, Roeko, Langenau, Germany) and a resin-based composite restorative filling material on top (EverX Posterior™ Stick Tech., Turku, Finland).

4.2.2.4 Load testing

After storage in ultrapure distilled water for 24h at 37.5°C, all the specimens were statically loaded. A universal testing machine (LR 30K plus, Lloyd, Sussex, UK, 1.0mm/min) was used to contact the specimen at an angle of 130º (Hjerppe *et al .,* 2011; Rosentritt *et al*., 2014), representing an average interincisal angle of people with normal

occlusion. A 0.5 mm-thick tin foil was used in between to ensure even distribution of the force during loading (Sailer *et al,*. 2009).

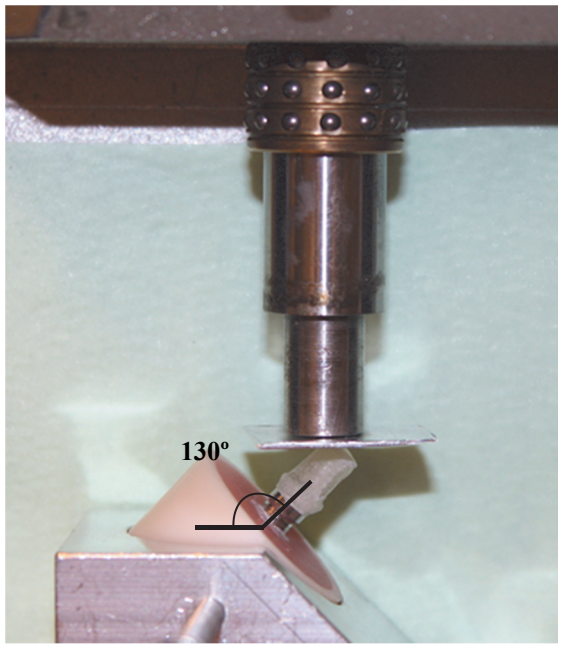

Figure 20: Loading of the abutment with a Universal testing machine at 130º.

4.2.3 Precision of fit

A scanning electron microscope (SEM) (LEO 1530 Gemini, Helmholtz Centrum, Berlin, Germany) was used to image the unidirectionally and bidirectionally reinforced fiber geometry and to measure the precision of fit of the screw-retained abutments. The abutments were cleaned ultrasonically in water for 10min, dried and screwed onto stainless steel replicas (RP implant replica Branemark Sytem®) according to the manufacturers´ recommendations. Before imaging with SEM the specimens were sputtered with gold (Bal-Tec SCD 050, Scotia, New York, USA). Magnifications of ×30, ×250 and ×1000 were carried out. The vertical misfit was measured with ×1000 magnification at 9 different locations and the mean values were reported for each abutment.

4.2.4 Statistical analysis

Statistical analysis was performed with Statistical Package for the Social Sciences (Version 21.0; SPSS. Inc, Chicago, Illinois). The distribution of data was normal, which was determined by the Kolmogorov-Smirnov test. Thus, the data were analyzed using one way analysis of variance (ANOVA) followed by Tukey's test. Differences were considered significant at 95% confidence level.

5 RESULTS AND DISCUSSION

5.1 General discussion

In vitro pre-clinical studies are necessary to introduce a newly developed material for implant abutment fabrication. Thus, the present study aimed to evaluate the use of E-glass fiber-reinforced composites (FRC) as an implant abutment material in terms of both bacterial attachment and mechanical properties. The main idea supporting the hypothesis was that FRCs have better biomechanical matching to living tissues compared to traditional implant abutment materials. Besides displaying a modulus of elasticity comparable to bone and dentin, they can be engineered to match a specific application site. Accordingly, they may reduce undesirable high stress concentration and enhance a more even stress distribution in the peri-implant tissues. The aims of the present study were of utmost interest since FRCs have recently gained interest as dental, orthopedic and cranial devices for load-bearing applications (Zhao *et al.,* 2009; Aitasalo *et al.,* 2014; Adbulmajeed *et al.,* 2015; Ballo *et al.,* 2015). Unfortunately there is a lack of studies regarding the bacterial adhesion and the mechanical properties of FRCs aimed to be used as an implant abutment material, therefore, these studies were designed to elucidate some characteristics on the potential use of FRCs in implant prosthetic dentistry.

Smooth surface textures (i.e, Sa <0.2 μm) and hydrophobic surfaces are recommended when characterizing materials for implant abutment materials. Both characteristics may prevent bacterial adhesion on biomaterials. The average roughness (S_a or R_a) is the most used parameter to measure surface roughness nevertheless; it is known that it may not always be sufficient to describe complex surface geometries. Additionally, since there is no standardized protocol for biomaterial surface characterization, an exhaustive correlation analysis of surface parameters, including roughness and wettability, was performed in order to obtain optimal surface parameters for biomaterial surface characterization. Hence, Study I aimed to characterize FRC surfaces and compare them to five widely used implant abutment materials. A further aim was to propose a set of surface parameters showing the highest discriminatory power to characterize biomaterials.

Evaluation of the bacterial adhesion is relevant since the vast majority of implant failures start with microbial colonization. Study II aimed to evaluate bacterial adhesion on FRC surfaces, and correlate with bacterial adhesion on current implant abutment materials. Thereby, the adhesion of *S. aureus* and *E. coli* on FRC surfaces was determined and related to roughness and wettability.

Following the adequate bacterial response of FRC, the mechanical properties of FRC either for an implant abutment or an oral implant application were analyzed (Study III). Fracture resistance to functional loads is one of the mechanical requirements when selecting an appropriate material for implant dentistry. Therefore, considering that the type of structure and fiber orientation have a significant influence on the mechanical properties of FRC, Study III was conducted to evaluate the load-bearing capacity of FRC abutments and one-piece FRC implants with two different types of fiber orientations (unidirectional vs. bidirectional) for oral anterior application.

5.2 Surface characterization

Results of the surface characterization (Figures 21 and 22) showed that FRC surfaces displayed the highest roughness values among the tested materials, but in the range of previous studies (Tanner *et al.,* 2003; Lassila *et al.,* 2009; Adbulmajeed *et al.,* 2014). These values were above the threshold roughness proposed by Bollen (Bollen *et al.,* 1997) suggesting that FRC surfaces could enhance bacterial adhesion and biofilm formation (Bollen *et al.,* 1997). Nevertheless, comparable FRC surfaces (Lassila *et al.,* 2009) did not harbor more bacteria compared to the most commonly used materials in restorative dentistry. On the other hand, this increased roughness could benefit the soft tissue attachment since rough abutment surfaces have shown increased fibroblast ingrowth in comparison to smooth textures (Nothdurft *et al.,* 2014).

In addition to the surface roughness, wettability plays a key role in many biological cell-substrate interactions. FRC surfaces displayed low external angles and subsequently, high internal contact angles (>90 degrees) that indicate poor wetting properties and thus, a hydrophobic caracter (Figure 23). The different wettability values obtained compared to a previous study could be attributed to the different fiber orientation (Adbulmajeed *et al.,* 2011b). In the present study fibers run perpendicular and vertical to the camera (fibers were cross-sectioned on the surface of the disks) in contrast to the previous study where fibers ran horizontal and parallel.

In general the characterization of the cast Co-Cr, DLMS Co-Cr, titanium, zirconia, and PEEK surfaces were in agreement with previous studies (Rosentritt *et al.,* 2009; Ivanova *et al.,* 2010; Adbulmajeed *et al.,* 2014; Ourahmoune *et al.,* 2014; Kim *et al.,* 2015). However, in the present study zirconia was shown to be rougher than previously analyzed zirconia (Att *et al.,* 2009). Contrary to that study, in the present study, zirconia did not undergo glazing procedures; this technique has been shown to reduce the surface roughness of zirconia (Sabrah *et al.,* 2013). In addition to this, DLMS cobalt-chrome exhibited the lowest roughness value. This finding is in agreement with previous studies that state that laser sintering procedures enhance the surfaces properties of metals compared to casting approaches (Oyagüe *et al.,* 2012; Castillo-Oyagüe *et al.,* 2013). In contrast, this finding is not in accordance with a study where the average roughness value

of DLMS cobalt-chrome was significantly higher compared to cast cobalt-chrome. The differences in chemical composition of the cobalt-chromium alloys analyzed may have affected these results (Kilicarslan & Ozcan, 2012).

Wettability values in general were also in agreement with previous studies except for zirconia which resulted to be the most hydrophilic material (highest contact angle value and thus the lowest internal angle). This may be explained by the fact that the examined surfaces were rougher than those in previous studies (Att *et al.,* 2009).

Topographical features of biomaterial surfaces are determinant in many biological cell-substrate reactions. Despite being highly relevant, there exists a lack of a standardized set of surface parameters to characterize biomaterials. One posible explanation is that there exist a large number of surface parameters in the literature which diminish the probability of identifying potential associations due to the vast variability. The present study was in accordance with previous studies that confirm that the most commonly used parameters to characterize biomaterials are redundant (Dong *et al.,* 1994; Crawford *et al.,* 2012; Webb *et al.,* 2013). Twenty-one parameters were reduced to six considering their efficiency in materials discrimination by means of correlation analysis and sensitivity testing in the differentiation between pairs of materials.

At the nanoscale (Table 8) the surface parameters showed poor correlations, nevertheless three clusters of non-correlated parameters were differentiated. The S_a-S_{max}-S_{min}-S_{pv}-S_q-S_z group displayed strong correlations, in contrast, the S_{mean}-S_{mid} and S_{sk}-S_{ku} groups were weakly correlated among themselves and with the former. Since strongly correlated parameters addressed the possibility of reducing interchangeable parameters and conversely, weak correlations pointed towards independence between parameters, a preliminary selection of surface parameters was performed. From the highly correlated group, S_a was selected to represent as shown by its superior sensitivity on the pair-wise material discrimination (Table 5). From the weakly correlated cluster of parameters, the lesser which correlated to S_a, were selected. Thus at the nanoscale the selected set of parameters was S_a,S_{ku}, and S_{mid}.

Conversely, at the microscale (Table 9) all the parameters were correlated challenging the selection of which parameter was best in surface characterization. Similarly to the nanoscale, the S_a parameter exhibited the highest sensitivity discrimination pairs of materials being therefore selected (Table 6). S_z was also selected due to the fact that it displayed the lower correlation value to S_a.

Nanoscale and microscale roughness parameters in general were not correlated (Table 10); this indicated the complementarity of these approaches. The combination of both techniques has also been previously claimed by authors aiming to overcome the limitations of each measuring device in the achievement of an efficient surface characterization (Tyrrell *et al.,* 2004; Guo *et al.,* 2011).

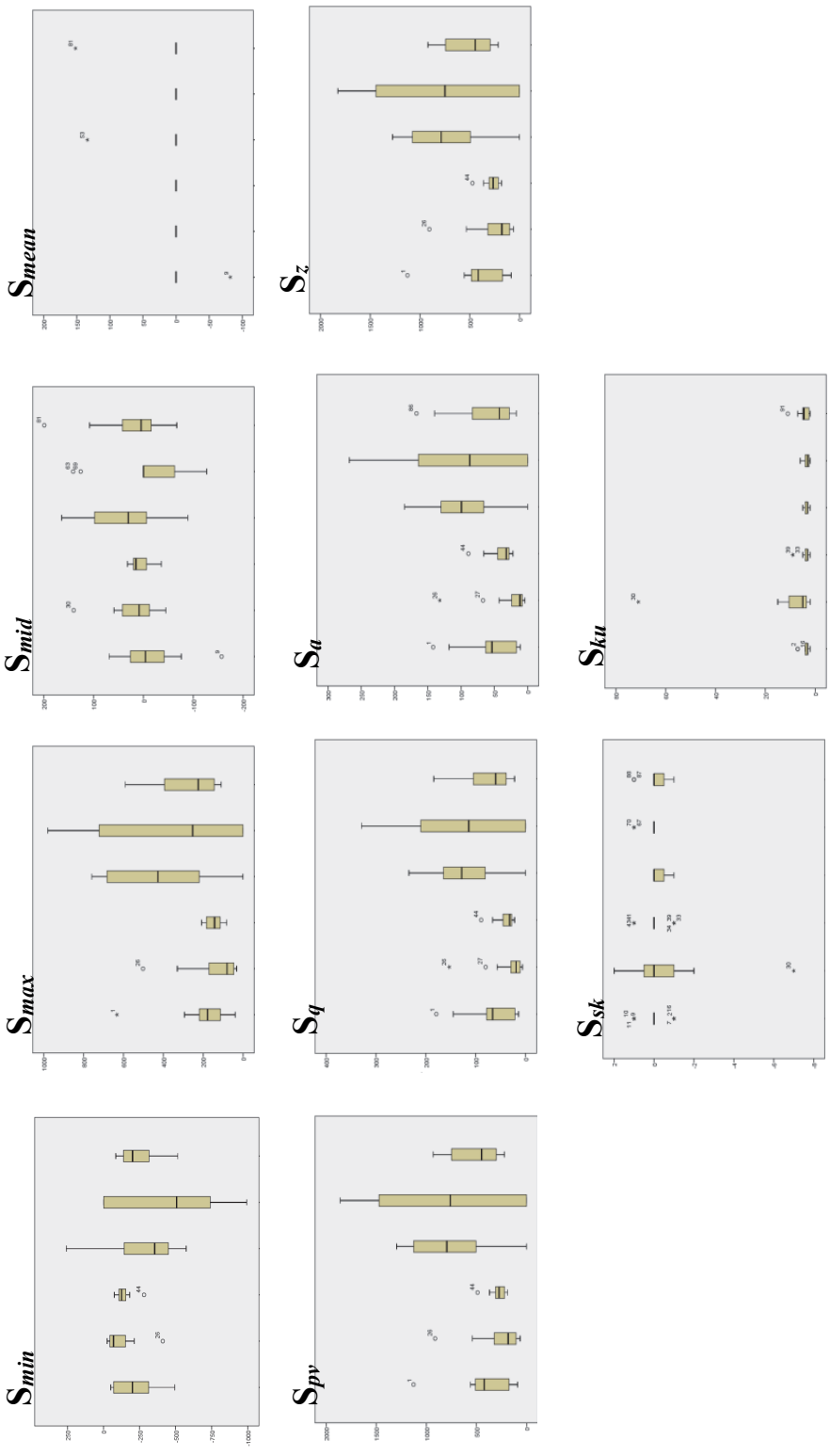

Figure 21: Box plot data of the descriptive anaysis of nanoscale roughness parameters including the median, minimum and maximum. Left to right cast Co-Cr, DLMS Co-Cr, titanium, zirconia, FRC, and PEEK.

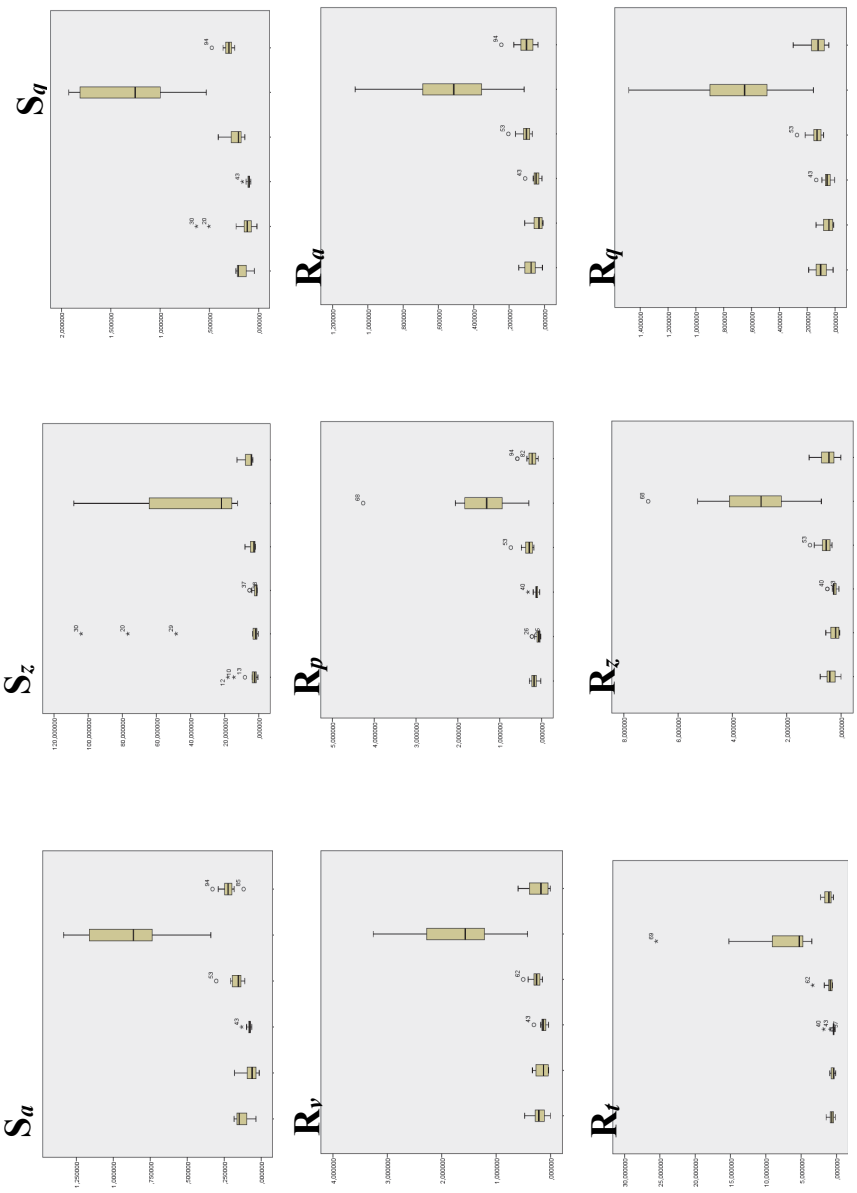

Figure 22: Box plot data of the descriptive anaysis of microscale roughness parameters including the median, minimum and maximum. Left to right cast Co-Cr, DLMS Co-Cr, titanium, zirconia, FRC, and PEEK.

Wettability values did not correlate with nanoroughness parameters whilst they poorly correlated with microroughness parameters (Tables 11 and 12). Previous studies have shown that smooth microscale surface characteristics (R_a less than 0.1 μm) have minor influence on the surface wettability of a surface (Busscher *et al*., 1994; Adbulmajeed *et al*., 2011). In those studies smooth surfaces displayed contact angles that ranged between 60º and 86º and the differences of the contact angles were related to the surface chemistry. The present study, is in agreement with those studies since all the smooth surfaces investigated (all the materials except for FRC) showed contact angle values within this given range. Accordingly, rough FRC surfaces showed a contact angles above 86º showing a similarity in the trend claimed by Wenzel (Wenzel, 1949).

S_a,S_{ku}, and S_{mid} at the nanoscale, S_a and S_z at the microscale and θ_{right} were the best parameters discriminating materials being therefore selected to represent the whole group of parameters. Thus, in Figures 24, 25 and 26 the materials are characterized according the screened parameters. The efficiency of the selected parameters is demonstrated by the fact that characterizing the materials with the proposed set agrees with early studies (Rosentritt *et al.,* 2009; Ivanova *et al.,* 2010; Adbulmajeed *et al.,* 2014; Ourahmoune *et al.,* 2014; Kim *et al.,* 2015). Hence, the adoption of this set will allow a more effective characterization of materials, in addtion to facilitating data comparisons.

Table 5: Results of Kruskal–Wallis test (p value) and Mann–Whitney U-test (number of different pairs of materials). Eficiency in discrimating pairs of materials by nanoscale roughness parameters.

	S_{min}	S_{max}	S_{mid}	S_{mean}	S_{pv}	S_a	S_q	S_z	S_{sk}	S_{ku}
Kruskal-Wallis*	0.03	0.20	0.10	0.40	0.01	0.01	0.01	0.01	0.60	0.03
Different pairs**	0	0	0	0	4	6	4	4	1	1

*Statistical significant differences $p<0.01$

**Statistical significant differences $p<0.003$

Table 6: Results of Kruskal–Wallis test (p value) and Mann–Whitney U-test (number of different pairs of materials). Eficiency in discrimating pairs of materials by microscale roughness parameters.

	S_a	S_z	S_q	R_p	R_v	R_z	R_t	R_a	R_q
Kruskal-Wallis*	<0.01	<0.01	<0.01	<0.01	<0.01	<0.01	<0.01	<0.01	<0.01
Different pairs**	11	8	8	10	7	8	9	9	9

*Statistical significant differences $p<0.01$

**Statistical significant differences $p<0.003$

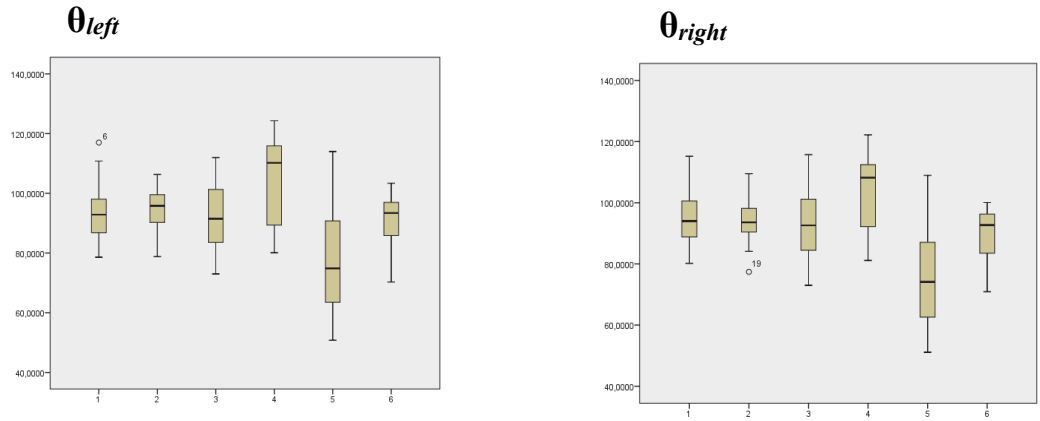

Figure 23: Box plot data of the descriptive anaysis of wettability parameters including the median, minimum and maximum. Left to right cast Co-Cr, DLMS Co-Cr, titanium, zirconia, FRC, and PEEK.

Table 7: Results of Kruskal–Wallis test (p value) and Mann–Whitney U-test (number of different pairs of materials). Eficiency in discrimating pairs of materials by wettability parameters.

	θ_{left}	θ_{right}
Kruskal-Wallis *p**	0.001	<0.01
Different pairs**	3	4

*Statistical significant differences $p<0.01$

**Statistical significant differences $p<0.00$

Table 8: Correlation matrix for nanoscale roughness parameters.

	S_{min}	S_{max}	S_{mid}	S_{mean}	S_{pv}	S_q	S_a	S_z	S_{sk}	S_{ku}
S_{min}	—	-.861**	.094	-.022	-.944**	-.919**	-.905**	-.943**	-.189	.077
S_{max}	-.861**	—	.260*	.206*	.967**	.921**	.902**	.967**	-.103	-.018
S_{mid}	.094	.260*	—	.294**	.077	.036	.035	.078	-.530**	.156
S_{mean}	-.022	.206*	.294**	—	.108	.100	.107	.104	-.088	-.094
S_{pv}	-.944**	.967**	.077	.108	—	.961**	.942**	1,000**	.049	-.057
S_q	-.919**	.921**	.036	.100	.961**	—	.993**	.963**	.154	-.235*
S_a	-.905**	.902**	.035	.107	.942**	.993**	—	.943**	.167	-.270**
S_z	-.943**	.967**	.078	.104	1**	.963**	.943**	—	.052	-.060
S_{sk}	-.189	-.103	-.530**	-.088	.049	.154	.167	.052	—	-.324**

*Statistical significant differences $p<0.05$

**Statistical significant differences $p<0.01$

Table 9: Correlation matrix for microscale roughness parameters.

	S_a	S_z	S_q	R_p	R_v	R_z	R_t	R_a	R_q
S_a	—	.755**	.941**	.844**	.699**	.810**	.841**	.866**	.856**
S_z	.755**	—	.875**	.646**	.584**	.653**	.712**	.653**	.664**
S_q	.941**	.875**	—	.769**	.656**	.749**	.798**	.794**	.792**
R_p	.844**	.646**	.769**	—	.847**	.955**	.886**	.965**	.963**
R_v	.699**	.584**	.656**	.847**	—	.930**	.783**	.877**	.874**
R_z	.810**	.653**	.749**	.955**	.930**	—	.882**	.960**	.959**
R_t	.841**	.712**	.798**	.886**	.783**	.882**	—	.886**	.896**
R_a	.866**	.653**	.794**	.965**	.877**	.960**	.886**	—	.989**
R_q	.856**	.664**	.792**	.963**	.874**	.959**	.896**	.989**	—

*Statistical significant differences $p<0.05$

**Statistical significant differences $p<0.01$

Table 10: Correlation matrix for nanoscale and microscale roughness parameters.

	S_a	S_z	S_q	R_p	R_v	R_z	R_t	R_a	R_q
S_{min}	-0.31**	-0.21	-0.25*	-0.27**	-0.18	-0.25*	-0.19	-0.28**	-0.27**
S_{max}	0.23*	0.15	0.23*	0.23*	0.17	0.21*	0.16	0.23*	0.22*
S_{mid}	-0.15	-0.16	-0.10	-0.04	-0.03	-0.04	-0.07	-0.07	-0.07
S_{mean}	0.06	0.03	0.06	0.04	0.03	0.04	0.15	0.03	0.03
S_{pv}	0.29**	0.20	0.27**	0.27**	0.19	0.25*	0.20	0.28**	0.27*
S_q	0.25*	0.14	0.21*	0.24*	0.16	0.20	0.19	0.23*	0.22*
S_a	0.21	0.09	0.16	0.21*	0.13	0.17	0.16	0.20	0.19
S_z	0.29**	0.19	0.27**	0.28**	0.19	0.25*	0.20	0.28**	0.27*
S_{sk}	0.07	0.09	0.02	0.06	0.10	0.07	0.16	0.07	0.08
S_{ku}	-0.24*	-0.02	-0.15	-0.17	-0.12	-0.09	-0.20	-0.15	-0.13

*Statistical significant differences $p<0.05$

**Statistical significant differences $p<0.01$

Table 11: Correlation matrix for wettability and nanoscale roughness parameters.

	S_{min}	S_{max}	S_{mid}	S_{mean}	S_{pv}	S_q	S_a	S_z	S_{sk}	S_{ku}	θ_{left}
θ_{left}	0.06	-0.06	-0.11	-0.08	-0.05	-0.05	-0.06	-0.04	-0.02	0.02	
θ_{right}	0.05	-0.05	-0.08	-0.08	-0.04	-0.04	-0.04	-0.04	0.03	0.03	0.97**

*Statistical significant differences $p<0.05$

**Statistical significant differences $p<0.01$

Table 12: Correlation matrix for wettability and microscale roughness parameters.

	S_a	S_z	S_q	R_p	R_v	R_z	R_t	R_a	R_q	θ_{left}
θ_{left}	-0.22*	-0.19	-0.21*	-0.18	-0.25*	-0.24*	-0.28**	-0.22**	-0.22**	
θ_{right}	-0.26*	-0.23*	-0.26*	-0.19	-0.25*	-0.25	-0.29*	-0.24*	-0.24*	0.97**

*Statistical significant differences $p<0.05$

**Statistical significant differences $p<0.01$

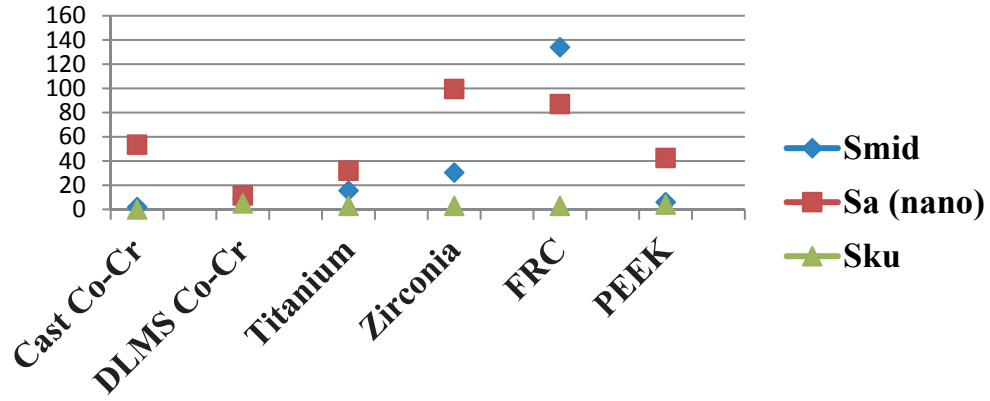

Figure 24: Characterization of the materials according to the selected nanoscale parameters.

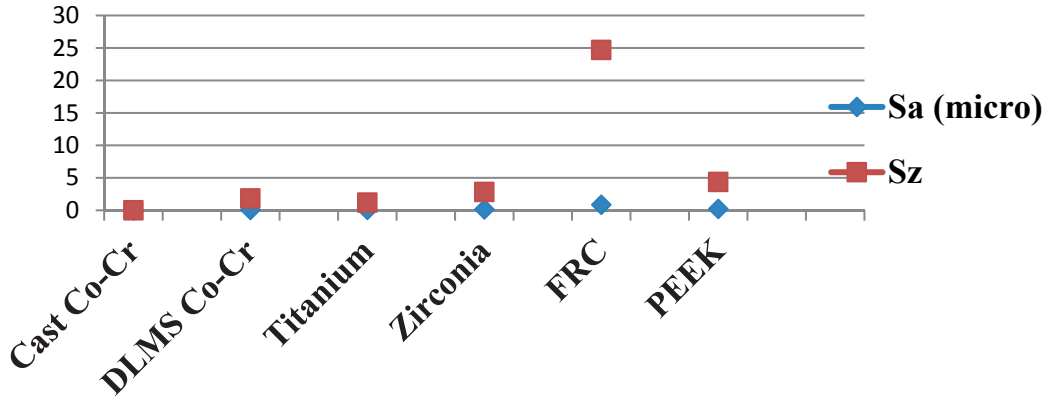

Figure 25: Characterization of the materials according to the selected microscale parameters.

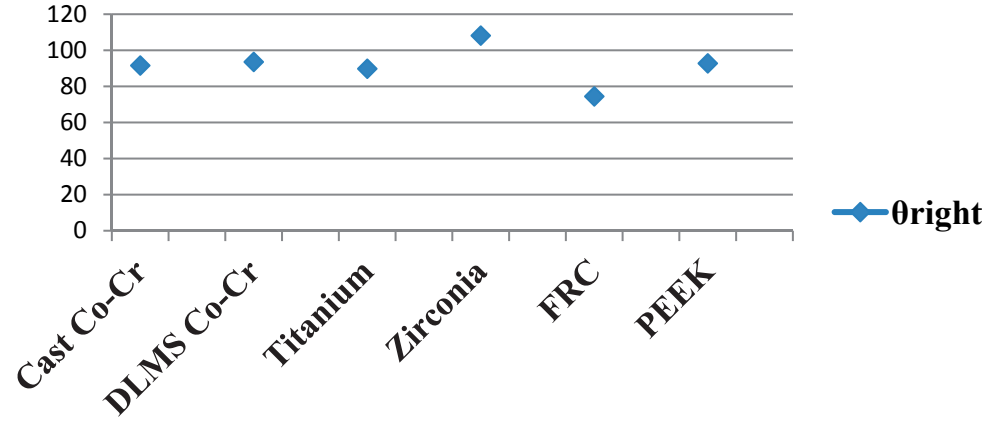

Figure 26: Characterization of the materials according to the selected wettability parameter.

5.3 Bacterial adhesion to FRC

The role of implant abutment surfaces has acquired increasing interest in in implant dentistry owing to its intimate connection to the peri-implant gingival tissues and thus, of utmost relevance in implant health preservation. Considering that biofilm formation on abutment surfaces, if not removed, creates a basis for future peri-implantitis, it is desirable that a material for implant abutment fabrication features low bacterial adhesion. The present findings are in agreement with previous studies which show that FRC surfaces feature adequate bacterial response (Tanner *et al.,* 2005; Lassila *et al.,* 2009). Thus, it can be postulated that the use of FRC does not increase the microbial adhesion.

It has been reported that the chemical composition and surface properties of biomaterials including roughness, nanoroughness, and wettability are determining factors in bacterial adhesion (Subramani *et al.,* 2009; Ivanova *et al.,* 2010). With increasing roughness, larger areas and retentive locations for bacterial adhesion are created. In addition to this, water adsorption is the initial event when a surface is first in contact with biologic environment (Kasemo, 2002) and the more or less hydrophilic/phobic characters of a surface determines the subsequent biologic processes, i.e. extracellular matrix adsorption (Anselme, 2000; Kasemo, 2002). Owing to the fact that in Study I the average surface value resulted to be the best parameter in the material discrimination at the nano and microscale, S_a was selected to characterize the materials. Therefore in the present study the average roughness at both scales (Figures 27 and 28) in addition to wettability value data (Figure 29) were correlated to bacterial adhesion (Figures 30 and 31).

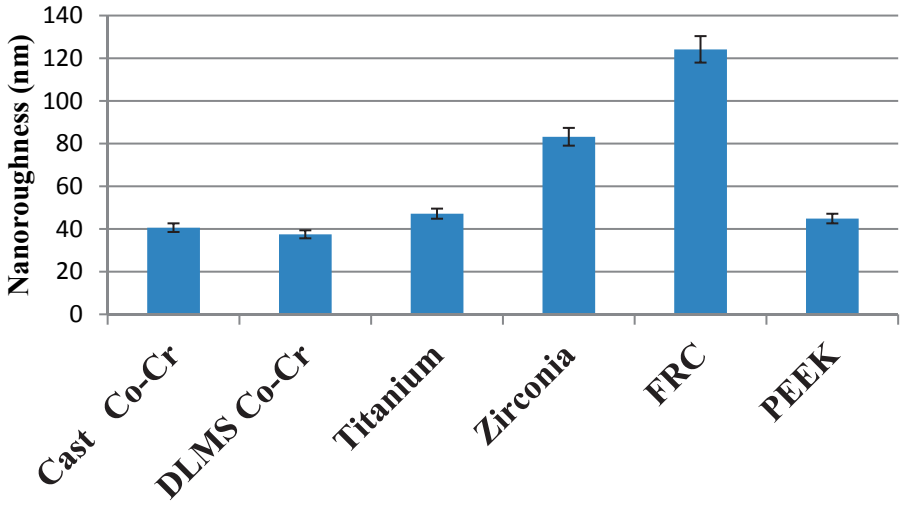

Figure 27: Median average roughness (S_a) and standard deviations of the experimental groups measured by AFM.

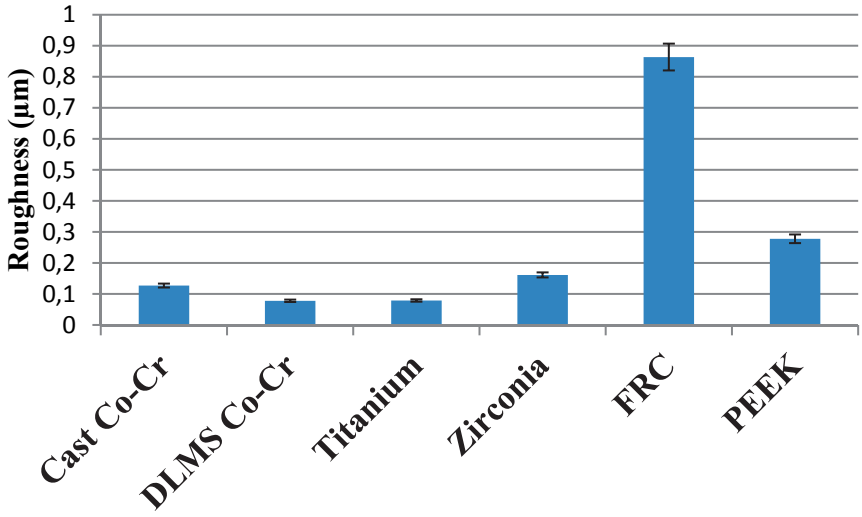

Figure 28: Median average roughness (S_a) and standard deviations of the experimental groups measured by WLI.

Figure 29 shows the average contact angle values obtained from the surfaces investigated. A high contact angle (>90 degrees) is an indication of poor wetting properties and thus hydrophobic character. On the contrary, a low contact angle addresses the enhanced wetting property and thus the hydrophilic character (O'Brien, 1997). The results show that FRC are hydrophobic materials that show poor wettability properties.

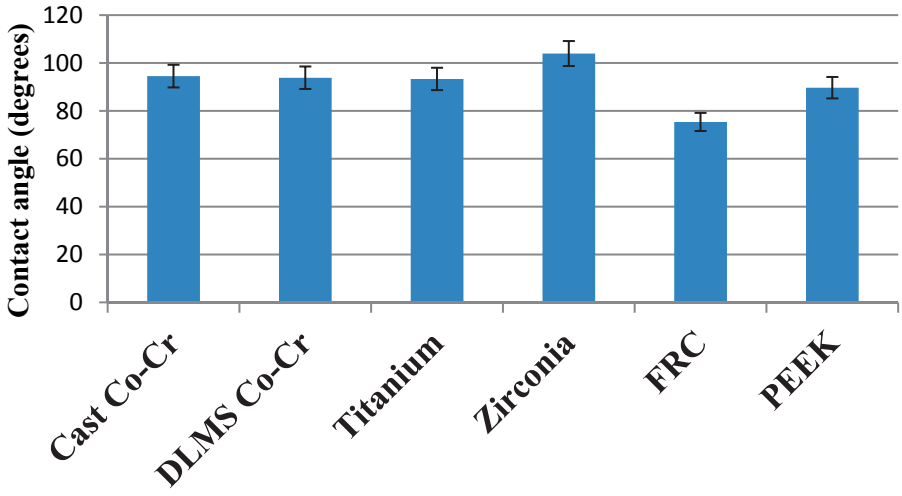

Figure 29: Mean contact angle values of the experimental group measured by the sessile drop method.

S. aureus has been shown to be a major contributor to implant related infections (Leonhardt *et al.,* 2003; Tortora *et al.,* 2004; Mombelli & Decaillet 2011). In addition to the Gram positive *S. aureus*, the Gram negative *E. coli* has been widely studied in the evaluation of biofilm formation on biomaterials (Mitik Dineva *et al.,* 2009; Ivanova *et al.,* 2010; Juan *et al.,* 2010; Zhang *et al.,* 2013); both species are generally used as models. Thus, the adhesion of *S. aureus* and *E. coli* was assessed at 2 and 24 hours of contact. Figure 30 shows the results of bacterial adhesion of both species after 2 hours of contact. Bacterial populations are expressed as colony-forming units (CFU/mm^2) obtained by the calculation of the average value of 16 measurements.

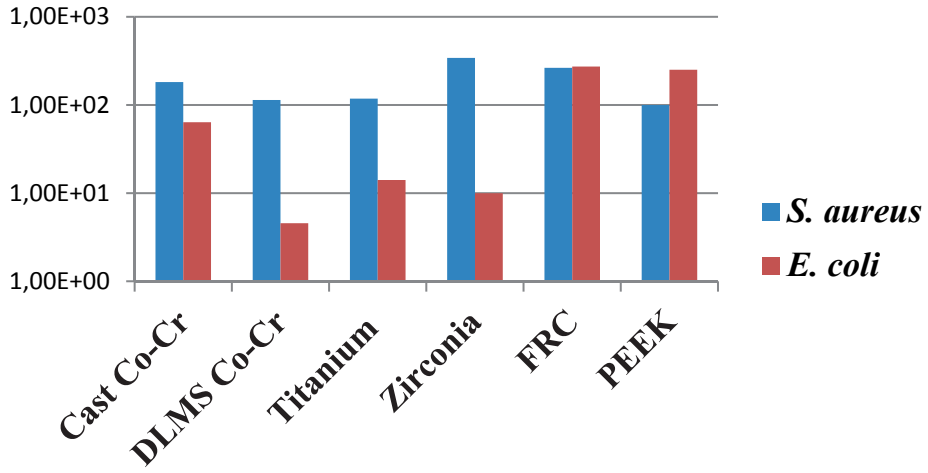

Figure 30: Bacterial adhesion after 2 hours of contact expressed as colony-forming units (CFU/mm^2).

The present data show that the initial biofilm formation is affected by the surface roughness. Subsequently, after two hours of contact, the smoothest surface (DLMS Co-Cr) featured the lowest bacterial counts while the roughest (FRC) displayed an opposite behavior. In this early adhesion stage, as expected, the "early colonizer" *S. aureus* was found in higher proportions. These differences in the binding behavior of the two species is in agreement with the ''attachment point'' theory which states that different microorganisms morphologies (i.e. spherical-cocci and rod-shaped bacili) exhibit different attachment patterns (Advincula *et al.,* 2007). Additionally, at this stage the previously stated threshold value of R_a 0.2 µm claimed by Bollen was confirmed (Bollen *et al.,* 1997). Amoroso et al. reported that this threshold value is related to the minimum bacterial size. They claimed that since most bacteria are larger in size, lower roughness values may not promote bacterial adhesion (Amoroso *et al.,* 2006).

Conversely, after 24 hours of contact (Figure 31) no differences were found in the numbers of bacteria adhered to FRC over the rest of the analyzed surfaces.

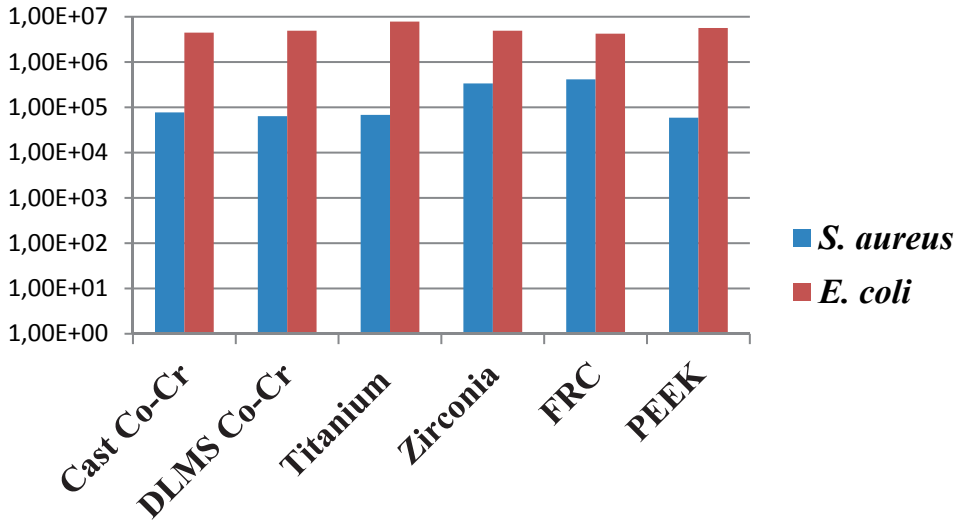

Figure 31: Bacterial adhesion after 24 hours of contact expressed as colony-forming units (CFU/mm^2).

Hence, according to these results it can be hypothesized that wettability is a major factor in microbial adhesion to FRC. The poor wettability characteristic shown by FRC surfaces may explain their adequate bacterial performance; despite being the roughest materials they showed the lowest hydrophilic properties. The present study like the presvious study of Lassila et al., observed that low-surface free contact angles which are an indication of high water contact angles (Duncan-Hewitt, 1990) resulted to be a major factor governing bacterial adhesion on E-glass FRC compared to roughness. Furthermore previous *in vivo* and *in vitro* studies have shown that bacterial adhesion to FRC resembles restorative composite, which nowadays is widely accepted (Tanner *et al.,* 2000; Lassila *et al.,* 2009). One explanation can be the similar composition organic polymer matrix (dimetacrilate monomer systems) and inorganic filler particles.

The present study is in agreement with previous *in vitro* and *in vivo* studies were the early bacterial adhesion was influenced by physic-chemical characteristics of the tested materials (Mitik Dineva *et al.,* 2009) nevertheless, on the later, mature biofilm compensated this differences (de Oliveira *et al.,* 2012; do Nascimento et al., 2013; Nascimento *et al*., 2014). This is in relatively disagreement with other authors (Bürgers *et al.,* 2010a; Bürgers *et al.,* 2010b). According to their results the adhesion and biofilm forming activity of *Candida albicans* on titanium surfaces strongly depend upon wettability and roughness seemed to play a secondary role. Contrary to this, when measuring the initial adhesion of *Streptococcus sobrinus* to differently textured titanium surfaces, they found it was primarily influenced by the roughness whereas the influence of wettability seemed to be of only minor importance. Subsequently it seems that significant differences can be expected when using different microbial species and

moreover Bürgers´ studies compared differently polished titanium and not different materials.

AFM imaging of the cultured bacteria, confirmed that FRC substrates do not provide good environmental conditions for bacterial growth. The large amount of exopolysaccharide can be clearly observed from micrographs which indicate a low rate of growth.

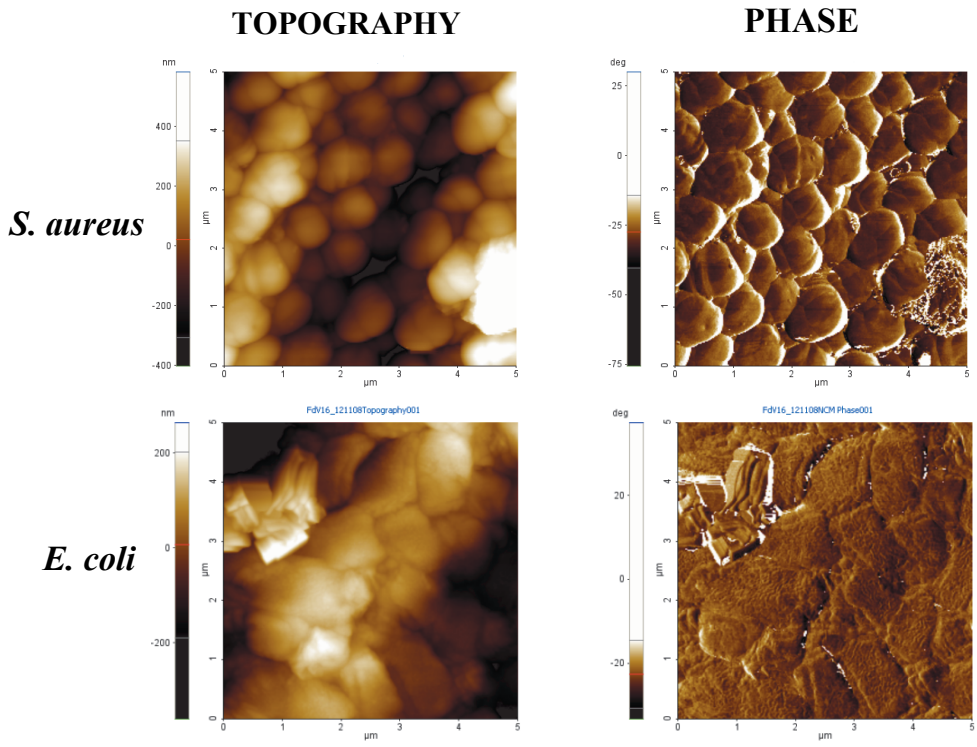

Figure 32: AFM topography and phase images on FRC substrates.

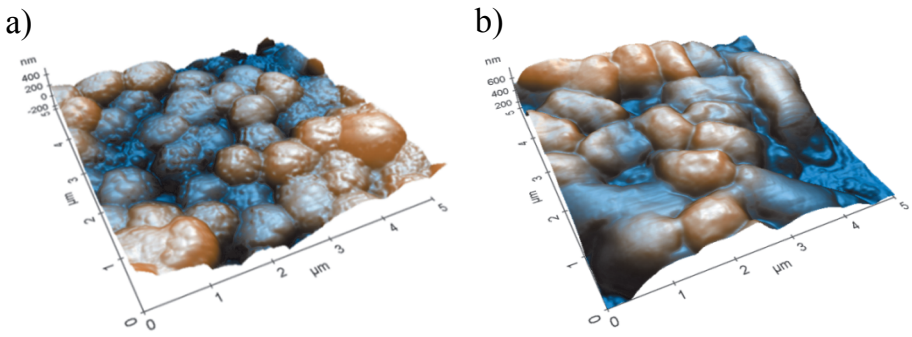

Figure 33: 3D bacteria adhesion images on FRC substrates obtained by AFM: a) *S. aureus* and b) *E. coli*.

Research on nanotechnology is gaining interest. Because bacteria are measured on the nanoscale (< 1μm), molecular and cellular events occur on the nanoscale. On the other hand, human gingival fibroblasts responsible for establishing the transmucosal connections between the oral environment and the underlying tissues are measured in micrometers. Because of this, the exploration of the surfaces where these biological reactions occur (bacterial adhesion and fibroblast attachment), are important when analyzing biomaterial surfaces. The present study also confirmed the role of resolution in scanning, as shown by the observed differences in the order of the materials according to their roughness values. For example, zirconia was rougher when analyzed by AFM than WLI.

Nanoengineered surfaces can modulate molecular and cellular events and subsequently, cell adhesion and proliferation predicting the overall biological response (Variola *et al.,* 2011). FRC surfaces allow the creation of a surface coating as in the case of lactose-modified chitosan (Chitlac) that can be bonded to BisGMA-TEGDMA resin polymer (Nganga *et al.,* 2013). In line with these thoughts, various in vitro studies have shown excellent antibacterial properties against *Staphylococcus aureus* and *Pseudomonas aeruginosa* when adding silver-polysaccharide silver nanoparticles coatings on FRC surfaces (Nganga *et al.,* 2013; Nganga *et al.,* 2014).

As the oral biofilm formation is a very complex process, it is clear that the results gathered inthis study cannot be completely transferred to the clinical performance of a biomaterial. Nevertheless, *Staphylococcus aureus* and *Escherichia coli* reflect two major types of biological and chemical organizations of the bacterial surface. Although our results cannot be mechanistically extended to all microbes, large differences with other oral pathogens are not expected.

5.4 Mechanical properties

Bidirectionally reinforced FRC abutments and one-piece FRC implants carry the potential to be used as alternative implant materials as shown by their high load-bearing capacity and enhanced ability to withstand breakage compared to those unidirectionally reinforced. Previously, one study evaluated the load-bearing capacity of FRC abutments, however, only unidirectional fibers were analyzed (Behr *et al.,* 2001). Therefore the present study is first in reporting the load bearing capacity of FRC abutments and implants with different types of fiber orientation. Furthermore the mode of failure and precision of fit were evaluated.

Three-point bending test was used to determine the mechanical properties of the two types of experimental FRC groups. Data is presented in Table 13.

Table 13: Comparison of the mechanical properties of one-piece unidirectional FRC with bidirectional FRC rods

	Unidirectional FRC	**Bidirectional FRC**
Flexural Strength (MPa)	1082.1 ± 174.5*	417.8 ± 82.2*
Flexural modulus (GPa)	34.7 ± 7.8*	14.8 ± 4.2*
Toughness (MPa)	1.1 ± 0.28	0.71 ± 0.17
Load-bearing capacity (N)	495.8 ± 48*	223.2 ± 54.8*

*p value <0.0001

Bidirectional FRC rods as expected, had inferior values compared to unidirectional FRC rods (Krenchel, 1964; Moritz *et al.,* 2014). The mode of failure of FRC rods under flexion has been described as complex. Under tension, load beams can fail either longitudinally or transversely and show shear failure within the matrix, the fiber-matrix interface or within the fiber (Issac, 1999). None of the rods failed catastrophically besides bidirectional FRC rods showed a greater ability to withstand breakage (Figure 34) since they prevented the characteristic interlaminar shear failure exhibited by unidirectional rods (Behr *et al.,* 2000; Abdulmajeed *et al.,* 2011a).

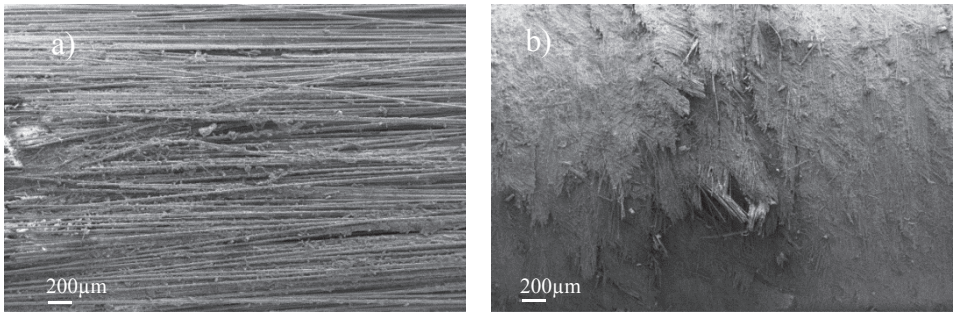

Figure 34: In the process of FRC fracture, unidirectional fibers (a) displayed intralaminar shear failure (delamination) due to the tension failures in the resin layers while, bidirectional fibers, (b) showed bending and fiber pull-out. This can be explained by the capacity of bidirectional fibers bridging the cracks in the resin providing resistance to crack propagation and crack opening before fiber pull-out.

Nevertheless, both groups displayed a elastic modulus similar to cortical bone and dentin and adequate strength that acknowledge them for load bearing applications such as abutments and implants in the oral anterior region (Brunski & Skalak, 1998; Black & Hastings 1998; Ritchie, 2009).

Load-bearing capacity under functional loading is a prerequisite for a material aimed to be used as an oral material. Therefore, the ISO 14801 test was performed (Hjerppe *et al.,* 2011; Rosentritt *et al.*, 2014). Accordingly the following testing conditions were adapted: (1) Implants were embedded in a resin with an elastic modulus similar to natural bone; (2) The implant shoulder was left uncovered to reproduce 3mm of bone resorption.

Furthermore to simulate the average interincisal angle (Hjerppe *et al.,* 2011; Rosentritt *et al.*, 2014) load was directed to contact the specimen at an angle of 130º. Load-bearing capacity data and standart deviations of the experimental group is presented in Table 14.

Table 14: Mean fracture values and standart deviations (SD) of the experimental groups. Same superscript letters indicate that data are not statistically different ($p<0.001$).

Experimental groups	Mean fracture loads (N)
Unidirectional screw-retained FRC abutment	220.5 ± 24.2^{a}
Bidirectional screw-retained FRC abutment	466.2 ± 43.0^{b}
One-piece unidirectional FRC implant abutment	733.2 ± 39.1^{c}
One-piece bidirectional FRC implant abutment	746.9 ± 41.8^{c}
Custom-made zirconia abutment	687.8 ± 69.4^{c}
Commercially available titanium abutment	1260 ± 201.7^{d}

This study revealed that one-piece FRC implants exhibited mean fracture loads far beyond the maximal incisal forces and were the best among FRC groups ($p<0.001$). It is known that the mechanical properties of FRC are influenced by changing the fiber orientation (Dyer *et al.,* 2005), however the one-piece group in this study did not show this. The minor effect of different fiber orientations on the strength of one-piece implant abutments could be attributed to the properties of high fiber vol.% of the bulk FRC structure. However, bidirectional fibers showed a higher resistance to breakage since they showed bending without fracture compared to the delamination showed by unidirectional fibers (Figure 35). This is explained by the different energy transfer of the two groups. While unidirectional fibers transfer the energy longitudinally from the abutment to the implant, bidirectional fibers, show an even load distribution.

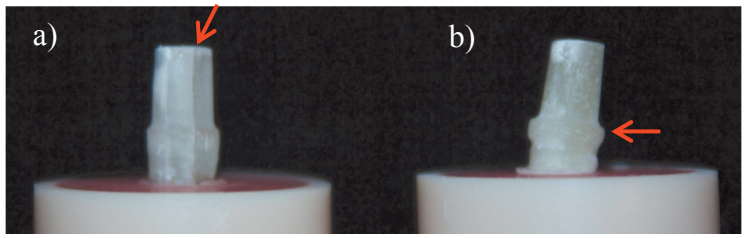

Figure 35: Representative fracture patterns of one-piece FRC implants: a) unidirectional and b) bidirectional.

Controversial results in success-rates of metallic one-piece implants have been reported. While some papers report high success rates (Parel & Schow, 2005; Hahn *et al.,* 2007) others show a significantly reduced success rates (Ostman *et al.,* 2007; Sennerby *et al.,* 2008). One possible explanation is that one-piece implants require shaping *in situ* immediatelly after implant insertion. Thus, when using metallic implants bone health can be potentially damaged owing to heat generation (Gross *et al.,* 1995; Gabay *et al.,* 2010). Unlike titanium, FRC is easy to grind and modify without heat generation. Additionally it shows osteoinductive properties when added to bioactive glass particles

(BAG). Both advantageous properties make one-piece FRC potential alternatives to metallic one-piece implants for immediate loading protocols (Ballo *et al.,* 2014).

Contrary to FRC implants, in FRC abutments the fiber structure had a significant influence on the load-bearing capacity. Unidirectional fibers failed when compressive loads where directed in the fiber direction, in contrast bidirectional fibers, provided optimal reinforcement showing fracture loads (p<0.001) above the maximum incisal forces. Similar to Behr et al.'s findings, in unidirectional FRC abutments, tensile stresses originated at the fiber-matrix interface resulted in slight reinforcement leading to catastrophic failure (Figure 36a) (Behr *et al.,* 2001). In contrast the bidirectional fibers improved the shock absorbing properties of the polymer matrix since bending failure was only observed (Figure 36b). The more flexible matrix achieved by the bidirectional reinforcement allowed abutment bending without fiber damage (e.g. delamination), transmitting the entire energy towards the screw.

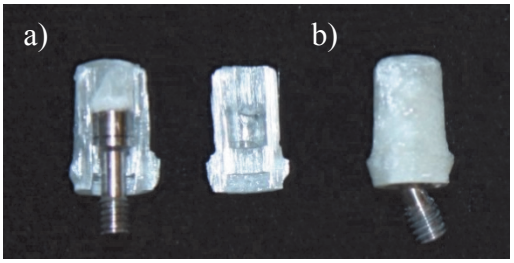

Figure 36: Representative fracture pattterns of FRC abutments: a) unidirectional and b) bidirectional.

In the present study, the load-bearing capacities of the control groups were within the range (944N for titanium and 480-831N for zirconium) of previous studies (Yildirim *et al.,* 2003; Dittmer *et al.,* 2012). Likewise, the failure modes of the control groups (i.e. zirconia and titanium) were comparable to earlier studies (Yildirim *et al.,* 2003; Dittmer *et al.,* 2012). The catastrophic failure (Figure 37a) exhibited by zirconia abutments may be explained by the reduced tolerance of zirconia to tensile loads that are generated around the screw (Tripodakis *et al.,* 1995; Att *et al.,* 2006). Titanium abutments showed plasticization of metallic components (i.e. implant hexagon- abutment hexagon) and screw bending (Figure 37b). Clinically, this leads to an undesirable scenario since it cannot be repaired and would probably require implant removal.

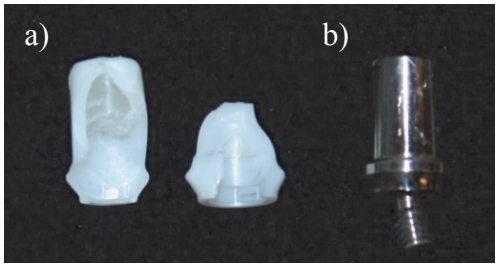

Figure 37: Representative fracture pattterns of:a) zirconia abutment and b) titanium abutment.

Scanning electron microscopy images have shown that the fiber distribution either in the multidirectional or unidirectional FRC groups corresponded with the desired geometry (Figure 38).

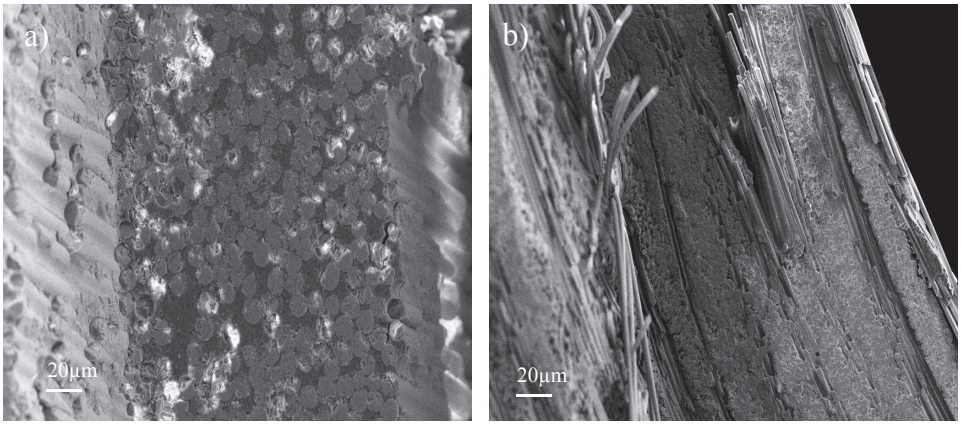

Figure 38: Scanning electron microscopic images of (a) unidirectional reinforced matrix and (b) bidirectional reinforced matrix of the tested materials at ×250 magnification.

The accuracy of passive fit has been previously evaluated by measuring implant abutment distances in relation to a reference group (Hjerppe *et al.,* 2011; Rosentritt *et al.,* 2014) as shown in Figure 39. The mean vertical gap distances and standard deviations in µm were as follows: unidirectional FRC: 0.0 ± 0.0; bidirectional FRC 5.30 ± 0.67; zirconia: 2.14 ± 0.40; and titanium: 4.60 ± 0.38 (Figure 39).

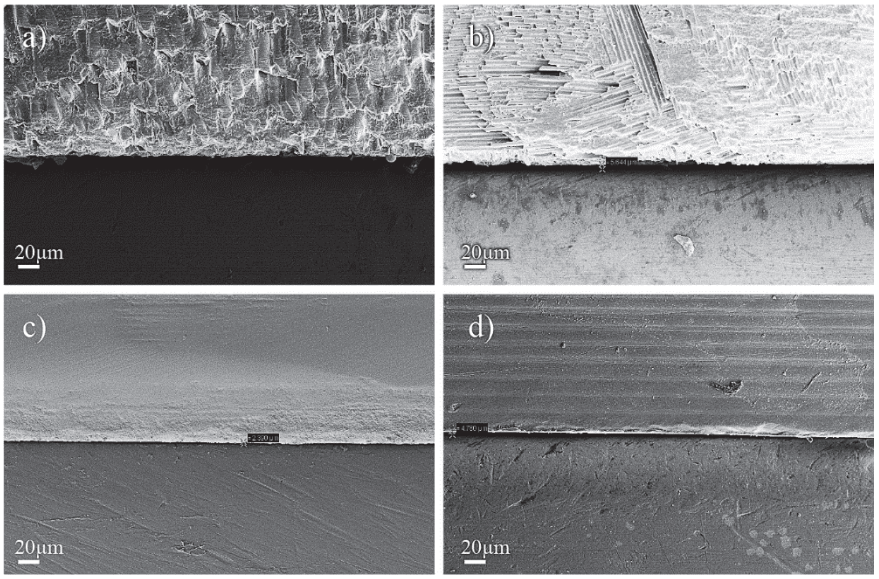

Figure 39: Precision of fit at x250 magnification: a) unidirectional FRC; b) bidirectional FRC; c) zirconia; and d) titanium.

Interestingly, the unidirectional FRC abutment material allowed to closing of the implant abutment gap compared to any other abutments evaluated in this study. The poor marginal fit reported for titanium abutments is because the used implants and abutments were from different manufacturers (Byrne *et al.,* 1998) Nevertheless, the range of misfit for all experimental groups in the current study is consistent with earlier studies and it can be considered as acceptable (Hjerppe *et al.,* 2011; Rosentritt *et al.,* 2014).

Optimization of screw-retained FRC abutments can be achieved via implementation of some constructional improvements: 1) the FRC specimens were hand-made resulting in voids. This could be avoided by utilizing vacuum–molding techniques which help remove trapped air bubbles in the resin during processing, 2) Regardless of the different materials examined all the specimens were milled by the same technique and had identical final shape. In FRC abutments the thin abutment walls may have lead to a substantial weakness of the restoration during loading. According to the present results by using a bulk FRC abutment a significant improvement in the performance may be achieved. Therefore the type of material should guide the shape and not opposite, 3) Bidirectional reinforcement significantly improved the anisotropic behavior of unidirectional reinforcement. However, the mechanical optimization for FRC composite structures for abutments may have to have a combination of unidirectional and bidirectional fiber structures and 4) in the area of the fracture initiation fiber reinforcement could be placed to increase the reinforcement efficiency.

Some limitations of the study need to be outlined. Cyclic load fatigue tests with water immersion are believed the best technique to evaluate fracture strength and long-term

survival of implant abutments (Behr *et al.,* 2001; Rosentritt *et al.,* 2014). Nevertheless, from a static load test significant relevant findings may arise (Yildirim *et al.,* 2003; Dittmer *et al.,* 2012) particularly when new materials are being tested. One variable, the screw design, could not be standardized as we aimed to follow the manufacturers' recommendations for the zirconium group. For the titanium and FRC abutments, the screw head had a tapering design, whereas the zirconia´s abutment screw head had a butt-joint design. In addition, the zirconia abutment screw had more threads than the other type. Additionally, this investigation did not include a full veneer crown in the model system. Higher load-bearing capacity values are expected with crowns due to stress shielding allowing a larger load to be applied before failure.

5.5 Future perspectives

In vitro mechanical testing plays a key role in the screening and validation of newly developed materials and structures. These results may influence the design of FRC abutments and implant structures. In addition to this, FRC materials show promising properties for implant abutments.

Future FRC surface properties could be optimized to prevent microbial adhesion by changing the surface of the fibers or also by incorporating antimicrobial agents to the polymer matrix. Taking into consideration the enhancement of the bidirectional reinforcement compared to unidirectional, further research including multidirectional reinforcement should be tested. In addition, cyclic fatigue loading with water immersion could be more representative of masticatory loading. Nevertheless, either in vivo bacterial and in vivo under loaded clinical tests will definitively validate the results.

6 CONCLUSIONS

Based on the studies developed in the present thesis the main findings and conclusions are:

1. FRC surfaces showed high roughness values and low wettability (hydrophobic) properties. Roughness quantification at two different scales gave complementary information. Wettability was not correlated with nanoroughness. In contrast, it was correlated with microroughness but this correlation was weak. S_a-S_{ku}-S_{mid} at the nanoscale, S_a- S_z at the microscale and one angle contact value are suggested for surface characterization.

2. FRC surfaces feature a bacterial response comparable to current implant abutment materials. This resulted to be true for both Gram positive (*S. aureus*) and Gram negative (*E. coli*) bacteria. Their poor wettability (hydrophobic) properties counteract the increased roughness preventing bacterial attachment. FRC do not estimulate the development of both young and mature biofilms.

3. Bidirectional reinforcement improved the performance of FRC abutments and one-piece implants Bidirectional FRC abutments showed significantly higher load-bearing capacity than unidirectional FRC abutments. Abutments and implants made of bidirectional fibers could be promising oral load-bearing devices.

ACKNOWLEDGEMENTS

The present thesis was developed at the Departments of Prosthetic Dentistry, Dental School and Pathology and Experimental Therapeutics, Medicine School at the University of Barcelona, Barcelona, Spain and Turku Clinical Biomaterial Centre–TCBC, Institute of Dentistry, University of Turku, Turku, Finland during the years 2011-2015.

Dear Friends and Collegues,

There are so many people to whom thanks I extend! This study would have not been posible without you. Many of you have been supportive unselfishly in achieving this work. I would like to mention a few people that meaningfully contributed to this thesis proyect.

First of all I would like to express my greatest gratitude to my two supervisors Professor Miquel Viñas and Professor Tomas Escuin for all their advice, support and knowledge that have guided me throughout this PhD journey. Prof. Viñas introduced me in the exciting and fun unknown world of microbiology. Prof. Escuin as well as Teresa Tomas have transmitted the passionatte knowledge of prosthodontics laboratory work. You have been determinant in my growth as a researcher!

I am grateful to Prof. Carlos Ascaso for his assessment in statistics. I also would like to give a warm thanks to Prof. Antonio Ros and Dr. Rafael Claramunt for their advice offered for the mechanical tests in Madrid

I am deeply thankful to Prof. Timo Narhi for inviting me to conduct one part of my research and finalize my thesis in Finland. The time spent in Finland in Prof Närhi´s group has been a great breakthrough in my development as a dental materials researcher. I was also fortunate to have an excellent mentor Dr. A Abdulmajeed.

I want to give a very special acknowledgement to Professor Pekka Vallittu and Lippo Lasilla head of the Turku Clinical Biomaterials Centre lab for challenging the creativity of the dental materials laboratory work. And for all the sauna moments!

In my daily work I have been accompanied with a helpful group of people. The group of students, researchers and staff of the Laboratory of Prosthetic Dentistry, the Department of Pathology and Experimental Therapeutics in Barcelona and Turku Clinical Biomaterials Centre (TCBC) in Turku made this work possible.

This dissertation would not have been possible without the financial support of several scholarships awarded by the University of Barcelona, Health University of Barcelona Campus and the Turku University Foundation.

My friends from Zarautz, Barcelona, and Turku. You have been direct witnesses of the whole project in good and bad moments. Thank you for all the shared moments you have been determinant in this whole process.

Lastly and most importantly, I would like to thank my family for all their support. To my sister Dr. Jeruka… she is my favourite dentist!, my brother Mikel a promising electronic engineer my brother in law Gerardo and to my parents Mertxe and Carmelo for your endless love and encouragement. The values of constancy, vision and honesty that I have learnt from you have guidelined this work inspiring me throughout the whole process. Mi little nephews Julen and Unai are among the greatest thing I have ever had… best wishes in your life! I will also like to thank my uncles and aunts for their support regardless of the distance.

Warmest regards,

Marina Etxeberria DDS, MSc,

Barcelona, Spain

REFERENCES

Abdulmajeed AA, Närhi TO, Vallittu PK, Lassila LV. (2011a) The effect of high fiber fraction on some mechanical properties of unidirectional glass fiber-reinforced composite. Dent Mater. 27:313-321.

Abdulmajeed AA, Lassila LV, Vallittu PK, Närhi TO. (2011b) The effect of exposed glass fibers and particles of bioactive glass on the surface wettability of composite implants. Int J Biomater. 2011:607971.

Abdulmajeed AA, Walboomers XF, Massera J, Kokkari AK, Vallittu PK, Närhi TO. (2014) Blood and fibroblast responses to thermoset BisGMA-TEGDMA/glass fiber-reinforced composite implants in vitro. Clin Oral Implants Res. 25:843-851.

Abdulmajeed AA, Willberg J, Syrjänen S, Vallittu PK, Närhi TO. (2015) In vitro assessment of the soft tissue/implant interface using porcine gingival explants. J Mater Sci Mater Med. 26:5385.

Advincula MC, Petersen D, Rahemtulla F, Advincula R, Lemons JE. (2007) Surface analysis and biocorrosion properties of nanostructured surface sol-gel coatings on Ti6Al4V titanium alloy implants. J Biomed Mater Res B Appl Biomater. 80:107-120.

Agustín-Panadero R, Serra-Pastor B, Roig-Vanaclocha A, Román-Rodriguez JL, Fons-Font A. (2015) Mechanical behavior of provisional implant prosthetic abutments. Med Oral Patol Oral Cir Bucal. 20:e94-102.

Aitasalo KM, Piitulainen JM, Rekola J, Vallittu PK. (2014) Craniofacial bone reconstruction with bioactive fiber-reinforced composite implant. Head Neck. 36:722-728.

Amoroso PF, Adams RJ, Waters MG, Williams DW. (2006) Titanium surface modification and its effect on the adherence of Porphyromonas gingivalis: an in vitro study. Clin Oral Implants Res. 17:633-637.

An YH, Friedman RJ. (1998) Concise review of mechanisms of bacterial adhesion to biomaterial surfaces. J Biomed Mater Res. 43:338-348.

Anselme K. (2000) Osteoblast adhesion on biomaterials. Biomaterials. 21:667-681.

Anusavice KJ, Phillips RW. (2012) Phillips' science of dental materials, 12th ed., Elsevier, St. Louis.

Att W, Kurun S, Gerds T, Strub JR. (2006) Fracture resistance of single-tooth implant-supported all-ceramic restorations after exposure to the artificial mouth. J Oral Rehabil. 33:380-386.

Att W, Takeuchi M, Suzuki T, Kubo K, Anpo M, Ogawa T. (2009) Enhanced osteoblast function on ultraviolet light-treated zirconia. Biomaterials. 30:1273-1280.

Ausschill TM, Arweiler NB, Brecx M, Reich E, Sculean A, Netuschil L. (2002) The effect of dental restorative materials on dental biofilm. Eur J Oral Sci. 110: 48-53.

Ballo AM, Akca EA, Ozen T, Lassila L, Vallittu PK, Närhi TO. (2009) Bone tissue responses to glass fiber-reinforced composite implants--a histomorphometric study. Clin Oral Implants Res. 2:608-615.

Ballo AM, Akca E, Ozen T, Moritz N, Lassila L, Vallittu P, Närhi TO. (2014a) Effect of implant design and bioactive glass coating on biomechanical properties of fiber-reinforced composite implants. Eur J Oral Sci. 122:303-309.

Ballo AM, Cekic-Nagas I, Ergun G, Lassila L, Palmquist A, Borchardt P, Lausmaa J, Thomsen P, Vallittu PK, Närhi TO. (2014b) Osseointegration of fiber-reinforced composite implants: Histological and ultrastructural observations. Dent Mater. 30:e384-395.

Behr M, Rosentritt M, Lang R, Handel G. (2001) Glass fiber-reinforced abutments for dental implants. A pilot study. Clin Oral Implants Res. 12:174-178.

Behr M, Rosentritt M, Handel G. (2003) Fiber-reinforced composite crowns and FPDs: a clinical report. Int J Prosthodont. 16: 239-243.

Belser UC, Schmid B, Higginbottom F, Buser D. (2004) Outcome analysis of implant restorations located in the anterior maxilla: a review of the recent literature. Int J Oral Maxillofac Implants. 19 Suppl:30-42.

Bergendal T, Ekstrand K, Karlsson U. (1995) Evaluation of implant-supported carbon/graphite fiber-reinforced poly (methyl methacrylate) prostheses. A longitudinal multicenter study. Clin Oral Implants Res. 6:246-253.

Bidra AS, Rungruanganunt P. (2013) Clinical outcomes of implant abutments in the anterior region: a systematic review. J Esthet Restor Dent. 25:159-176.

Binnig G, Quate CF, Gerber C. (1986) Atomic force microscope. Phys Rev Lett. 56:930.

Björk N, Ekstrand K, Ruyter E. (1985) Carbon/graphite fiber reinforced polymer implant bridge prostheses. Swed Dent J Suppl; 28: 77-84.

Black J, Hastings GW. (1998) Handbook of Biomaterials Properties,Chapman & Hall, London UK.

Bollen CM, Papaioanno W, Van Eldere J, Schepers E, Quirynen M, van Steenberghe D. (1996) The influence of abutment surface roughness on plaque accumulation and peri-implant mucositis. Clin Oral Implants Res. 7:201-211.

Bollen CM, Lambrechts P, Quirynen M. (1997) Comparison of surface roughness of oral hard materials to the threshold surface roughness for bacterial plaque retention: a review of the literature. Dent Mater. 13:258-269.

Bowen RL. (1963) Properties of a silica-reinforced polymer for dental restorations. J Am Dent Assoc. 66:57-64.

Brown SA, Hastings RS, Mason JJ, Moet A. (1990) Characterization of short-fibre reinforced thermoplastics for fracture fixation devices. Biomaterials. 11:541-547.

Brunski JB, Skalak R. (1998) Biomechanical considerations for craniofacial implants, in Osseointegration in Craniofacial Reconstruction, Branemark P-I, Tolman DE editors, Quintessence Publishing Co., Inc., Carol Stream, IL, Chapter 2, 15-36.

Busscher HJ, Van Pelt AWJ, De Boer P, De Jong HP, Arends J. (1984) The effect of surface roughening of polymers on measured contact angles of liquids. Colloids and Surfaces. 9:319-331.

Bürgers R, Hahnel S, Reichert TE, Rosentritt M, Behr M, Gerlach T, Handel G, Gosau M. (2010a) Adhesion of Candida albicans to various dental implant surfaces and the influence of salivary pellicle proteins. Acta Biomater. 6:2307-2313.

Bürgers R, Gerlach T, Hahnel S, Schwarz F, Handel G, Gosau M. (2010b) In vivo and in vitro biofilm formation on two different titanium implant surfaces. Clin Oral Implants Res. 21:156-164.

Busscher HJ, Rinastiti M, Siswomihardjo W, Van der Mei HC. (2010) Biofilm formation on dental restorative and implant materials. J Dent Res. 89:657-665.

Byrne D, Houston F, Cleary R, Claffey N. (1998) The fit of cast and premachined implant abutments. J Prosthet Dent. 80:184-192.

Castillo-Oyagüe R, Lynch CD, Turrión AS, López-Lozano JF, Torres-Lagares D, Suárez-García MJ. (2013) Misfit and microleakage of implant-supported crown copings obtained by laser sintering and casting techniques, luted with glass-ionomer, resin cements and acrylic/urethane-based agents. J Dent. 41:90-96.

Crawford RJ, Webb HK, Truong VK, Hasan J, Ivanova EP. (2012) Surface topographical factors influencing bacterial attachment. Adv Colloid Interface Sci. 1:142-149.

Darvell BW. (2006) Materials Science for Dentistry. 8th edition, Darvell BW,Pokfulam.

de Groot P, Deck L. (1995) Surface profiling by analysis of white-light interferograms in the spatial frequency domain. J Mod Opt. 42:389-401.

de Oliveira GR, Pozzer L, Cavalieri-Pereira L, de Moraes PH, Olate S, de Albergaría Barbosa JR. (2012) Bacterial adhesion and colonization differences between zirconia and titanium implant abutments: an in vivo human study. J Periodontal Implant Sci. 42:217-223.

Dittmer MP, Dittmer S, Borchers L, Kohorst P, Stiesch M. (2012) Influence of the interface design on the yield force of the implant-abutment complex before and after cyclic mechanical loading. J Prosthodont Res. 56:19-24.

do Nascimento C, da Rocha Aguiar C, Pita MS, Pedrazzi V, de Albuquerque Junior RF, Ribeiro RF. (2013) Oral biofilm formation on the titanium and zirconia substrates. Microsc Res Tech. 76:126-132.

Dong WP, Sullivan PJ, Stout KJ. (1994) Comprehensive study of parameters for characterising three-dimensional surface topography: III: Parameters for characterising amplitude and some functional properties. Wear. 178:29-43.

Dorobantu LS, Gray MR. (2010) Application of atomic force microscopy in bacterial research. Scanning. 32:74-96.

Dorobantu LS, Goss GG, Burrell RE. (2012) Atomic force microscopy: a nanoscopic view of microbial cell surfaces. Micron. 43:1312-1322.

Duncan JP, Freilich MA, Latvis CJ. (2000) Fiber-reinforced composite framework for implant-supported overdentures. J Prosthet Dent. 84:200-204.

Duncan-Hewitt W. (1990) Nature of the hydrophobic effect. In: Doyle R, RosenbergM, editors, Microbial cell surface hydrophobicity.Washington DC: American Society for Microbiology, 39-73.

Dyer SR, Lassila LV, Jokinen M, Vallittu PK. (2004) Effect of fiber position and orientation on fracture load of fiber-reinforced composite. Dent Mater. 20:947-955.

Dyer SR, Lassila LV, Jokinen M, Vallittu PK. (2005) Effect of cross-sectional design on the modulus of elasticity and toughness of fiber-reinforced composite materials. J Prosthet Dent. 94:219-226.

Elias CN, Lima JHC, Valiev R, Meyers MA. (2008) Biomedical applications of titanium and its alloys. Jom, 60(3), 46-49.

Erkmen E, Meriç G, Kurt A, Tunç Y, Eser A. (2011) Biomechanical comparison of implant retained fixed partial dentures with fiber reinforced composite versus conventional metal frameworks: a 3D FEA study. J Mech Behav Biomed Mater. 4:107-116.

Ferrario VF, Sforza C, Serrao G, Dellavia C, Tartaglia GM. (2004) Single tooth bite forces in healthy young adults. J Oral Rehabil. 31:18-22.

Fombellida F, Martos F. (2004) Cirugía mucogingival. Team Work Media España. 12:371-428.

Freilich MA, Meiers JC, Duncan JP, Goldberg AJ. (2000) Fiber reinforced composites in clinical dentistry. 1st ed. Chicago: Quintessence Publishing Co. Inc.1-8.

Freilich MA, Duncan JP, Alarcon EK, Eckrote KA, Goldberg AJ. (2002) The design and fabrication of fiber-reinforced implant prostheses. J Prosthet Dent. 88:449-454.

Gabay E, Cohen O, Machtei EE. (2010) Heat production during prosthetic preparation of a one-piece dental implant. Int J Oral Maxillofac Implants. 25:1131-1136.

Gadelmawla ES, Koura MM, Maksoud TMA, Elewa IM, Soliman, HH. (2002) Roughness parameters. J Mater Process Tech. 123:133-145.

Garoushi S, Säilynoja E, Vallittu PK, Lassila L. (2013) Physical properties and depth of cure of a new short fiber reinforced composite. Dent Mater. 29:835-841.

Gittens RA, McLachlan T, Olivares-Navarrete R, Cai Y, Berner S, Tannenbaum R, Schwartz Z, Sandhage KH, Boyan BD. (2011) The effects of combined micron-/submicron-scale surface roughness and nanoscale features on cell proliferation and differentiation. Biomaterials. 32:3395-3403.

Gittens RA, Olivares-Navarrete R, Cheng A, Anderson DM, McLachlan T, Stephan I, Geis-Gerstorfer J, Sandhage KH, Fedorov AG, Rupp F, Boyan BD, Tannenbaum R, Schwartz Z. (2013) The roles of titanium surface micro/nanotopography and wettability on the differential response of human osteoblast lineage cells. Acta Biomater. 9:6268-6277.

Gohring TN, Roos M. (2005) Inlay-fixed partial dentures adhesively retained and reinforced by glass fibers: clinical and scanning electron microscopy analysis after five years. Eur J Oral Sci. 113:60-69.

Gomes AL, Montero J. (2011) Zirconia implant abutments: a review. Med Oral Patol Oral Cir Bucal. 16:50-55.

Gorth DJ, Puckett S, Ercan B, Webster TJ, Rahaman M, Bal BS. (2012) Decreased bacteria activity on Si3N4 surfaces compared with PEEK or titanium. Int J Nanomedicine. 7:4829-4829.

Gregersen T. (1978) Rapid method for distinction of Gram-negative from Gram-positive bacteria. Appl Microbiol Biotechnol. 5:123-127.

Groessner-Schreiber B, Hannig M, Dück A, Griepentrog M, Wenderoth DF. (2004) Do different implant surfaces exposed in the oral cavity of humans show different biofilm compositions and activities? Eur J Oral Sci. 112:516-522.

Gross M, Laufer BZ, Ormianar Z. (1995) An investigation on heat transfer to the implant-bone interface due to abutment preparation with high-speed cutting instruments. Int J Oral Maxillofac Implants. 10:207-212.

Hahn JA. (2007) Clinical and radiographic evaluation of one-piece implants used for immediate function. J Oral Implantol. 33:152-155.

Hahnel S, Wieser A, Lang R, Rosentritt M. (2014) Biofilm formation on the surface of modern implant abutment materials. Clin Oral Implants Res. 24.:10.1111/clr.12454

Ham M, Powers BM. (2014) Roughness parameter selection for novel manufacturing processes. Scanning. 36:21-29.

Herbst D, Dullabh H, Sykes L, Vorster C. (2013) Evaluation of surface characteristics of titanium and cobalt chromium implant abutment materials. SADJ. 68:350, 352-6.

Hjalmarsson L. (2009) On cobalt-chrome frameworks in implant dentistry. Swed Dent J Suppl. 201:3-83.

Hjerppe J, Lassila LV, Rakkolainen T, Närhi T, Vallittu PK. (2011) Load-bearing capacity of custom-made versus prefabricated commercially available zirconia abutments. Int J Oral Maxillofac Implants. 26:132-138.

Hove LH, Holme B, Young A, Tveit AB. (2008) The protective effect of TiF4, SnF2 and NaF against erosion-like lesions in situ. Caries Res. 42:68-72.

Hulterström M, Nilsson U. (1994) Cobalt-chromium as a framework material in implant-supported fixed prostheses: a 3-year follow-up. Int J Oral Maxillofac Implants. 9:449-454.

Imazato S, McCabe JF, Tarumi H, Ehara A, Ebisu S. (2001) Degree of conversion of composites measured by DTA and FTIR. Dent Mater. 17:178-183.

ISO 10477. (1992) Dentistry — Polymer-based crown and bridge materials;

ISO 14801. (2007) Dentistry — Implants dynamic fatigue test for endooseous dental implants;.

Ivanova EP, Truong VK, Wang JY, Berndt CC, Jones RT, Yusuf II, Peake I, Schmidt HW, Fluke C, Barnes D, Crawford RJ. (2010) Impact of nanoscale roughness of titanium thin film surfaces on bacterial retention. Langmuir. 2:1973-1982.

Jackson N. (2008) Principles of interferometry. In Jets from Young Stars II, Springer Berlin Heidelberg. 193-218.

Jemt T. (1986) Modified single and short-span restorations supported by osseointegrated fixtures in the partially edentulous jaw. J Prosthet Dent. 55:243-247.

Juan L, Zhimin Z, Anchun M, Lei L, Jingchao Z. (2010) Deposition of silver nanoparticles on

titanium surface for antibacterial effect. Int J Nanomedicine. 5:261-267.

Jung RE, Holderegger C, Sailer I, Khraisat A, Suter A, Hammerle CH. (2008) The effect of all-ceramic and porcelain-fused-to-metal restorations on marginal peri-implant soft tissue color: a randomized controlled clinical trial. Int J Periodontics Restorative Dent. 28:357-365.

Kaiser TM, Brinkmann G. (2006) Measuring dental wear equilibriums—the use of industrial surface texture parameters to infer the diets of fossil mammals. Palaeogeogr, Palaeoclimatol, Palaeoecol. 239:221-240.

Kasemo B. (2002). Biological surface science. Surf Sci. 500:656-677.

Kilicarslan MA, Ozkan P. Evaluation of retention of cemented laser-sintered crowns on unmodified straight narrow implant abutments. (2013) Int J Oral Maxillofac Implants. 28:381-387.

Kim HK, Heo SJ, Koak JY, Kim SK. (2009) In vivo comparison of force development with various materials of implant-supported prostheses. J Oral Rehabil. 36:616-625.

Kim YS, Shin SY, Moon SK, Yang SM. (2015) Surface properties correlated with the human gingival fibroblasts attachment on various materials for implant abutments: A multiple regression analysis. Acta Odontol Scand. 73:38-47.

Krenchel H. (1963) Fibre Reinforcement (Ph.D. thesis). Copenhagen: Technical University of Denmark.

Kurtz SM, Devine JN. (2007) PEEK biomaterials in trauma, orthopedic, and spinal implants. Biomaterials. 28:4845-4869

Lassila LV, Nohrström T, Vallittu PK. (2002) The influence of short-term water storage on the flexural properties of unidirectional glass fiber-reinforced composites. Biomaterials. 23:2221-2229.

Lassila LV, Tanner J, Le Bell AM, Narva K, Vallittu PK. (2004) Flexural properties of fiber reinforced root canal posts. Dent Mater. 20:29-36.

Lassila LV, Garoushi S, Tanner J, Vallittu PK, Söderling E. (2009) Adherence of Streptococcus mutans to Fiber-Reinforced Filling Composite and Conventional Restorative Materials. Open Dent J. 4:227-232.

Lemons JE. (1998) Unanticipated outcomes: dental implants. Implant Dent. 7:351-354.

Leonhardt A, Bergstrom C, Lekholm U. (2003) Microbiologic diagnostics at titanium implants. Clin Implant Dent Relat Res. 5:226-232.

Leprince J, Palin WM, Mullier T, Devaux J, Vreven J, Leloup G. (2010) Investigating filler morphology and mechanical properties of new low-shrinkage resin composite types. J Oral Rehabil. 37:364-376.

Lewis S, Beumer J 3rd, Hornburg W, Moy P. (1988) The "UCLA" abutment. Int J Oral Maxillofac Implants. 3:183-189.

Lim YJ, Oshida Y. (2001) Initial contact angle measurements on variously treated dental/medical titanium materials. Biomed Mater Eng. 11:325-341.

Liu X, Lin J, Ding P. (2013) Changes in the surface roughness and friction coefficient of orthodontic bracket slots before and after treatment. Scanning. 35: 265-372

Luangruangrong P, Cook NB, Sabrah AH, Hara AT, Bottino MC. (2014) Influence of full-contour zirconia surface roughness on wear of glass-ceramics J Prosthodont. 23:198-205.

Mannocci F, Sherriff M, Watson TF, Vallittu PK. (2005) Penetration of bonding resins into fibre-reinforced composite posts: a confocal microscopic study. Int Endod J. 38:46-51.

McCabe JF. (1990) Applied dental materials. London, Blackwell.

Meiers JC, Duncan JP, Freilich MA, Goldberg, AJ. (1998) Preimpregnated, fiber-reinforced prostheses. Part II. Direct applications: splints and fixed partial dentures. Quintessence international, Berlin, Germany. 9:761-768.

Mitik-Dineva N, Wang J, Truong VK, Stoddart P, Malherbe F, Crawford RJ, Ivanova EP. (2009) Escherichia coli, Pseudomonas aeruginosa, and Staphylococcus aureus attachment patterns on glass surfaces with nanoscale roughness. Current microbiology. 58:268-273.

Mombelli A, Decaillet F. (2011) The characteristics of biofilms in peri-implant disease. J Clin Periodontol. 38:203-213.

Moritz N, Strandberg N, Zhao DS, Mattila R, Paracchini L, Vallittu PK, Aro HT. (2014) Mechanical properties and in vivo performance of load-bearing fiber-reinforced composite intramedullary nails with improved torsional strength. J Mech Behav Biomed Mater. 40:127-139.

Nascimento Cd, Pita MS, Fernandes FH, Pedrazzi V, de Albuquerque Junior RF, Ribeiro RF. (2014) Bacterial adhesion on the titanium and zirconia abutment surfaces. Clin Oral Implants Res. 25:337-343.

Nganga S, Travan A, Marsich E, Donati I, Söderling E, Moritz N, Paoletti S, Vallittu PK. (2013) In vitro antimicrobial properties of silver-polysaccharide coatings on porous fiber-reinforced composites for bone implants. J Mater Sci Mater Med. 24:2775-2785.

Nganga S, Moritz N, Kolakovic R, Jakobsson K, Nyman JO, Borgogna M, Travan A, Crosera M, Donati I, Vallittu PK, Sandler N. (2014) Inkjet printing of Chitlac-nanosilver--a method to create functional coatings for non-metallic bone implants. Biofabrication. 22:6:041001.

Noiset O, Schneider YJ, Marchand-Brynaert J. (2000) Adhesion and growth of CaCo2 cells on surface-modified PEEK substrata. J Biomater Sci Polym Ed. 11:767-86.

Nothdurft FP, Fontana D, Ruppenthal S, May A, Aktas C, Mehraein Y, Lipp P, Kaestner L. (2014) Differential Behavior of Fibroblasts and Epithelial Cells on Structured Implant Abutment Materials: A Comparison of Materials and Surface Topographies. Clin Implant Dent Relat Res.

Nowicki B. (1985) Multiparameter representation of surface roughness. Wear. 102:161-176.

O'Brien WJ. (2013) Dental materials and their selection, 2nd ed. Chicago:Quintessence; 1997. p. 40.

Ohl A, Schroder K, Keller D, Meyer-Plath A, Bienert H, Husen B, Rune GM. (1999) Chemical micropatterning of polymeric cell culture substrates using low-pressure hydrogen gas discharge plasmas. J Mater Sci Mater Med. 10:747-754.

Ohtonen J, Vallittu PK, Lassila LVJ. (2013) Effect of monomer composition of polymer matrix on flexural properties of glass fibre-reinforced orthodontic archwire. Eur J Orthodont. 35:110-114.

Ostman PO, Hellman M, Albrektsson T, Sennerby L. (2007) Direct loading of Nobel Direct and Nobel Perfect one-piece implants: a 1-year prospective clinical and radiographic study. Clin Oral Implants Res. 18:409-418.

Ourahmoune R, Salvia M, Mathia TG, Mesrati N. (2014) Surface morphology and wettability of sandblasted PEEK and its composites. Scanning. 36:64-75.

Oyagüe RC, Sánchez-Turrión A, López-Lozano JF, Montero J, Albaladejo A, Suárez-García MJ. (2012) Evaluation of fit of cement-retained implant-supported 3-unit structures fabricated with direct metal laser sintering and vacuum casting techniques. Odontology. 100:249-253.

Paphangkorakit J, Osborn JW. (1997) The effect of pressure on a maximum incisal bite force in man. Arch Oral Biol. 42:11-7.

Paquette DW, Brodala N, Williams RC. (2006) Risk factors for endosseous dental implant failure. Dent Clin North Am. 50:361-374.

Parel SM, Schow SR. (2005) Early clinical experience with a new one-piece implant system in single tooth sites. J Oral Maxillofac Surg. 63:2-10.

Park JH, Wasilewski CE, Almodovar N, Olivares-Navarrete R, Boyan BD, Tannenbaum R, Schwartz Z. (2012) The responses to surface wettability gradients induced by chitosan nanofilms on microtextured titanium mediated by specific integrin receptors. Biomaterials. 33:7386-7393.

Pegueroles M, Aparicio C, Bosio M, Engel E, Gil FJ, Planell JA, Altankov G. (2010) Spatial organization of osteoblast fibronectin matrix on titanium surfaces: effects of roughness, chemical heterogeneity and surface energy. Acta Biomater. 6:291-301.

Perea L, Matinlinna JP, Tolvanen M, Lassila LV, Vallittu PK. (2014) Fiber-reinforced composite fixed dental prostheses with various pontics. J Adhes Dent. 16:161-168.

Pereira A, Hernández P, Martinez J, Pérez JA, Mathia TG. (2014) Surface topographic characterization for polyamide composite injection molds made of aluminum and copper alloys. Scanning. 36:39-52.

Prestipino V, Inberg A. (1993) Esthetic High-Strength Implant Abutments. Part I. J Esthet Dent. 5:29-36.

Poortinga AT, Bos R, Busscher HJ. (1999) Measurement of charge transfer during bacterial adhesion to an indium tin oxide surface in a parallel plate flow chamber. J Microbiol Methods. 38:183-189.

Poortinga AT, Bos R, Busscher HJ. (2001) Charge transfer during staphylococcal adhesion to tinox coatings with different specific resistivity. Biophys Chem. 91: 273-279.

Quante K, Ludwig K, Kern M. (2008) Marginal and internal fit of metal-ceramic crowns fabricated with a new laser melting technology. Dent Mater. 2:1311-1315.

Radford DR, Sweet SP, Challacombe SJ, Walter JD. (1998) Adherence of Candida albicans to denture-base materials with different surface finishes. J Dent. 26:577-583

Ramage G, Martinez JP, Lopez-Ribot, JL. (2006) Candida biofilms on implanted biomaterials: a clinically significant problem. FEMS Yeast Res. 6: 979-986.

Rimondini L, Farè S, Brambilla E, Felloni A, Consonni C, Brossa F, Carrassi A. (1997) The effect of surface roughness on early in vivo plaque colonization on titanium. J Periodontol. 68:556-562.

Rimondini L, Cerroni L, Carrassi A, Torricelli P. (2002) Bacterial colonization of zirconia ceramic surfaces: an in vitro and in vivo study. Int J Oral Maxillofac Implants. 17:793-798.

Ritchie RO, Buehler M.J., Hansma P. (2009) Plasticity and toughness in bone. Phys. Today. 62:41-47

Roach M. (2007) Base metal alloys used for dental restorations and implants. Dent Clin North Am. 51:603-627.

Rochford ET, Poulsson AH, Salavarrieta Varela J, Lezuo P, Richards RG, Moriarty TF. (2014) Bacterial adhesion to orthopaedic implant materials and a novel oxygen plasma modified PEEK surface. Colloids Surf B Biointerfaces. 113:213-222.

Rosa MB, Albrektsson T, Francischone CE, Schwartz Filho HO, Wennerberg A. (2012) The influence of surface treatment on the implant roughness pattern. J Appl Oral Sci. 20:550-555.

Rosentritt M, Behr M, Bürgers R, Feilzer AJ, Hahnel S. (2009) In vitro adherence of oral streptococci to zirconia core and veneering glass-ceramics. J Biomed Mater Res B Appl Biomater. 91:257-263.

Rosentritt M, Hagemann A, Hahnel S, Behr M, Preis V. (2014) In vitro performance of zirconia and titanium implant/abutment systems for anterior application. J Dent. 42:1019-1026.

Rosen BG, Anderberg C, Ohlsson R. (2008) Parameter correlation study of cylinder liner roughness for production and quality control. Proc Inst Mech Eng B J Eng. 222:1475-1487.

Ruyter IE. (1995) Physical and chemical aspects related to substances released from polymer materials in an aqueous environment. Adv Dent Res. 9:344-347.

Sailer I, Sailer T, Stawarczyk B, Jung RE, Hämmerle CH. (2009) In vitro study of the influence of the type of connection on the fracture load of zirconia abutments with internal and external implant-abutment connections. Int J Oral Maxillofac Implants. 24:850-858.

Sabrah AH, Cook NB, Luangruangrong P, Hara AT, Bottino MC. Full-contour Y-TZP ceramic surface roughness effect on synthetic hydroxyapatite wear. (2013) Dent Mater. 29:666-673.

Salton MRJ. (1953) Studies of the bacterial cell wall: IV. The composition of the cell walls of some gram-positive and gram-negative bacteria. Biochimica et biophysica acta. 10:512-523.

Sawase T, Wennerberg A, Hallgren C, Albrektsson T, Baba K. (2000) Chemical and topographical surface analysis of five different implant abutments. Clin Oral Implants Res. 11:44-50.

Scarano A, Piattelli M, Caputi S, Favero GA, Piattelli, A. (2004) Bacterial adhesion on commercially pure titanium and zirconium oxide disks: an in vivo human study. J Periodontol. 75: 292-296.

Scheirs J. (2000) Compositional and failure analysis of polymers: a practical approach. John Wiley and Sons Inc, New York.

Sennerby L, Rocci A, Becker W, Jonsson L, Johansson LA, Albrektsson T. (2008) Short-term clinical results of Nobel Direct implants: a retrospective multicentre analysis. Clin Oral Implants Res. 19:219-226.

Siddiqi A, Payne AG, De Silva RK, Duncan WJ. (2011) Titanium allergy: could it affect dental implant integration? Clin Oral Implants Res. 22:673-680.

Sicilia A, Cuesta S, Coma G, Arregui I, Guisasola C, Ruiz E, Maestro A. (2008) Titanium allergy in dental implant patients: a clinical study on 1500 consecutive patients. Clin Oral Implants Res. 19: 823-835.

Smith DC. (1961)The acrylic denture: mechanical evaluation of midline fracture. Br Dent J. 110:257-267.

Stawarczyk B, Beuer F, Wimmer T, Jahn, D, Sener B, Roos M, Schmidlin PR. (2013) Polyetheretherketone—A suitable material for fixed dental prostheses? J Biomed Mater Res. 101:1209-1216.

Stenhagen KR, Hove LH, Holme B, Taxt-Lamolle S, Tveit AB. (2010) Comparing different methods to assess erosive lesion depths and progression in vitro. Caries Res. 44:555-61.

Subramani K, Jung RE, Molenberg A, Hammerle CH. (2009) Biofilm on dental implants: a review of the literature. Int J Oral Maxillofac Implants. 24:616-626.

Tanner J, Vallittu PK, Soderling E. (2000) Adherence of streptococcus mutans to an E-glass fiber-reinforced composite and conventional restorative materials used in prosthetic dentistry. J Biomed Mater Res. 49: 250-256.

Tanner J, Carlén A, Söderling E, Vallittu PK. (2003) Adsorption of parotid saliva proteins and adhesion of Streptococcus mutans ATCC 21752 to dental fiber-reinforced composites. J Biomed Mater Res B Appl Biomater. 66:391-398.

Tanner J, Robinson C, Söderling E, Vallittu P. (2005) Early plaque formation on fibre-reinforced composites in vivo. Clin Oral Investig. 9:154-160.

Tetè S, Mastrangelo F, Traini T, Vinci R, Sammartino G, Marenzi G, Gherlone E. (2008) A macro- and nanostructure evaluation of a novel dental implant. Implant Dent. 17:309-320.

Tetelman ED, Babbush CA. (2008) A new transitional abutment for immediate aesthetics and function. Implant Dent. 17:51-58.

Teughels W, Van Assche N, Sliepen I, Quirynen M. (2006) Effect of material characteristics and/or surface topography on biofilm development. Clin Oral Implants Res. 17:68-81.

Thomas TR. (1981) Characterization of surface roughness. Precis Eng . 3:97-104.

Tortora GJ, Funke BR, Case CL. (2004) Microbiology: an Introduction. 8th Edition, Pearson Education Copyright (c)(Ed) ISBN: 0805376143 p 894

Tripodakis AP, Strub JR, Kappert HF, Witkowski S. (1995) Strength and mode of failure of single implant all-ceramic abutment restorations under static load. Int J Prosthodont. 8:265-272.

Truong VK, Lapovok R, Estrin YS, Rundell S, Wang JY, Fluke CJ, Crawford RJ, Ivanova EP. (2010) The influence of nano-scale surface roughness on bacterial adhesion to ultrafine-grained titanium. Biomaterials. 31:3674-3683.

Tsang CSP, Ng H, Mc Millan AS. (2007) Antifungal susceptibility of Candida albicans biofilms on

titanium discs with different surface roughness. Clin Oral Investig. 11:361-368.

Tyrrell JW, Dal Savio C, Krüger-Sehm R, Danzebrink, HU. (2004) Development of a combined interference microscope objective and scanning probe microscope. Rev Sci Instrum. 75:1120-1126.

Uctasli S, Tezvergil A, Lassila LV, Vallittu PK. (2005) The degree of conversion of fiber-reinforced composites polymerized using different light-curing sources. Dent Mater. 21:469-475.

Uppal M, Ganesh A, Balagopal S, Kaur G. (2013) Profilometric analysis of two composite resins' surface repolished after tooth brush abrasion with three polishing systems. J Conserv Dent. 16:309-313.

Vallittu PK, Lassila VP, Lappalainen R. (1994) Transverse strength and fatigue of denture acrylic-glass fiber composite. Dent Mater. 10:116-121.

Vallittu PK. (1998) Experiences of the use of glass fibres with multiphase acrylic resin systems. In: Vallittu PK. editor. The first symposium on fibre reinforced plastics in dentistry in the proceedings of the 22nd annual EPA conference.. Paper II.

Vallittu PK. (1999) Flexural properties of acrylic resin polymers reinforced with unidirectional and woven glass fibers. J Prosthet Dent. 81:318-326.

Vallittu PK. (2004) Survival rates of resin-bonded, glass fiber–reinforced composite fixed partial dentures with a mean follow-up of 42 months: A pilot study. J Prosthet Dent. 91:241-246.

Vallittu PK. (2009) Interpenetrating polymer networks (IPNs) in dental polymers and composites. J Adhes Sci Technol. 23:961-972.

Variola F, Brunski JB, Orsini G, de Oliveira PT, Wazen R, Nanci A. (2011) Nanoscale surface modifications of medically relevant metals: state-of-the art and perspectives. Nanoscale. 3:335-353.

Viñas M, Regué M, Lorén JG. (1991) Bacterial envelopes and antibiotics. PPU Editorial (promociones Publicaciones Universitarias) Barcelona. ISBN 8476658834.

Vishu S. (2007) Handbook of plastics testing and failure analysis. 3rd ed. John Wiley and Sons, Inc. New York.

Wang L, Garcia FC, Amarante de Araújo P, Franco EB, Mondelli RF. (2004) Wear resistance of packable resin composites after simulated toothbrushing test. J Esthet Restor Dent. 16:303-14; 314-5.

Wennerberg A, Albrektsson T. (2000) Suggested guidelines for the topographic evaluation of implant surfaces. Int J Oral Maxillofac Implants. 15:331-344.

Whitehead KA, Colligon J, Verran J. (2005) Retention of micro- bial cells in substratum surface features of micrometer and sub-micrometer dimensions. Colloid Surf B Biointerfaces. 41:129-138.

Whitehouse DJ. (1982) The parameter rash—is there a cure? Wear. 83:75-78.

Webb HK, Truong VK, Hasan J, Fluke C, Crawford RJ, Ivanova EP. (2012) Roughness parameters for standard description of surface nanoarchitecture. Scanning. 34:257-263.

Webb HK, Boshkovikj V, Fluke CJ, Truong VK, Hasan J, Baulin VA, Lapovok R, Estrin Y, Crawford RJ, Ivanova EP. (2013) Bacterial attachment on sub-nanometrically smooth titanium substrata. Biofouling. 29:163-170.

Wenzel RN. (1949) Surface roughness and contact angle. J Phys Colloid Chem 53:1466-1467

Williams DF. (1999) The Williams Disctionary of Biomaterials Liverpool: Liverpool University Press.

Yang Y, Zhou J, Liu X, Zheng M, Yang J, Tan J. (2015) Ultraviolet light-treated zirconia with different roughness affects function of human gingival fibroblasts in vitro: The potential surface modification developed from implant to abutment. J Biomed Mater Res B Appl Biomater. 103:116-124.

Yildirim M, Fischer H, Marx R, Edelhoff D. (2003) In vivo fracture resistance of implant-supported all-ceramic restorations. J Prosthet Dent. 90:325-331.

Zhang X, Li Z, Yuan X, Cui Z, Bao H, Li X, Liu Y, Yang X. (2013) Cytotoxicity and antibacterial property of titanium alloy coated with silver nanoparticle-containing polyelectrolyte multilayer. Mater Sci Eng C Mater Biol Appl. 33:2816-2820.

Zarb GA, Albrektsson T, Branemark PI. (1985) Tissue-integrated prostheses: osseointegration in clinical dentistry. Quintessence. 241-282.

Zarb GA, Schmitt A. (1990) The longitudinal clinical effectiveness of osseointegrated dental implants: the Toronto study. Part I: surgical results. J Prosthet Dent. 63:451-457.

Zupancic R, Legat A, Funduk N. (2006) Tensile strength and corrosion resistance of brazed and laser-welded cobalt-chromium alloy joints. J Prosthet Dent. 96: 273-282.

Zhao DS, Moritz N, Laurila P, Mattila R, Lassila LV, Strandberg N, Mäntylä T, Vallittu PK, Aro HT. (2009) Development of a multi-component fiber-reinforced composite implant for load-sharing conditions. Med Eng Phys. 31:461-469.

ORIGINAL PUBLICATIONS

Useful Surface Parameters For Biomaterial Discrimination

MARINA ETXEBERRIA[1], TOMAS ESCUIN[2], MIQUEL VINAS[3], CARLOS ASCASO[4]

[1]*Doctoral student, Department of Dentistry and Department of Pathology and experimental therapeutics, Dentistry School, University of Barcelona, Feixa Llarga s/n, 08907 Hospitalet de Llobregat, Barcelona, Spain*
[2]*Associate Professor, Laboratory of Prosthetic Dentistry, Dentistry School, University of Barcelona, Feixa Llarga s/n, 08907 Hospitalet de Llobregat, Barcelona, Spain*
[3]*Professor, Department of Pathology and Experimental Therapeutics, Medical and Dentistry Schools, University of Barcelona, Feixa Llarga s/n, 08907 Hospitalet de Llobregat, Barcelona, Spain*
[4]*Professor, Department of Public Health, Medical School, University of Barcelona, Villarroel 170, 08036 Barcelona, Barcelona, Spain*

ABSTRACT

Topographical features of biomaterials' surfaces are determinant when addressing their application site. Unfortunately up to date there has not been an agreement regarding which surface parameters are more representative in discriminating between materials. Discs (n=16) of different currently used materials for implant prostheses fabrication, such as cast cobalt-chrome, direct laser metal soldered (DLMS) cobalt-chrome, titanium grade V, zirconia (Y-TZP), E-glass fiber-reinforced composite and polyetheretherketone (PEEK) were manufactured. Nanoscale topographical surface roughness parameters generated by atomic force microscopy (AFM), microscale surface roughness parameters obtained by white light interferometry (WLI) and water angle values obtained by the sessile-water-drop method were analyzed in order to assess which parameter provides the best optimum surface characterization method. Correlations between nanoroughness, microroughness and hydrophobicity data were performed to achieve the best parameters giving the highest discriminatory power. A subset of 6 parameters for surface characterization were proposed. AFM and WLI techniques gave complementary information. Wettability did not correlate with any of the nanoroughness parameters while it however showed a weak correlation with microroughness parameters.

INTRODUCTION

Surface features significantly condition many technological and biomedical applications of biomaterials (Ham and Powers, 2014). Surface roughness and surface wettability can significantly determine major aspects of biological interactions and, subsequently, allow to predict the eventual failure or success of an implant-prosthetic treatment (Park *et al.,* 2012; Gittens *et al.,* 2013). Surface modification strategies attempt to modulate the surface properties of biomaterials in order to affect cell-substrate interactions and improve the overall biological response (Ivanova *et al.,* 2010). Furthermore, in order to accomplish this purpose a detailed characterization of surface topography must be achieved.

Characterization of surface roughness is complex as it depends on both the intrinsic properties of the material and manufacturing procedures and conditions (De Chiffre *et al.,* 2000). In an attempt to have a more extensive and clear description, a wide variety of surface roughness parameters (RPs) have been developed. This has been termed as "the parameter rash" by Whitehouse (Whitehouse, 1982). Nevertheless, inconsistencies have been reported when describing surface topographies, in part due to the lack of standardized methods. Nowadays a wide set of parameters are being used; however, it seems that there is an urgent need to reduce the number of parameters in order to achieve a general standardization to facilitate comparisons and reduce cost.

The parameter reduction method is effective at selecting the RP to represent a surface (Nowicki, 1985; Rosén *et al.*, 2008; Ham and Powers, 2014). This method is based on the analysis of strong and weak correlations between RPs; correlated RPs highlight the similarity between them; conversely, non-correlated RPs underline the difference among them. Highly correlated RPs are redundant and

thereby one can be selected to represent the whole group. In contrast, poorly correlated RPs provide complementary information being thereby best discriminating between materials (Nowicki, 1985).

Progress in nanotechnologies has led to the development of nanometer resolution technologies allowing research and visualization at a scale in which interactions between bacterial cells and biomaterials' surfaces occur. Atomic Force Microscopy (AFM) is the most powerful tool for topographical characterization at the nanometer and sub-nanometer scales (Binnig *et al.,* 1986; Dorobantu and Gray, 2010). AFM topography imaging is non-destructive and widely used in life sciences which provides high-resolution characterization of surface topography, biomolecules, membranes and cells at the nanoscale. White Light Interferometry (WLI) is a type of computerized optical interference microscopy. Its use has rapidly widespread as a quality control of microscale engineering processes and has been used to analyze surface roughness and cell adhesion at the microscale (Hove *et al.,* 2007). This method has been shown to be fast, non-destructive and accurate. The combination of both techniques has been proposed to improve the measuring efficiency of AFM for the surface characterization of biomaterials (Tyrrell *et al.,* 2004; Guo *et al.,* 2011).

To characterize surface structure, the present study examined six different dental materials for implant abutment manufacture using an atomic force microscope (AFM) for high resolution analysis, white light interferometry (WLI) and the drop-sessile-water method. From both techniques, amplitudinal roughness parameters were determined, which are so far the most cited surface parameters for surface characterization Ivanova *et al.,* 2010; Gittens *et al.,* 2013; Webb *et al.,* 2013). These are obtained from the height values of a given profile (denoted by R) or surface (denoted by S). The aim of this study was to attempt the combination of surface parameters resulting in an optimum surface description.

MATERIALS AND METHODS

Specimen preparation

Disks 10 mm in diameter and two mm thick were manufactured (n = 16) from six different implant abutment materials. The tested materials were: cast cobalt-chrome (Co-Cr), direct laser metal soldered selective laser melted (DLMS) Co-Cr disks, Titanium grade V disks, Zirconia (Y-TZP) disks, E-glass fiber-reinforced composite and polyetheretherketone (PEEK). The disks were manufactured as previously described (Etxeberria *et al.,* 2014).

Cast cobalt-chromium disks

Acrylic resin (pattern resin® LS, GC Corp.) disks of the desired final shape were fabricated and casted by induction (Ducatron Série 3 UGIN'Dentaire. Seyssins. France) using Co-Cr (Wirobond C® alloy, BEGO, Bremer Goldschlägerei Wilh. Herbst GmbH & Co. KG, Bremen, Germany). After casting, the sprues were eliminated with the aid of carbide discs at low speed. The castings were sandblasted with 110-μm aluminum oxide particles (Korox®, Bego, Bremen, Germany) under 3 bar pressure to remove oxide films and residual investment.

DLMS cobalt-chromium disks

The disk shaped specimens were designed in a 3D software package and saved in an industry standard stereolithography (STL) format. The standard DLMS (direct laser metal soldering) manufacturing method by EOSINT M 270 (EOSINT 270 GmbH Electro Optical Systems, Munich,Germany) was used to fabricate the disks.

Both the cast and the DLMS Co-Cr disks were polished in three stages: (a) using a hard rubber disk at 15,000 rpm; (b) then with a soft rubber disk at 15,000 rpm, and finally (c) using a soft brush with a polishing paste at 1400 rpm. Each polishing phase lasted 90 seconds.

Titanium disks

Machined and polished titanium grade V disks were provided by Klockner® (Klockner-Soadco S.L., Andorra).

Zirconia disks

Zirconia (Y-TZP) disks were supplied by Dentisel (Dentisel S.L., Barcelona, Spain).

FRC disks

E-glass FRC disks, prepared from rods, were provided by Bioloren® (Bioloren, S.r.L, Saronno, Varese, Italy).

PEEK disks

Polyetheretherketone (PEEK) disks were obtained from rods and were supplied by Tekniimplant® (Tekniimplant S.L., Barcelona, Spain).

Table 1. Summary of roughness parameters (Stout *et al.,* 1994).

Surface characterization technique	Symbol	Parameter
Atomic force microscopy	S_{max}	Maximum height of the surface
	S_{min}	Minimum height of the surface
	S_{mid}	Median height of the surface
	S_{mean}	Mean height of the surface
	S_{pv}	Peak to valley height
	S_a	Arithmetical mean deviation of surface roughness
	S_q	Root-mean-square deviation of surface topography
	S_z	Ten point height of surface topography
	S_{sk}	Skewedness of topography height distribution
	S_{ku}	Kurtosis of topography height distribution
White light interferometry	S_a	Arithmetical mean deviation of surface roughness
	S_z	Ten point height of surface topography
	S_q	Root-mean-square deviation of surface topography
	R_p	Maximum peak height of the roughness profile
	R_v	Maximum valley depth of the roughness profile
	R_z	Ten point height of the roughness profile
	R_t	Total height of the roughness profile
	R_a	Arithmetical mean deviation of the roughness profile
	R_q	Root-mean-square deviation of the roughness profile
Wettability	θ_{left}	Left contact angle
	θ_{right}	Right contact angle

All disks were handled by their lateral walls not to damage the disks' surfaces**.** In addition were gently cleaned using a cotton pellet with ethanol and dried under warm dry air.

CHARACTERIZATION

Atomic Force Microscopy

The surface topographies of the tested materials were characterized at the nanoscale using AFM (XE-70, Park Systems, Korea). Images with the areas of 5 × 5 μm² were scanned in the standard non-contact mode. The probe was supported on a rectangular-shaped cantilever tip (tip radius: < 10 nm, f=± 300 kHz, spring constant= ± 40 N/m, silicon coating). The scan rate was 0.6 Hz and the resolution 256 × 256 pixels. Representative roughness parameters S_{Min}, S_{Max}, S_{Mid}, S_{Mean}, S_{pv}, S_q, S_a, S_z, S_{sk} and S_{ku} described in Table 1 were calculated from the roughness values obtained by AFM and processed by XEI image processing software (Park Systems).

White light interferometry

The surface topographies of the tested materials were characterized at the microscale using a white light interferometer microscope (LeicaSCAN DCM3D, Leica Microsystems, Switzerland). A 50×/0.50 Mirau objective was utilized. The threshold was set to 1.0% and the Gaussian filter to 25 μm. Vertical scanning interferometry mode images with the areas of 250.64 × 190.90 μm² were obtained. Image data-analyses were performed using Leica map DCM 3D, version 6.2.6561 (Leica Microsystems, Switzerland) and R_p ,R_v, R_z, R_t, R_a, R_q, S_a, S_z, and S_q roughness parameters described in Table 1 were calculated.

Surface wettability

External water contact angles were analyzed with the sessile-water-drop method at room temperature (Gittens *et al.,* 2013; Truong *et al.,* 2010). A 10 μl drop of MilliQ-quality water was placed onto the center of each specimen using an injector. Digital photographs were taken (Nikon D70) and the determination of the external contact angle was done using IMAT software (CCIT, Barcelona, Spain). Two contact angles (θ_{left} and θ_{right}) per disk were obtained.

Statistical analysis

The surface nanoroughness, microroughness and wettability data did not follow a normal distribution. Therefore, a non-parametric ANOVA statistical analysis was carried out for data comparisons. Quantitative data analysis including the median, minimum and maximum were computed for each parameter. Spearman's rank correlation coefficient was used to express the degree of pair-wise association among nanoroughness parameters, microroughness parameters, and wettability. In order to identify statistical differences among the materials, Kruskal–Wallis and Mann-Whitney U test were performed with the Bonferroni adjustment

Table 2. Median, minimum and maximum values of nanoscale surface parameters in nanometres. Results of Kruskal–Wallis (*p*-value) and Mann–Whitney *U*-test with Bonferroni correction (number of pairs of materials with statistically significant differences).

	Cast Co-Cr	DLMS Co-Cr	Titanium	Zirconia	FRC	PEEK	Kruskal-Wallis p^*	Different pairs**
S_{min}	-200.5 (-494; -57)	-69 (-411; -25)	-125 (-181; -75)	-355 (-573; 258)	-507 (-993; -1)	-207 (-515; -85)	0.03	0
S_{max}	178 (51; 633)	80.5 (32; 502)	143 (82; 201)	427 (1; 759)	253 (1; 980)	194 (110; 591)	0.2	0
S_{mid}	-2 (-157; 69)	8.5 (-45; 140)	15.5 (-36; 32)	30.5 (-89; 164)	0.0 (-127; 141)	-6 (-67; 199)	0.1	0
S_{mean}	0.0 (-82; -0)	0.0 (0.0; 0.0)	0.0 (0.0; 0.0)	0.0 (0; -134)	0.0 (0.0; 0.0)	0.0 (0; -152)	0.4	0
S_{pv}	427 (128; 112)	183.5 (64; 91)	265.5 (189; 37)	795.5 (1; 1297)	761 (2; 1860)	457 (221; 932)	0.01	4
S_a	53.5 (11; 142)	11.5 (4; 132)	32 (22; 31.5)	99.5 (0; 185)	87 (0; 268)	42.5 (17; 167)	0.01	6
S_q	66 (14; 179)	19 (6; 153)	32 (22; 66)	128 (0; 234)	114 (0; 329)	61 (22; 184)	0.01	4
S_z	421 (106; 1126)	179 (61; 906)	259 (182; 363)	787.5 (1; 1276)	750 (2; 1825)	445 (216; 920)	0.01	4
S_{sk}	0 (-1; 1)	0 (-7; 2)	0 (-1; 1)	0 (-1; 0)	0 (0; 1)	0 (-1; 1)	0.6	1
S_{ku}	3.5 (2; 7)	5 (2; 71)	3 (2; 9)	3 (2; 5)	3 (2; 6)	4 (2; 11)	0.03	1

*Statistically significant differences $p<0.01$
**Different pairs of materials as determined by Mann–Whitney *U*-test $p<0.003$

Table 3. Median, minimum and maximum values of microscale surface parameters. Results of Kruskal–Wallis (*p*-value) and Mann–Whitney *U*-test with Bonferroni correction (number of pairs of materials with statistically significant differences).

	Cast Co-Cr	DLMS Co-Cr	Titanium	Zirconium	FRC	PEEK	Kruskal-Wallys p^*	Different pairs
S_a	0.15 (0.04; 0.18)	0.06 (0.01; 0.18)	0.08 (0.08; 0.63)	0.15 (0.11; 0.30)	0.87 (0.34; 1.33)	0.22 (0.18; 0.32)	<0.01	11
S_z	2.44 (0.54; 18.1)	1.83 (0.31;104.14	1.19 (0.88; 5.46)	2.83 (1.87; 8.08)	24.71 12.5; 108.41)	4.37 (3.4; 12.78)	<0.01	8
S_q	0.21 (0.44; 0.23)	0.21 (0.02; 0.63)	0.11 (0.08, 0.16)	0.21 (0.14; 0.41)	1.31 (0.53; 1.92)	0.31 (0.24; 0.47)	<0.01	8
R_p	0.17 (0.02; 0.29)	0.06 (0.02; 0.23)	0.12 (0.04; 0.32)	0.29 (0.18; 0.73)	1.26 (0.30; 4.26)	0.22 (0.11; 0.57)	<0.01	10
R_v	0.21 (0.00; 0.47)	0.12 (0.03; 0.33)	0.14 (0.03; 0.30)	0.25 (0.14; 0.50)	1.40 (0.41; 3.26)	0.21 (0.00; 0.59)	<0.01	7
R_z	0.41 (0.00; 0.76)	0.19 (0.05; 0.56)	0.27 (0.08; 0.50)	0.54 (0.33; 1.14)	2.64 (0.72; 7.10)	0.45 (0.00; 1.17)	<0.01	8
R_t	0.66 (0.16; 1.45)	0.37 (0.10; 0.94)	0.41 (0.20;1.80)	0.88 (0.56; 3.36)	5.42 (3.49; 25.51)	1.07 (0.48; 2.23)	<0.01	9
R_a	0.07 (0.01; 0.01)	0.03 (0.00; 0.11)	0.05 (0.13; 0.10)	0.10 (0.68; 0.20)	0.51 (0.11; 1.07)	0.11 (0.04; 0.24)	<0.01	9
R_q	0.10 (0.01; 0.18)	0.04 (0.01; 0.13)	0.06 (0.83; 0.13)	0.13 (0.00; 0.27)	0.69 (0.15; 1.48)	0.13 (0.05; 0.30)	<0.01	9

*Statistically significant differences $p<0.01$
**Different pairs of materials as determined by Mann–Whitney *U*-test $p<0.003$

according to the number of tests performed. Total data were analyzed in SPSS 2 to provide descriptive statistics and to perform non-parametric testing. Statistical analysis was performed with Statistical Package for the Social Sciences (Version 21.0; SPSS. Inc, Chicago, Illinois). Hypotheses were contrasted with an alpha error of 5% and estimations with 95% confidence level.

RESULTS

Overall results of the measurements on the surfaces are summarized in Tables 2 to 4. Tables 2, 3 and 4 describe the median, minimum and maximum values computed for each surface parameter carried out of 16 estimations per each material.

Table 4. Median, minimum and maximum values of external contact angle measurements. Results of Kruskal–Wallis (*p*-value) and Mann–Whitney *U*-test with Bonferroni correction (number of pairs of materials with statistically significant differences).

	Cast Co-Cr	DLMS Co-Cr	Titanium	Zirconia	FRC	PEEK	Kruskal-Wallis *p**	Different pairs**
θ_{left}	91.1 (78.6; 117)	95.8 (78.8; 106.3)	88.3 (73; 111.6)	110.2 (80.1; 124.3)	75.3 (50.8; 114)	93.5 (70.3; 103.4)	0.001	3
θ_{right}	91.6 (80.2; 115.2)	93.6 (77.4; 109.5)	89.8 (73; 115.7)	108.2 (81.1; 122.2)	74.5 (51.1; 109)	92.8 (70.9; 100.1)	0.0	4

*Statistically significant differences $p<0.01$
**Different pairs of materials as determined by Mann–Whitney *U*-test $p<0.003$

Correlation coefficient calculations are presented from Table 5 to Table 7: among nanoscale roughness parameters and wettability (Table 5); among microscale roughness parameters and wettability (Table 6) and finally Table 7 summarizes the correlations between nanoscale and microscale roughness parameters. At the nanoscale, roughness parameters showed poor correlations however 3 clusters of parameters are differentiated. A highly correlated group (r>0.86) comprised by S_a-S_{max}-S_{min}-S_{pv}-S_q-S_z in addition to S_{mean}-S_{mid} and S_{sk}-S_{ku} groups that are weakly correlated (r = 0.29 and r = -0.32 respectively) among themselves. Contrary to the nanoscale, at the microscale all the parameters are correlated (r>0.58). Nevertheless, two subgroups are slightly differently related by their correlation degree: the profile roughness parameters and the surface roughness parameters. Contact angles (θ_{left} and θ_{right}) are highly correlated (r = 0.97) among themselves regardless of the scale. Wettability did not correlate with any of the nanoroughness parameters in contrast it showed a weak and negative correlation with microroughness parameters. Correlation analysis of nano and microescale parameters in Table 7 presented few and weak correlations.

Results of Kruskal–Wallis ($p<0.01$) and Mann-Whitney U test ($p<0.003$) (Tables 2, 3) show that S_a roughness parameter exhibited the highest discrimination power at both scales.

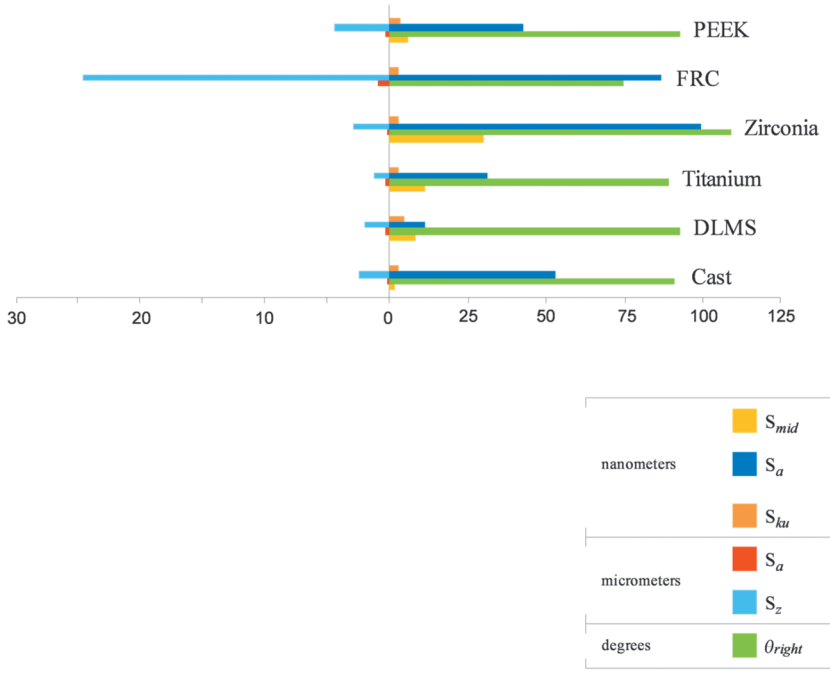

Figure 1. Characterization of the materials according to the selected parameters.

Table 5. Correlation matrix showing correlation coefficients (r values) for nanoscale roughness parameters and wettability.

	S_{min}	S_{max}	S_{mid}	S_{mean}	S_{pv}	S_q	S_a	S_z	S_{sk}	S_{ku}	θ_{left}
S_{max}	-0.86**										
S_{mid}	0.09	0.26*									
S_{mean}	-0.02	0.20*	0.29**								
S_{pv}	-0.94**	0.96**	0.07	0.10							
S_q	-0.91**	0.92**	0.04	0.10	0.96**						
S_a	-0.90**	0.90**	0.03	0.10	0.94**	0.99**					
S_z	0.18	0.96**	0.08	0.10	1.00**	0.96**	0.94**				
S_{sk}	-0.18	-0.10	-0.53**	-0.09	0.05	0.15	0.17	0.05			
S_{ku}	0.07	-0.01	0.16	-0.09	-0.06	-0.23*	-0.27**	-0.06	-0.32**		
θ_{left}	0.06	-0.06	-0.11	-0.08	-0.05	-0.05	-0.06	-0.04	-0.02	0.02	
θ_{right}	0.05	-0.05	-0.08	-0.08	-0.04	-0.04	-0.04	-0.04	0.03	0.03	0.97**

**$p < 0.01$
*$p < 0.05$

Table 6. Correlation matrix showing correlation coefficients (r values) for microscale roughness parameters and wettability.

	S_a	S_z	S_q	R_p	R_v	R_z	R_t	R_a	R_q	θ_{left}
S_z	0.75**									
S_q	0.94**	0.87**								
R_p	0.84**	0.65**	0.77**							
R_v	0.69**	0.58**	0.66**	0.85**						
R_z	0.81**	0.65**	0.75**	0.95**	0.93**					
R_t	0.84**	0.71**	0.79**	0.88**	0.78**	0.99**				
R_a	0.87**	0.65**	0.79**	0.96**	0.88**	0.96**	0.88**			
R_q	0.85**	0.66**	0.79**	0.96**	0.87**	0.96**	0.89**	0.99**		
θ_{left}	-0.22*	-0.19	-0.21*	-0.18	-0.25*	-0.24*	-0.28**	-0.22**	-0.22**	
θ_{right}	-0.26*	-0.23*	-0.26*	-0.19	-0.25*	-0.25	-0.29*	-0.24*	-0.24*	0.97**

**$p < 0.01$
*$p < 0.05$

Table 7. Correlation matrix showing correlation coefficients (r values) for microscale and nanoscale roughness parameters.

	S_a	S_z	S_q	R_p	R_v	R_z	R_t	R_a	R_q
S_{min}	-0.31**	-0.21	-0.25*	-0.27**	-0.18	-0.25*	-0.19	-0.28**	-0.27**
S_{max}	0.23*	0.15	0.23*	0.23*	0.17	0.21*	0.16	0.23*	0.22*
S_{mid}	-0.15	-0.16	-0.10	-0.04	-0.03	-0.04	-0.07	-0.07	-0.07
S_{mean}	0.06	0.03	0.06	0.04	0.03	0.04	0.15	0.03	0.03
S_{pv}	0.29**	0.20	0.27**	0.27**	0.19	0.25*	0.20	0.28**	0.27*
S_q	0.25*	0.14	0.21*	0.24*	0.16	0.20	0.19	0.23*	0.22*
S_a	0.21	0.09	0.16	0.21*	0.13	0.17	0.16	0.20	0.19
S_z	0.29**	0.19	0.27**	0.28**	0.19	0.25*	0.20	0.28**	0.27*
S_{sk}	0.07	0.09	0.02	0.06	0.10	0.07	0.16	0.07	0.08
S_{ku}	-0.24*	-0.02	-0.15	-0.17	-0.12	-0.09	-0.20	-0.15	-0.13

**$p < 0.01$
*$p < 0.05$

Characterization of the tested materials

Results of the characterization of the analyzed materials showed that FRC was found to be the roughest while DLMS Co-Cr resulted the smoothest. Zirconia was shown to be the most hydrophilic whereas FRC resulted the most hydrophobic material. Finally, in Figure 1 a graphic representation of the discrimination of the materials according to the selected parameters is described.

DISCUSSION

Several attempts have been made to establish a set of surface parameters giving the optimum surface description for the discrimination of materials (Stout *et al.,* 1994; Crawford *et al.,* 2012; Webb *et al.,* 2013). However, the statistical dependence of the surface parameters has rarely been analyzed. The present study is in agreement with previous studies that state that the commonly used parameters to characterize biomaterials are redundant (Stout *et al.,* 1994; Crawford *et al.,* 2012;

Webb *et al.,* 2013). A set of six parameters giving the highest discriminatory power (S_a,$S_{ku,}$ and S_{mid} at the nanoscale, S_a and S_z at the microscale and θ_{right}) where selected out of 21 parameters to represent the whole group of parameters.

The poor correlations exhibited among the nanoscale surface parameters are in agreement with previous studies (Rosén *et al.,* 2008). However the strong correlations displayed by the S_a-S_{max}-S_{min}-S_{pv}-S_q-S_z cluster of parameters means that the determination of one of the parameters automatically leads to the definition of the others. S_{mean}-S_{mid} and S_{sk}-S_{ku} groups are not correlated thereby they provide additional complementary information. The present results may be explained by the fact that all the highly correlated parameters are height descriptors, S_{mean}, S_{mid} are normality height descriptors and S_{sk}, S_{ku} describe the spatial surface topography. Regarding the most correlated group, the criteria for selecting the parameter to represent the group was based on the most sensitive parameter in the materials discrimination which was found to be S_a (Table 2). From the less correlated groups, the criteria for selecting the parameter was the lesser correlation of parameters. Hence, a preliminary set of three independent parameters, S_a, S_{mid} and S_{ku} was selected.

S_a (or its counterpart R_a) is one of the most commonly used parameters to quantify surface topography (Whitehead *et al.,* 2005; Truong *et al*., 2010; Crawford *et al*., 2012). It quantifies the "absolute" magnitude of surface heights but in contrast, is insensitive to the spatial distribution of the heights. Similarly to previous studies, our results highlight that the S_a value is insufficient for the surface discrimination of biomaterials at the nanoscale and spatial surface descriptors are needed for an optimized surface characterization (Ivanova *et al.,* 2010; Webb *et al.,* 2012). In practical terms, kurtosis values describe the shape of the distribution of the heights; (i.e. normal distributions have kurtosis value of 3 while sharper distributions have higher values and rounded distributions have lower). In the present study, DLMS Co-Cr and PEEK showed the smoothest surfaces at the nanoscale obtaining kurtosis values > 3 compared to the rest of materials, which had values of < 3. On the other hand, the zero value for S_{sk}, (skewedness is a measure of the symmetry of height distribution) reflects symmetrical height distribution and these results are corroborated by a zero value for S_{mean}. This may be explained by the fact that the materials underwent polishing procedures. It is evident that these parameters (kurtosis and skewedness) are material-dependent and that either one or the other or both should be addressed depending on the required information (Crawford *et al.,* 2012). To the author´s knowledge, S_{mid} has not been addressed before.

The applicability of the first subset of parameters has also played a role in determining bacterial adhesion. Thereby, in the study of Webb et al. the S_a, S_q and S_{max} parameters gathered similar bacterial counts in contrast to S_{sk} and S_{ku} (Webb *et al.,* 2013).

In contrast to the nanoscale, at the microscale, all the roughness parameters are correlated (Table 5) nevertheless, profile values are slightly differently related by their correlation degree to surface values. These findings are comparable to previous studies (Nowicki, 1985; Rosén et al 2008; Ham and Powers, 2014); however, the different correlation values obtained by Ham et al. is due to the different averaging methods. In their study the mean of 3 calculations was computed while in ours the median of 16 calculations. Due to the fact that all the parameters are correlated, the selection of the best set of roughness parameter for is hindered. Therefore, S_a was selected to represent the whole group of parameters for being the most sensitive parameter on the pair-wise material discrimination at the microscale (Table 3).

This result is confirmed by recent studies which recommended the selection of S values as they are obtained from the surface and thus are more representative compared to those obtained from the profile (Webb *et al* 2013). In the present study, S_z shows the lowest correlation value with S_a and with the rest of parameters and thus could be considered as a useful complementary roughness parameter. The efficiency of both parameters determined as the average and the maximum values has been widely used for material discrimination (Gorlenko *et al.,* 1981; Nowicki, 1985; Gittens *et al.,* 2013). Thus at the microscale subset, the two selected parameters are S_a and S_z.

The few and weak correlations encountered among nano and microroughness (Table 7) suggest that both techniques give complementary information and thus it is of paramount concern to include two different scales. These results are in agreement with previous authors' recommendations of using optical measuring methods such as white light interferometry to expand the AFM measuring range and to improve roughness measuring efficiency (Tyrrell *et al.,* 2004; Guo *et al.,* 2011). Therefore, in general S_a-S_{ku}-S_{mid} at the nanoscale and S_a-S_z at the microscale are not

correlated being confirmed the complementarity of both groups of parameters.

As first described by Wenzel, an intimate relationship between surface roughness and wettability exists (Wenzel, 1949). Nevertheless, this correlation was not observed at the nanoscale. Likewise in a recent study, no correlation was found between roughness and wettability at the nanoscale (Gittens *et al.,* 2013). While wettability values did not correlate with nanoroughness parameters, they correlated poorly with microroughness parameters. The negative correlation encountered indicates that as the roughness value increases the external angle contact value decreases and vice versa. This is explained by Wenzel´s method that states that roughness induces hydrophobicity (Wenzel, 1949) and has been confirmed in previous studies (Gittens *et al.,* 2011; Webb *et al.,* 2013).

The selected parameters are efficient in characterizing and differentiating between materials and the obtained characterizations are in agreement with previous studies (Ivanova *et al.,* 2010 Rosentritt *et al.,* 2009; Adbulmajeed *et al.,* 2014; Ourahmoune *et al.,* 2014; Kim *et al.,* 2015). FRC exhibited the highest roughness value Sa <0.2 μm among the tested materials values but in the range of previous studies (Tanner *et al.,* 2003; Garoushi *et al*., 2009; Adbulmajeed *et al.,* 2014). In contrast, DLMS Co-Cr obtained the lowest roughness value. This finding is in agreement with recent studies that support the notion that the powder additive manufacturing layer by layer improves the surface compared to the conventional casting methods (Oyagüe *et al.,* 2012; Castillo-Oyagüe, 2013). However, this finding is not in accordance with a recent study where the average roughness value of DLMS was significantly higher compared to cast Co-Cr. One explanation could be differences in the composition of the used metal alloys (Kilicarslan and Ozcan, 2012).

Previous studies have shown that smooth microscale surface characteristics (R_a less than 0.1 μm) have minor influence on the surface wettability of a surface (Busscher *et al*., 1994; Adbulmajeed *et al*., 2011). In those studies smooth surfaces displayed contact angles that ranged between 60º and 86º and the differences of the contact angles were related to the surface chemistry. The present study, is in agreement with those studies since all the smooth surfaces investigated (all the materials except for FRC) showed contact angle values within this given range. Accordingly, rough FRC surfaces showed a contact angles above 86º showing a similarity in the trend claimed by Wenzel (Wenzel, 1949). Wettability values in general are also in agreement with previous studies except for the Zirconia which showed the highest contact angle value roughness can be considered This may be explained by the fact that the surfaces were rougher than in previous studies (Att *et al.,* 2009). On the other hand, FRC showed the lowest wettability, which may be explained by the influence of fibers on the wettability behavior of composite materials (Adbulmajeed *et al.,* 2014).

The limitations of measuring devices may introduce errors during data acquisition which may reflect on the final surface characterization. For instance, even the very sharp tip of an AFM shows limitations, and the optical methods are limited when recording small wavelength components. In addition to this, filtering techniques should be considered with care.

Correlation tests can be carried out to systematize the choice of a set of parameters when multiple parameters have to be reduced. The selection of parameters should be founded on the results of the degree of correlation between the multiple parameters and the required properties regarding their application site. This set of parameters was efficient in differentiating between six types of materials at the nano and microscale. The adoption of this proposed set of parameters will enable universal comparisons.

CONCLUSIONS

The present study proposes 6 parameters for characterizing biomaterial surfaces:

S_a-S_{ku}-S_{mid} at the nanoscale, S_a-S_z at the microscale and one angle contact value are suggested for surface characterization.

Roughness quantification at two different scales gave complementary information.

Wettability was not correlated with nanoroughness. In contrast, it was correlated with rough surfaces at the microscale.

REFERENCES

Abdulmajeed AA, Walboomers XF, Massera J, Kokkari AK, Vallittu PK, Närhi TO. 2014. Blood and fibroblast responses to thermoset BisGMA-TEGDMA/glass fiber-reinforced composite implants in vitro. Clin Oral Implants Res. 25:843-851.

Abdulmajeed AA, Lassila LV, Vallittu PK, Närhi TO. 2011. The effect of exposed glass fibers and particles of

bioactive glass on the surface wettability of composite implants. Int J Biomater. doi: 10.1155/2011/607971

Att W, Takeuchi M, Suzuki T, Kubo K, Anpo M, Ogawa T. 2009. Enhanced osteoblast function on ultraviolet light-treated zirconia. Biomaterials 30:1273–1280.

Binnig G, Quate CF, Gerber C. 1986. Atomic force microscope. Phys Rev Lett 56:930-933.

Busscher H J, Van Pelt AWJ, De Boer P, De Jong HP, Arends J. 1984. The effect of surface roughening of polymers on measured contact angles of liquids. *Colloids and Surfaces*, *9*(4), 319-331.

Castillo-Oyagüe R, Lynch CD, Turrión AS, López-Lozano JF, Torres-Lagares D, Suárez-García MJ. 2013. Misfit and microleakage of implant-supported crown copings obtained by laser sintering and casting techniques, luted with glass-ionomer, resin cements and acrylic/urethane-based agents. J Dent. 41:90-96.

Crawford RJ, Webb HK, Truong VK, Hasan J, Ivanova EP. 2012. Surface topographical factors influencing bacterial attachment. Adv Colloid Interface Sci 179–182:142–149.

De Chiffre L, Lonardo P, Trumpold H, Lucca DA, Goch G, Brown CA, Raja J, Hanse HN. Quantitative characterisation of surface texture. CIRP Annals-Man Tech. 49: 635-652.

Dong WP, Sullivan PJ, Stout KJ. 1994. Comprehensive study of parameters for characterising three-dimensional surface topography: III: Parameters for characterizing amplitude and some functional properties, Wear 178:29-43.

Dorobantu LS and Gray MR. 2010. Application of atomic force microscopy in bacterial research. Scanning 32:74-96.

Etxeberria M, López-Jiménez L, Merlos A, Escuín T, Viñas M. 2013. Bacterial adhesion efficiency on implant abutments: a comparative study. Int Microbiol 16:235-242.

Gittens RA, McLachlan T, Olivares-Navarrete R, Cai Y, Berner S, Tannenbaum R, Schwartz Z, Sandhage KH, Boyan BD. 2011. The effects of combined micron-/submicron-scale surface roughness and nanoscale features on cell proliferation and differentiation. Biomaterials 32:3395-3403.

Gittens RA, Olivares-Navarrete R, Cheng A, Anderson DM, McLachlan T, Stephan I, Geis-Gerstorfer J, Sandhage KH, Fedorov AG, Rupp F, Boyan BD, Tannenbaum R, Schwartz Z. 2013. The roles of titanium surface micro/nanotopography and wettability on the differential response of human osteoblast lineage cells. Acta Biomater 9:6268-6277.

Gorlenko OA. 1981. Assessment of surface roughness parameters and their interdependence. Precis Eng 3:105-108.

Guo T, Wang S, Dorantes-Gonzalez DJ, Chen J, Fu X, Hu X. 2011. Development of a hybrid atomic force microscopic measurement system combined with white light scanning interferometry. Sensors 12:175-188.

Ham M, Powers BM. 2014. Roughness parameter selection for novel manufacturing processes. Scanning 36:21-29.

Hove LH, Holme B, Young A, Tveit AB. 2007. The erosion-inhibiting effect of TiF4, SnF2, and NaF solutions on pellicle-covered enamel in vitro. Acta Odontol Scand 65:259-264.

Ivanova EP, Truong VK, Wang JY, Berndt CC, Jones RT, Yusuf II, Peake I, Schmidt HW, Fluke C, Barnes D, Crawford RJ. 2010. Impact of nanoscale roughness of titanium thin film surfaces on bacterial retention. Langmuir 26:1973-1982.

Kilicarslan MA, Ozkan P. 2012. Evaluation of retention of cemented laser-sintered crowns on unmodified straight narrow implant abutments. Int J Oral Maxillofac Implants 28:381-387.

Kim YS, Shin SY, Moon SK, Yang SM. 2015. Surface properties correlated with the human gingival fibroblasts attachment on various materials for implant abutments: A multiple regression analysis. Acta Odontol Scand 73:38-47.

Lassila LV, Garoushi S, Tanner J, Vallittu PK, Söderling E. 2009. Adherence of Streptococcus mutans to Fiber-Reinforced Filling Composite and Conventional Restorative Materials. Open Dent J 4:227-232.

Nowicki B. 1985. Multiparameter representation of surface roughness. Wear 102:161-176.

Ourahmoune R, Salvia M, Mathia TG, Mesrati N. 2014. Surface morphology and wettability of sandblasted PEEK and its composites. Scanning 36:64-75.

Oyagüe RC, Sánchez-Turrión A, López-Lozano JF, Montero J, Albaladejo A, Suárez-García MJ. 2012. Evaluation of fit of cement-retained implant-supported 3-unit structures fabricated with direct metal laser sintering and vacuum casting techniques. Odontology 100:249-253.

Park JH, Wasilewski CE, Almodovar N, Olivares-Navarrete R, Boyan BD, Tannenbaum R, Schwartz Z. 2012. The responses to surface wettability gradients induced by chitosan nanofilms on microtextured titanium mediated by specific integrin receptors. Biomaterials 33:7386-7393.

Rosén BG, Anderberg C, Ohlsson R. 2008. Parameter correlation study of cylinder liner roughness for production and quality control. Proceedings of the Institution of Mechanical Engineers. Part B: Journal of Engineering Manufacture 222:1475-1487.

Rosentritt M, Behr M, Bürgers R, Feilzer AJ, Hahnel S. 2009. In vitro adherence of oral streptococci to zirconia core and veneering glass-ceramics. J Biomed Mater Res B Appl Biomaterials 91:257-263.

Tanner J, Carlén A, Söderling E, Vallittu PK. 2003. Adsorption of parotid saliva proteins and adhesion of Streptococcus mutans ATCC 21752 to dental fiber-reinforced composites. J Biomed Mater Res B Appl Biomater 15:391-398.

Truong VK, Lapovok R, Estrin YS, Rundell S, Wang JY, Fluke CJ, Crawford RJ, Ivanova EP. 2010. The influence of nano-scale surface roughness on bacterial adhesion to ultrafine-grained titanium. Biomaterials 31:3674-3683.

Tyrrell JW, Dal Savio C, Krüger-Sehm R, Danzebrink HU. 2004. Development of a combined interference microscope objective and scanning probe microscope. Rev Sci Inst 75: 1120-1126.

Webb HK, Boshkovikj V, Fluke CJ, Truong VK, Hasan J, Baulin VA, Lapovok R, Estrin Y, Crawford RJ, Ivanova EP. 2013. Bacterial attachment on sub-nanometrically smooth titanium substrata. Biofouling 29:163-170.

Webb HK, Truong VK, Hasan J, Fluke C, Crawford RJ, Ivanova EP. 2012. Roughness parameters for standard description of surface nanoarchitecture. Scanning 34:257-263.

Whitehead KA, Colligon J, Verran J. 2005. Retention of micro-bial cells in substratum surface features of micrometer and sub-micrometer dimensions. Colloid Surf B Biointerfaces 41:129-138.

Whitehouse DJ. 1982. The parameter rash—is there a cure? Wear 83:75-78.

Wenzel RN. 1949. Surface roughness and contact angle. J Phys Colloid Chem 53:1466-1467.

RESEARCH ARTICLE

INTERNATIONAL MICROBIOLOGY (2013) 16:235-242
doi: 10.2436/20.1501.01.199 ISSN 1139-6709 www.im.microbios.org

INTERNATIONAL MICROBIOLOGY
OPEN ACCESS

Bacterial adhesion efficiency on implant abutments: A comparative study

Marina Etxeberria,[1,2] Lidia López-Jiménez,[1] Alexandra Merlos,[1] Tomás Escuín,[2] Miguel Viñas[1]*

[1]Laboratory of Molecular Microbiology and Antimicrobials. Department of Pathology and Experimental Therapeutics, University of Barcelona, Barcelona, Spain. [2]Laboratory of Prosthodontics, Department of Dentistry, Medical and Dentistry Schools, University of Barcelona, IDIBELL, Barcelona, Spain

Received 28 October 2013 · Accepted 5 December 2013

II

Summary. The attachment of *Escherichia coli* ATCC 25922 and *Staphylococcus aureus* ATCC 28213 onto six different materials used to manufacture dental implant abutments was quantitatively determined after 2 and 24 h of contact between the materials and the bacterial cultures. The materials were topographically characterized and their wettability determined, with both parameters subsequently related to bacterial adhesion. Atomic force microscopy, interferometry, and contact angle measurement were used to characterize the materials' surfaces. The results showed that neither roughness nor nano-roughness greatly influenced bacterial attachment whereas wettability strongly correlated with adhesion. After 2 h the degree of *E. coli* attachment markedly differed depending on the material whereas similar differences were not observed for *S. aureus*, which yielded consistently higher counts of adhered cells. Nevertheless, after 24 h the adhesion of the two species to the different test materials no longer significantly differed, although on all surfaces the numbers of finally adhered *E. coli* were higher than those of *S. aureus*. [**Int Microbiol** 2013; 16(4):235-242]

Keywords: implant abutments · glass fiber · bacterial adhesion · nano-roughness · wettability · biomaterials

Introduction

Bacteria can grow as sessile forms (biofilms) on almost all surfaces and under almost any environmental condition. In most infectious diseases, particularly those arising from infected implants and medical devices, bacterial growth as biofilms plays a crucial role in disease pathogenesis [6]. Among all known biofilms occurring in pathologic settings, those in the oral cavity provide a good model system and as such have been extensively studied [13]. Oral biofilms are formed by a wide variety of gram-positive and gram-negative bacteria species and are a consistent feature of oral infections, mainly caries, periodontitis, and endodontitis, but they are also involved in infection-related implant failures, so-called peri-implantitis [23]. The adhesion and development of microbial biofilms depend upon the characteristics of the microbes that form them, but also on the environmental conditions. Chemical and surface properties such as roughness, nano-roughness, and wettability are relevant in controlling bacterial adhesion [28].

*Corresponding author: M. Viñas
Laboratory de Microbiologia Molecular
Facultat de Medicina. Universitat de Barcelona
Feixa Llarga s/n
08907 Hospitalet de Llobregat, Spain
Tel. +34-934024265
E-mail: mvinyas@ub.edu

One of the main goals of oral implantology is to significantly reduce the risk of infection, e.g., by altering the local environment such that it is less favorable for bacterial biofilm formation. Accordingly, the elucidation of the mechanisms underlying bacterial adhesion, colonization, and biofilm development on prosthetic devices and implant surfaces is currently an area of great interest in both clinical and biomedical research. From a biomechanical engineering standpoint, the physical properties of implant surfaces can be optimized by taking advantage of recent progress in both materials science and nanotechnology. By modulating cell-substrate interactions, for example, the biological response of the infectious agent can be determined [2,23,27].

The effect of surface topography on cell attachment has received significant attention, with several recently published studies highlighting the critical role in cellular adherence played by nanotopography [19,20,22]. Nano-engineered surfaces can directly influence bacterial behavior, as shown in studies demonstrating that these cells align in the anisotropic direction of microscale ridges and grooves [14]. Based on these findings, a possible approach to restrict biofilm formation involves the use of materials whose surface properties hinder biofilm development, particularly in the early stages of implantation [13]. Different strategies can be adopted to achieve this purpose, such as by altering the nanoscale surface topography. However, there is no consensus regarding whether increased surface roughness correlates either positively or negatively with the extent of bacterial attachment. Clearly, materials enhancing biofilm formation should be discarded even if they have excellent mechanical properties.

Metals, ceramics, polymers, and composites are currently used to manufacture prosthetic implant abutments. Among these materials, glass fiber-reinforced composites (glass-FRC) are a promising low-cost alternative to metal alloys, metal ceramics, and ceramic restorations. Indeed, in the last few years glass-FRCs have been used successfully in a variety of dental applications [1,10]. Implant-supported fixed prostheses of glass-FRC may also offer a suitable alternative [5,11], but the potential and limitations of this promising material have not been adequately evaluated.

A few studies have specifically examined the effect of the nanoscale morphology of dental implant abutment materials, and especially titanium, on surface-bacteria interactions in vitro. However, little is known about the extent of bacterial attachment on nanometrically characterized implant abutment surfaces, whether of titanium or other metals. Experimental approaches to explore topography with respect to bacterial adhesion include experimental bacteriology, atomic force microscopy (AFM), interferometry, and wettability measurements. In this study, we analyzed and compared the surface properties, roughness, and wettability of six test materials used in the manufacture of implant abutments in terms of the adhesion of the gram-positive bacterium *Staphylococcus aureus* and the gram-negative bacterium *Escherichia coli*. Our aim was to evaluate the biocompatibility of glass-FRC and the potential application of this material in dentistry.

Materials and methods

Dental materials. Disks 10 mm in diameter and 2 mm thick were manufactured from each of six different implant abutment materials. The tested materials were: (i) Cast cobalt-chromium disks obtained from acrylic resin patterns (Pattern Resin LS, GC Corp.) and invested with phosphate-bonded investment material (CM-20 Cendrex+Métaux, Biel/Bienne, Switzerland) as indicated by the manufacturer (BEGO, Bremer Goldschlägerei Wilh. Herbst, Bremen, Germany). Casting was accomplished using Co-Cr Wirobond C alloy (BEGO). After melting and casting by induction (Ducatron Série 3 UGIN'Dentaire, Seyssins, France), the disks were sandblasted with 110-µm aluminum oxide particles (Korox, BEGO) under 3 bar pressure to remove oxide films and residual investment. (ii) Selective laser melted (SLM) Co-Cr disks (BEGO). Both the cast and the SLM Co-Cr disks were polished in three stages: (a) using a hard rubber disk at 15,000 rpm; (b) then with a soft rubber disk at 15,000 rpm, and (c) using a soft brush with a polishing paste at 1400 rpm. Each polishing phase lasted 90 s. (iii) Machined and polished titanium grade V disks (Klockner-Soadco, Andorra). (iv) Zirconia (Y-TZP) disks (Dentisel, Barcelona, Spain). (v) Glass-FRC disks, prepared from rods (Bioloren, Saronno, Varese, Italy). And (vi) polyetheretherketone (PEEK) disks, prepared from rods (Teknimplant, Barcelona, Spain). All disks were handled by their lateral walls. They were gently cleaned using a cotton pellet with ethanol and dried under warm dry air.

Surface characterization. The disk surfaces were analyzed by three different methods: (i) Atomic force microscopy. It was carried out with an AFM XE-70 (Park Systems, Korea) in non-contact mode. The rectangular-shaped cantilever (ACTA Si-cantilevers, Park Systems) had a force constant of 40 N/m, a resonance frequency of 300 kHz, and a tip radius with a curvature of <10 nm. All AFM variables, including scan rate and set point, were optimized for the type of sample measured. Scan areas were 5 × 5 µm², with a scan rate of 0.6 Hz and a resolution of 256 × 256 pixels. AFM images were processed using a scanning probe image processor XEI (Park Systems), correcting the plane of the AFM image for possible coupling of the lateral plane and the *z*-axis, caused by the instrument. The height, area, and volume of the surfaces were determined via polygon/ellipse/circle methods, in which a suitable shape is best fitted to the image. The average surface roughness (Ra) was calculated. (ii) White light interferometry; the specimens were visualized on a white light interferometer microscope (LeicaSCAN DCM3D, Leica Microsystems, Switzerland), which is a computerized optical interference microscope operating in the vertical scanning interferometry mode and producing a topographic image. The objective used was Leica N Plan H 50×/0.50, with an Mirau-interferometer objective lens and an image resolution of 250.64 × 190.90 µm². Images were analyzed using the software Leica map DCM 3D 6.2.6561 version (Leica Microsystems); the threshold was set to 1.0% and the Gauss filter to 25 µm. Ra was determined. And (iii) surface wettability measurements; they were conducted by measuring the contact angle using the sessile water-drop method [13,24]. Briefly, 10 µl of MilliQ-quality water was dropped onto the center of each specimen using an injector. Digital photo-

Table 1. Bacterial adhesion expressed as colony-forming units (CFU)/mm² (average of 16 determinations). SLM, selective laser melted; PEEK polyetheretherketone

	Staphylococcus aureus		*Escherichia coli*	
Material	CFU/mm² (2 h)	CFU/mm² (24 h)	CFU/mm² (2 h)	CFU/mm² (24 h)
Cast Co-Cr	1.82×10^2	7.74×10^4	6.38×10^1	4.46×10^6
SLM Co-Cr	1.14×10^2	6.38×10^4	4.56	4.92×10^6
Titanium	1.18×10^2	6.83×10^4	1.41×10^1	7.84×10^6
Zirconia	3.42×10^2	3.37×10^5	1.00×10^1	4.92×10^6
GF-reinforced composite	2.64×10^2	4.15×10^5	2.73×10^2	4.24×10^6
PEEK	1.00×10^2	5.92×10^4	2.51×10^2	5.65×10^6

graphs were taken (Nikon D70) and the resulting images were analyzed using IMAT software (CCIT, Barcelona, Spain). Sixteen samples were measured in each group, with each disk measured twice.

Bacterial strains and culture media. Two collection bacterial strains were used to assess the adhesion properties of gram-negative and gram-positive bacteria on the test materials: *Escherichia coli* strain ATCC 25922 and *Staphylococcus aureus* strain ATCC 28213, respectively. Both strains were maintained on trypticase soy agar (TSA, Sharlau, Barcelona, Spain) plates. Adhesion experiments were carried out using two colonies selected from the plates to inoculate trypticase soy broth (TSB, Scharlau). The cultures were incubated at 37 ºC in a rotary shaker at 240 rpm in air for 18 h, at which time they had reached the late exponential phase of growth.

Adhesion experiments. Disks to be used in the bacterial assays were sterilized in an autoclave (121 ºC, 15 min). The above-described overnight cultures were diluted in TSB to the desired concentration (10^6 colony forming units [CFU]/ml in TSB), as determined spectrophotometrically. For the adhesion experiment, the disks were covered with a suspension of the bacterial culture and incubated at 37 ºC with gentle (60 rpm.) shaking. samples were taken 2 and 24 h later, processing the disks by washing them four times in Ringer's 1/4 to remove unattached bacteria and then placing them in test tubes containing 1 ml of Ringer's 1/4. The tubes were submerged in an ultrasonic water bath for 3 min, vigorously vortexed for 1 min, and then treated ultrasonically again for 3 min to release the surface-attached bacteria. Serial dilutions (10^0 to 10^{-7}) of these suspensions were used to inoculate agar plates, which were incubated for 48 h. Colonies were then scored and counted. The detachment of biofilm-forming bacteria from the disks was monitored by microscopic visualization of the disks after sonication and vortexing.

Atomic force microscopy imaging. Bacteria were cultured in liquid media in which disks of tested materials were submerged; disks were then washed four-fold by using Ringer's 1/4 and allowed to dry on air. Samples were imaged in air by using an atomic force microscope XE-70 [Park Systems]. All images were collected in non-contact mode by using rectangular-shaped silicon cantilevers with a spring constant of ± 40 N/m and a resonance frequency of ±300 kHz. The upper surface of these cantilevers (the opposite side of the tip) is coated with aluminium to enhance the laser beam reflectivity. The data acquired during the surface scanning were converted into images of topography, amplitude and phase; and analysed by using XEP and XEI software (Park Systems). On topography images, it becomes possible to observe the shape, structure and differences of the sample surface, amplitude images accentuating the edges gives roughness and height information. Finally, the phase images show variations in elasticity and viscoelasticity of the sample. The four types of image were simultaneously acquired with scan size of 25 µm² at a scan rate of 0.6 Hz.

Table 2. Roughness values as determined by interferometry and atomic force miscroscopy. SLM, selective laser melted; PEEK, polyetheretherketone

	Roughness	Nanoroughness
	White light interferometry	Atomic force interferometry
Material	Ra (µm)	Ra (nm)
Cast Co-Cr	0.0776	48
SLM Co-Cr	0.0388	14
Titanium	0.0474	29
Zirconia	0.108	136
GF-reinforced composite	0.553	236
PEEK	0.113	59

Results

Bacterial adhesion of gram-positive *S. aureus* and gram-negative *E. coli* onto disks of the tested materials were compared. The results are summarized in Table 1. Surface roughness, determined as the mean arithmetic surface roughness (Ra), was characterized by interferometry and AFM, as shown in Table 2. The angles formed between water and the test materials resulted to be as follows: the lowest angle (75º 64′) was formed on zirconia, followed by cast Co-Cr (79º 71′); three of the tested materials gave quite similar angles: SLM Co-Cr (85º 4′), Titanium (84º 23′) and PEEK (89º 75′), whereas the highest value corresponded to GF-reinforced composite (113º 36′). A set of selected images showing the surface roughness are presented for comparison in Fig. 1 (interferometry) and Fig. 2 (AFM).

Imaging of bacterial cells grown as sessile forms onto the different tested material surfaces allowed to distinguish details concerning adhesion and morphologies. Fig. 3 shows two AFM images of both *E. coli* and *S. aureus* when developing biofilms onto glass-FRC.

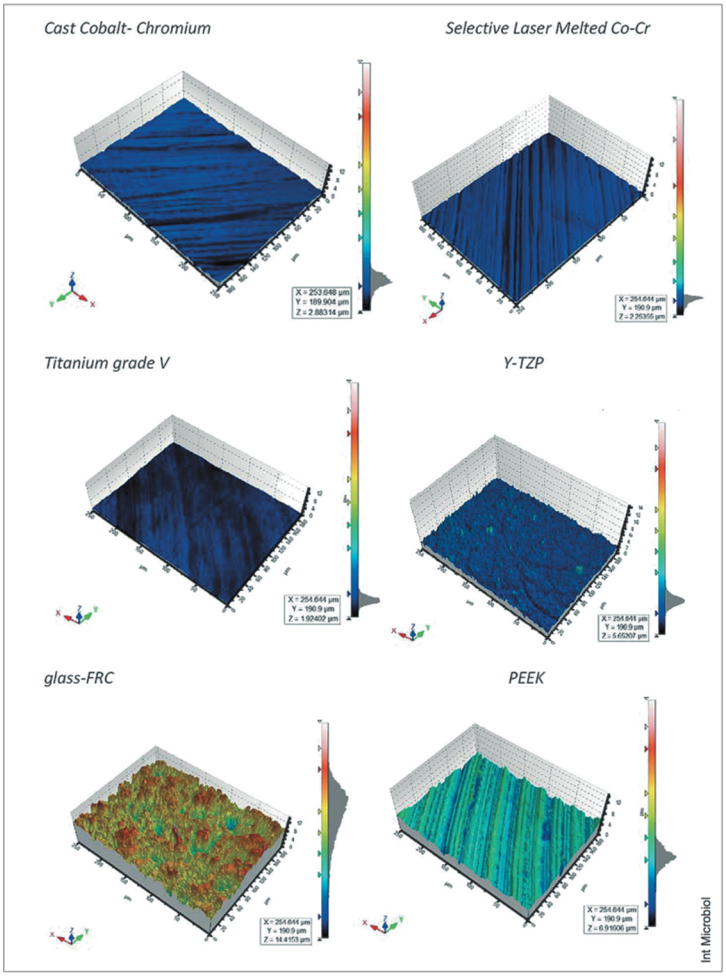

Fig. 1. Interferometry images of the six surface materials tested. **(A)** Cast cobalt- chromium. **(B)** Selective laser melted cobalt-chromium. **(C)** Titanium. **(D)** Zirconia (Y-TZP). **(E)** Glass-FRC. **(F)** PEEK polyetheretherketone.

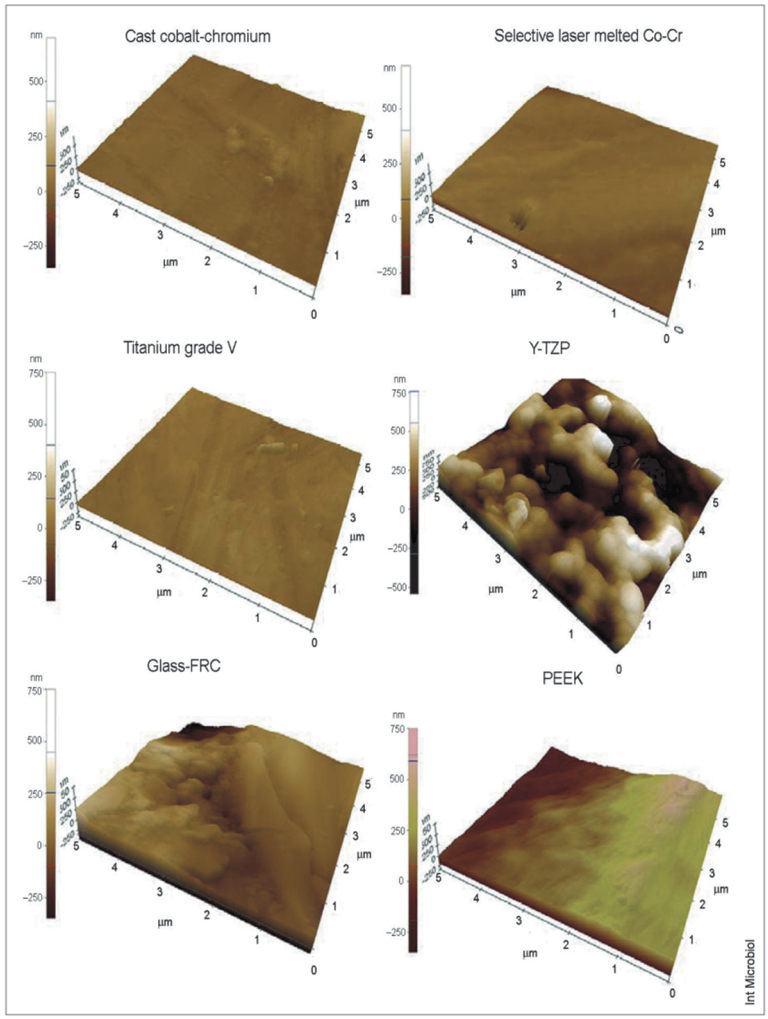

Fig. 2. AFM imaging of the six surface materials tested. **(A)** Cast cobalt-chromium. **(B)** Selective laser melted cobalt-chromium. **(C)** Titanium. **(D)** Zirconia (Y-TZP). **(E)** Glass-FRC. **(F)** PEEK polyetheretherketone.

Discussion

The ability of bacteria to form biofilms is among the most relevant factors in the pathogenesis of peri-implantitis and periodontitis. Since both gram-positive and gram-negative bacteria cause oral infections, in this study representatives of each one (*E. coli* and *S. aureus*) were used to determine bacterial adhesion to the six tested materials. Our primary aim was to compare the efficiency of bacterial adhesion onto implant abutments currently in use, especially glass-FRC in order to assess its potential advantages. This focus reflects current interest in glass-FRC as an alternative to traditionally used materials. A recent report, showed that the use of glass-FRC for implant abutment or restoration material could significantly reduce physical stresses in the bone-implant contact area by

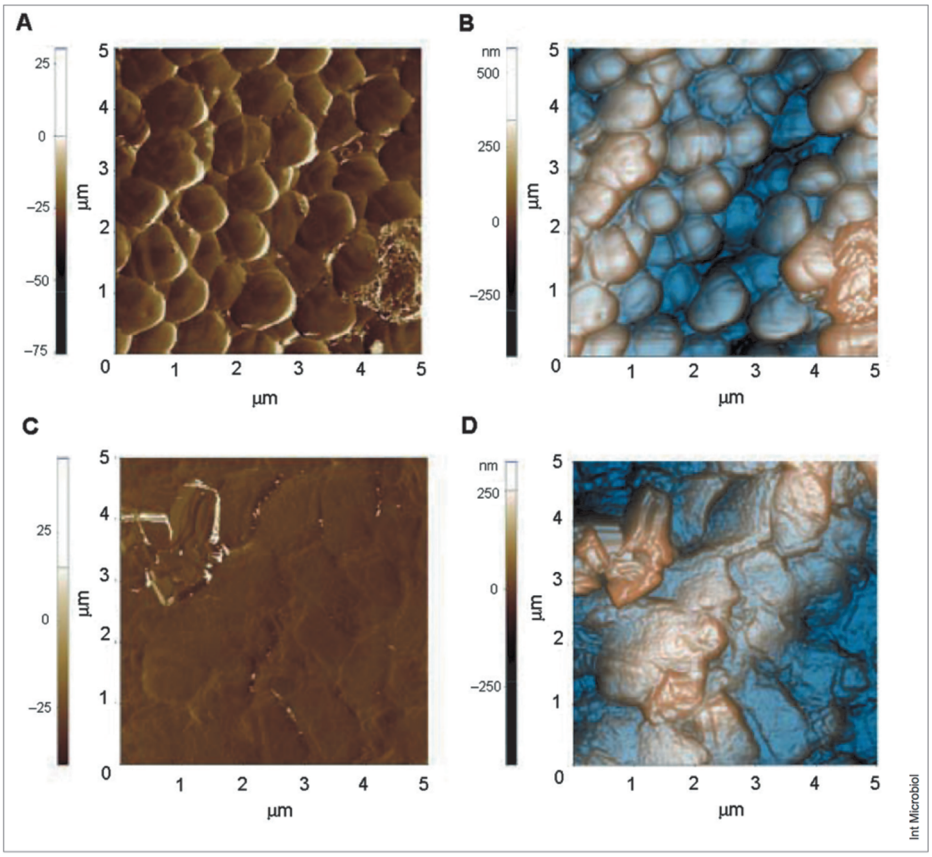

Fig. 3. AFM imaging on glass-FRC disks: (**A**) *Staphylococcus aureus* phase; (**B**) *S. aureus* topography; (**C**) *Escherichia coli* phase; (**D**) *E. coli* topography.

acting as shock-absorbers and thus minimize the risk of eventual peri-implant bone loss [18]. However, there is still much to be learned about the potential application of glass-FRC. Progress in nanotechnology allows the design and production of materials, including biomaterials, with surface properties tailored to a given application. Today, one of the main focuses of biomaterials research is the physico-chemical properties of surfaces that determine bacterial adhesion [25].

In this study, the surface parameters of dental materials were measured using three different methodologies. In surface roughness analyses, we found important differences between the studied materials, with glass-FRC being significantly rougher than the other biomaterials examined, both at micro- and nano-scales. Interferometry measurements of surface roughness showed higher values for glass-FRC than for either zirconia (5-fold) or titanium (10-fold). Similar results were obtained with AFM, which showed that the nano-roughness of glass-FRC was twice that of zirconia and eight times that of titanium. Nonetheless, the high Ra value of glass-FRC falls within the clinically acceptable range [4,25] (Table 2). The most highly polished surface was that of SLM chrome cobalt, followed by titanium. This result contradicts a previous report in which significantly greater differences in the Ra values of similar materials, including laser sinterized chrome cobalt, were reported, although in that study a profilometer was used whereas our measurements were obtained with AFM [16].

Likewise, zirconia was much rougher when assessed using AFM rather than interferometry. The discrepancy could be due to the well-recognized differences in roughness depending on the measurement method used and to the fact that zirconia surfaces are strongly affected by the material preparation procedure. In a recent study, glazing procedures were shown to reduce the surface roughness of Y-TZP [20]. In our study, AFM imaging demonstrated strong surface differences between zirconia and cast Co- Cr, laser sinterized Co-Cr, and titanium (Fig. 2).

There have been a few reports examining the relationship between nanoscale topographical details and bacterial adhesion. Microbial adhesion was shown to be sensitive to nanoscale topography (commonly accepted with feature sizes <100 nm) but universal rules of attachment have yet to be determined. For example, some investigators have observed that the attachment of certain bacteria is higher on surfaces with nanophase than with conventional topographies [15,20], while others have found a bacteria-repelling effect of nanophase materials [19]. Our results, like those of do Nascimento et al. [7,8], do not provide insights into the relationship between roughness and bacterial adhesion.

In bacterial attachment, contact between the cell and the surface is maximized. This process is aided by the ability of bacteria to assume different morphologies and to alter the number and size of their appendages, such as flagella or pili, or the amount of capsular material depending on the topographical details of the target surface or the physiological state or growth phase [14]. Gains in our knowledge of adhesion properties have important implications for the bioengineering of materials not only for use in the oral cavity but also with respect to a wide range of medical devices.

Wettability is another key determinant of bacterial adhesion efficiency. In our study, the degree of surface hydrophobicity positively correlated with the degree of surface roughness, with the roughest surface exhibiting the highest surface hydrophobicity. This correlation is in accordance with the Wenzel model, which explains roughness-induced hydrophobicity [27], and with a 2011 study reporting similar roughness-wettability correlations [15].

Our conclusions regarding bacterial adhesion are based on experiments with two different bacterial species, *S. aureus* and *E. coli*, as mechanisms of adhesion are strongly dependent upon the structure of the bacterial envelope and thus reflect the two major types of biological and chemical organization of the bacterial surface. Although our results cannot be mechanistically extended to all microbes, large differences with other oral pathogens are not expected. As seen from the data in Table 1, the dependence of adhesion on the physicochemical properties of the test materials was already evident after 2 h of incubation, since the most polished surface adsorbed the lowest amount of bacteria and vice-versa. After 24 h, differences in bacterial adhesion to the test surfaces were no longer significant, consistent with the findings in previous reports [3, 9]. While at 2 h *S. aureus* adhered more efficiently, by 24 h *E. coli* adhesion had increased.

Bacterial growth on glass-FRC was similar to that measured on titanium, confirming the results obtained in a previous study [17].The absence of a difference between the different surfaces may have been due to their wettability, since glass-FRC, is less wettable than the other materials tested. More research is needed assessing these aspects and other possible factors that may have influenced the results.

Acknowledgements.We thank Teresa Tomas for her excellent technical assistance in the preparation of the dental materials. This work was partially supported by "Ajuts a la Recerca" awarded to the School of Dentistry, University of Barcelona. The generous gift of abutment materials from Bego (Bremen, Germany), Klockner-Soadco (Andorra), Dentisel (Barcelona, Spain), Bioloren (Varese, Italy) and Tekniimplant (Barcelona, Spain) is gratefully acknowledged.

Competing interests. None declared

References

1. Adbulmajeed A, Walboomers X F, Massera J, Kokkari A K, Vallittu P K, Närhi TO (2013) Blood and fibroblast responses to thermoset BisGMA-TEGDMA/glass fiber-reinforced composite implants *in vitro*. Clin Oral Implants Res first published online: 16 apr 2013.doi: 10.1111/clr.12151
2. Anselme K, Davidson P, Popa AM, Giazzon M, Liley M, Ploux L (2010) The interaction of cells and bacteria with surfaces structured at the nanometre scale. Acta Biomater 6:3824-3846
3. Almaguer-Flores A, Olivares-Navarrete R, Wieland M, Ximénez-Fyvie LA, Schwartz Z, Boyan BD (2012) Influence of topography and hydrophilicity on initial oral biofilm formation on microstructured titanium surfaces *in vitro*. Clin Oral Implants Res 23:301-307
4. Barbosa SH, Zanata RL, Navarro MFL, Nunes OB (2005) Effect of different finishing and polishing techniques on the surface roughness of microfilled, hybrid and packable composite resins. Braz Dent J 16:39-44
5. Behr M, Rosentritt M, Lang R, Handel G. (2001) Glass fiber-reinforced abutments for dental implants. A pilot study. Clin Oral Implants Res 12:174-178
6. Costerton W, Veeh R, Shirtliff M, Pasmore M, Post, C. Ehrlich, G. (2003) The application of biofilm science to the study and control of chronic bacterial infections. J Clin Invest. 112:1466-1477
7. do Nascimento C, da Rocha Aguiar C, Pita MS, Pedrazzi V, de Albuquerque RF Jr, Ribeiro RF (2013) Oral biofilm formation on the titanium and zirconia substrates. Microsc Res Tech 76:126-132
8. do Nascimento C, Pita MS, Fernandes FHNC, Pedrazzi V, de Albuquerque RF Jr, Ribeiro RF (2013) Bacterial adhesion on the titanium and zirconia abutment surfaces. Clin Oral Implants Res 00:1-7; first published online:doi: 10.1111/clr.12093

9. Egawa M, Miura T, Kato T, Saito A, Yoshinari M (2013) In vitro adherence of periodontopathic bacteria to zirconia and titanium surfaces. Dent Mater J 32:101-106
10. Fischer H, Weber M, Eck M, Erdrich A, Marx R (2004) Finite element and experimental analyses of polymer-based dental bridges reinforced by ceramic bars. J Biomech 37:289-294
11. Freilich MA, Meiers JC, Duncan JP, Eckrote KA, Goldberg AJ (2002) Clinical evaluation of fiber-reinforced fixed bridges. J Am Dent Assoc 133:1524-1534
12. Gittens RA, Olivares-Navarrete R, Cheng A, et al. (2013) The roles of titanium surface micro/nanotopography and wettability on the differential response of human osteoblast lineage cells. Acta Biomater 9:6268-6277
13. Gorth DJ, Puckett S, Ercan B, Webster TJ, Rahaman M, Bal BS (2012) Decreased bacteria activity on Si_3N_4 surfaces compared with PEEK or titanium. Int J Nanomedicine 7:4829-4840
14. Hsu L, Fang J, Borca-Tasciuc DA, Worobo RW, Moraru CI (2013) The effect of micro- and nanoscale topography on the adhesion of bacterial cells to solid surfaces. Appl Environ Microbiol 79:2703-2712
15. Ivanova EP, Truong VK, Webb HK, Baulin VA, Wang JY, Mohammodi N, Wang F, Fluke C, Crawford RJ (2011) Differential attraction and repulsion of *Staphylococcus aureus* and *Pseudomonas aeruginosa* on molecularly smooth titanium films. Sci Rep 1:165-177
16. Kilicarslan MA, Ozkan P (2012) Evaluation of retention of cemented laser-sintered crowns on unmodified straight narrow implant abutments. Int J Oral Maxillofac Implants 28:381-387
17. Lassila LV, Garoushi S, Tanner J, Vallittu PK, Söderling E (2009) Adherence of *Streptococcus mutans* to fiber-reinforced filling composite and conventional restorative materials. Open Dent J 4:227-232
18. Magne P, Silva M, Oderich E, Boff LL, Enciso R. (2013) Damping behavior of implant-supported restorations. Clin Oral Implants Res 24:143-148
19. Puckett S D, Taylor E, Raimondo T, Webster TJ (2010) The relationship between the nanostructure of titanium surfaces and bacterial attachment. Biomaterials 31:706-713
20. Rizzello L, Sorce B, Sabella S, Vecchio G, Galeone A, Brunetti V, Cingolani R, Pompa PP (2011) Impact of nanoscale topography on genomics and proteomics of adherent bacteria. ACS Nano 5:1865-1876
21. Sabrah AH, Cook NB, Luangruangrong P, Hara AT, Bottino MC (2013) Full-contour Y-TZP ceramic surface roughness effect on synthetic hydroxyapatite wear. Dent Mater 29:666-673
22. Singh AV, Patil R, Thombre DK, Gade WN (2013) Micro-nanopatterning as tool to study the role of physicochemical properties on cell-surface interactions. J Biomed Mater Res A 101:3019-3032
23. Subramani K, Jung RE, Molenberg A. Hämmerle CH (2009) Biofilm on dental implants: a review of the literature. Int J Oral Maxillofac Implants 24:616-626
24. Truong VK, Lapovok R, Estrin YS, Rundell S, Wang JY, Fluke CJ, Crawford RJ, Ivanova EP (2010) The influence of nano-scale surface roughness on bacterial adhesion to ultrafine-grained titanium. Biomaterials 31:3674-3683
25. Uçtaşli MB, Bala O, Güllü A (2004) Surface roughness of flowable and packable composite resin materials after finishing with abrasive discs. J Oral Rehabil.31:1197-1202
26. Variola F, Brunski J, Orsini G, Tambasco de Oliveiran P, Wazen R, Nanci, A. (2011) Nanoscale surface modifications of medically-relevant metals:state-of-the art and perspectives. Nanoscale 3:335-3532
27. Wenzel RN (1949) Surface roughness and contact angle. J Phys Colloid Chem 53:1466-1467
28. Zareidoost A, Yousefpour M, Ghaseme B, Amanzadeh A (2012) The relationship of surface roughness and cell response of chemical surface modification of titanium. J Mater Sci Mater Med 23:1479-1488

Keywords

Fiber-Reinforced Composite
Fiber Orientation
Implant Abutment
Load-bearing Capacity

Authors

Marina Etxeberria *
(DDS, MSc)

Aous A. Abdulmajeed #
(DDS, PhD)

Tomas Escuin Δ
(DDS, MSc, PhD)

Miguel Vinas †
(PhD)

Lippo V.J. Lassila ‡
(DDS)

Timo O. Närhi §
(DDS, PhD)

Address for Correspondence

Marina Etxeberria *

Email: marinaetxebe@hotmail.com

Tel: +358 (0)2 333 8527

* *Turku Clinical Biomaterials Centre (TCBC), University of Turku, Itäinen Pitkäkatu 4B, 20520 Turku, Finland*

\# *Department of Prosthetic Dentistry, Institute of Dentistry, University of Turku, Lemminkäisenkatu 2, 20520 Turku, Finland*

Δ *Laboratory of Prosthetic Dentistry, Dental School,. University of Barcelona, Feixa Llarga s/n, 08907 Hospitalet de Llobregat, Barcelona, Spain*

† *Department of Pathology and Experimental Therapeutics, Medicine School, University of Barcelona, Feixa Llarga s/n, 08907 Hospitalet de Llobregat, Barcelona, Spain*

‡ *Turku Clinical Biomaterials Centre (TCBC), University of Turku, Itäinen Pitkäkatu 4B, 20520 Turku, Finland*

§ *Department of Prosthetic Dentistry, University of Turku, Turku, Finland and Clinic of Oral Diseases, Turku University Central Hospital, Turku, Finland. Lemminkäisenkatu 2, 20520 Turku, Finland*

Received: 15.01.2015
Accepted: 07.05.2015

doi: 10.1992/EJPRD_1434Etxeberria08

Load-Bearing Capacity of Fiber-Reinforced Composite Abutments and One-Piece Implants

ABSTRACT

Fiber-reinforced composites (FRC) can potentially help in a physiologic stress transmission due to its excellent biomechanical matching with living tissues. Novel one-piece FRC implants and abutments with two different fiber orientations were loaded until failure to assess the load-bearing capacity, fracture patterns, and precision of fit. The one-piece FRC implants showed significantly higher load-bearing capacity compared to FRC abutments regardless of the fiber orientation ($p<0.001$). For FRC abutments, bidirectional abutments showed significantly higher loads compared to unidirectional abutments ($p<0.001$). The type of structure and fiber orientation are strong determinant factors of the load-bearing capacity of FRC implants and abutments.

INTRODUCTION

Current implant systems cannot adjust to occlusal loads similarly as natural teeth with sound periodontal ligaments. Therefore, occlusal loads are transmitted directly to the underlying tissues unless these loads are balanced by shock-absorber elements.[1,2] This transmission of energy is influenced by the material and design of the implant restoration.

Contrary to biomimetic principles, the mechanical properties of traditional implant and prosthetic materials (i.e. metals and ceramics) are superior to the ones of bone and dentine.[3] However, the stiffness of traditional materials in addition to the corresponding load transfer to the surrounding tissues does not appear to affect the long term behavior of implants.[4,5] Nevertheless, it can be postulated that a resilient material would mimic the biomechanics of natural dentition and thus help in transmitting physiologic forces to the underlying tissues.

In the past, the acrylic resin occlusion approach aimed to reduce the load applied on metallic implants. Contrary to this assumption, acrylic resin materials did not have shock-dampening ability and showed high incidence of resin fractures and metallic substructure overloading.[6,7] Metal-composite abutments have recently been proposed as shock-absorber elements.[8,9] However, the poor bonding between composite and metals resulted in weak points showing metal substructure exposure. This fact could be attributed to the mismatch of the modulus of elasticity of both materials.

Fiber-reinforced composites (FRC) seem to fulfill stress principles as these materials are characterized by a low elastic modulus which is close to living tissues but have high fracture and tensile strength.[10] Fiber-reinforced

composite materials have been successfully used in restorative and prosthetic dentistry for many years. Its close elastic modulus with dentine allows fabrication of load-bearing substructures without metallic framework. Satisfactory results have been observed after five years of fatigue testing.[11]

The clinical use of FRC implants has shown success in cranial reconstructions.[12] In addition effective FRC implant have been developed in orthopaedics for load-bearing applications.[13,14]

FRC surfaces have shown excellent biocompatibility in oral soft and hard tissues,[15,16] along with a bacterial response similar to current implant abutment materials.[17] Additionally, FRC materials possess several advantages such as good esthetic properties, avoidance of artifacts at CT and MRI imaging, allowance of computer-aid-designing computer-aid-manufacturing (CAD-CAM), and the permission of intraoral adjustments rendering them potential candidates in implant dentistry. However there is still a lack of scientific data about the structural aspects of FRC oral implant devices.

Structural properties of FRC ought to fulfill clinical performance criteria. FRC show directional physical properties hence, a proper design of the fiber orientation is essential to withstand the multidirectional loads existing in the oral cavity. Susceptibility to delamination has been one of the major drawbacks for failure of FRC in high stress-bearing applications.[18] This may be explained by the anisotropic behavior of unidirectional FRC structures. Thereby, design strategies including multidirectional reinforcement to minimize the highly anisotropic behavior of unidirectional FRC could be favorable, although the fracture strength may decrease.

The physiologic maximum bite forces in the incisor area have been reported to range between 40 to 370N.[19,20] Nonetheless, higher parafunctional loads (e.g. bruxism) must be taken into account when selecting a material for oral stress-bearing device. Static load testing until fracture (i.e. load-bearing capacity) is the most commonly used test in preclinical strength assessment/screening of newly developed materials. To the best of our knowledge, there are no published reports that compare the effect of different structural designs of FRC for oral load-bearing applications. Hence, the aims of this *in vitro* study were to evaluate the influence of structure type on the load-bearing capacity, fracture patterns, and precision of fit of FRC implants and abutments.

MATERIALS AND METHODS

Table 1 shows the materials used for the fabrication of FRC specimens.

THREE-POINT BENDING TEST

Rod-shaped Ø 4.0mm and 66mm length unidirectional (longitudinally oriented) and cross-sectioned in plain-weave (concentrically oriented) fiber rods were manufactured as described previously.[10] Briefly, the fibers were pre-impregnated for 48h with light-polymerizable BisGMA-TEGDMA (50-50%) in an incubator (D 06062, Modell 600) at 37°C. Subsequently, they were subjected to an initial polymerization using a light-emitting diode (LED) polymerizing unit (Elipar S10) for 2 min per side. The irradiance was 950 mW/cm2 measured using a curing radiometer. Subsequently, the rods were post-cured in a Targis Power unit for 25 min at 95 °C. Additionally, in order to optimize the degree of monomer conversion (CD%), the substrates were post-polymerized for 24 hours in hot-air oven at 120°C. Three-point bending test was used to determine the flexural strength, flexural modulus, toughness, and load-bearing capacity of FRC rods (n=9). The specimens were tested with a universal testing device (LR 30K plus) adapted to ISO 10477:92 standards[21] (crosshead speed 5.0 mm/min), and the stress-strain curves were recorded with a PC-computer program (Nexygen).

Table 1. Materials used for the fabrication of FRC abutments.

Product	Description	Manufacture	Lot no.	Composition
***E-glass fiber**	Unidirectional fiber	Ahlstrom, Karhula, Finland	11372313	55% SiO_2, 15% Al_2O_3, 22% CaO, 6% B_2O_3, 0.5% MgO, and >1.0% Fe + Na + K
***E-glass fiber**	Bidirectional fiber	Ahlstrom, Karhula, Finland	240299	55% SiO_2, 15% Al_2O_3, 22% CaO, 6% B_2O_3, 0.5%MgO, and >1.0% Fe + Na + K
Stick Resin	Light curing resin	Stick Tech, Turku, Finland	54031672	BisGMA-** TEGDMA*** (50-50%)

* E-glass, electrical glass.
** Bis-GMA, bisphenol A-glycidyl dimethacrylate.
*** TEGDMA, triethylenglycoldimethacrylate.

FRACTURE LOAD TEST

Four different experimental FRC groups in addition to two control groups were prepared (n=6), as follows:

- Experimental group A: One-piece unidirectional FRC implant. Unidirectional fiber rods (longitudinally oriented) were manufactured as described previously,[10] and the one-piece implants were prepared from the rods using CAD/CAM technology (Zirkonzahn).
- Experimental group B: One-piece bidirectional FRC implant. Cross-sectioned in plain-weave fiber rods (concentrically oriented) were manufactured as described previously,[10] and the one-piece implants were prepared from the rods using CAD/CAM technology (Zirkonzahn).
- Experimental group C: Unidirectional FRC abutment. Unidirectional fiber rods (longitudinally oriented) were manufactured as described previously,[10] and the abutments were prepared using CAD/CAM technology (Zirkonzahn) and connected to external hexagon implants (size 3.75/11.5 Lance).
- Experimental group D: Bidirectional FRC abutment. Cross-sectioned in plain-weave fiber rods (concentrically oriented) were manufactured as described previously,[10] and the abutments were prepared using CAD/CAM technology (Zirkonzahn) and connected to external hexagon implants (size 3.75/11.5 Lance).
- Group E: Custom-made zirconia abutment (control group). Custom-made zirconia abutments (ICE Zircon translucent, Zirkonzahn, Gais, Italy) were prepared using CAD/CAM technology (Zirkonzahn), and connected to external hexagon implants (size 3.75/11.5 Lance).
- Group F: Commercially available titanium abutment (control group). External hexagonal commercially available titanium grade V abutments (Teknimplant) were connected to external hexagon implants (3.75/11.5 Lance).

FABRICATION OF THE ABUTMENTS AND ONE-PIECE IMPLANTS

A commercially available screw retained titanium abutment was shaped at 7.2mm length to simulate a central incisor abutment and served as the master abutment. The master abutment was scanned (Zirkonzahn) for fabrication of identical abutments for groups C, D, and E. The abutments were fixed onto an implant with external hexagonal abutment joint design (size 3.75/11.5 Lance). Figure 1 shows one-piece implants and abutments.

Figure 1: Representative images of the experimental groups, left to right: one-piece unidirectional FRC implant; one-piece bidirectional FRC implant; unidirectional FRC abutment; bidirectional FRC abutment; zirconia abutment; titanium abutment.

Table 2. Comparison of the mechanical properties of one-piece unidirectional FRC with bidirectional FRC implants.

	Unidirectional FRC	Bidirectional FRC	p*
Flexural strength (MPa)	1082.1 ± 174.5	417.8 ± 82.2	<0.0001
Flexural modulus (GPa)	34.7 ± 7.8	14.8 ± 4.2	<0.0001
Toughness (MPa)	1.1 ± 0.28	0.71 ± 0.17	0.007
Load-bearing capacity (N)	495.8 ± 48	223.2 ± 54.8	<0.0001

* Statistical significant differences between the respective values

LOAD TESTING

According to the ISO 14801[22], 36 standardized acrylic holders were custom made using a cold curing resin (Vertex™). Implants were inserted on the acrylic holders and attached using a dual-cure resin cement (RelyX™ Ultimate). The platform of the implants was positioned 3mm above the custom-made holder to simulate vertical bone resorption to mimic the worst-case scenario as recommended by ISO standard. Experimental FRC groups were manually fixed on the implants, while zirconia and titanium abutments were fixed according to the manufacturer´s instructions. The access holes were cleaned with ethanol (95%) and then conditioned with Scothbond™ Universal adhesive, and closed by placing a cotton pellet (Ø 2mm, Roeko) and short-fiber composite filling material (everX Posterior™) into the access hole. After storage in ultra pure distilled water for 24h at 37.5°C all the specimens were statically loaded using a universal testing machine (LR 30K plus). A crosshead speed of 1.0mm/min was directed on the abutments to contact the specimen at an angle of 135° according to the average interincisal angle.[23,24] A 0.5mm thick foil was used in between to ensure even force distribution during the loading. Loading was continued until fracture after which each specimen was examined to locate and determine the mode of failure. A representative specimen of each test group was observed by optical microscope (Wild M3Z).

SEM IMAGING

One abutment from each group was cleaned ultrasonically in water for 10 minutes, then dried and screwed onto stainless steel replicas (RP implant replica Branemark Sytem®) according to the manufacturers´ recommendations. The replica-abutment interface was sputtered with gold and examined with a scanning electron microscope (SEM) (LEO 1530 Gemini). SEM images of the unidirectionally and bidirectionally reinforced abutments at 1000× and 30× and the marginal gap at the implant-abutment interfaces at 250× magnification were obtained. The vertical misfit was measured at 9 different locations and the mean values were reported for each abutment.

STATISTICAL ANALYSIS

Statistical analysis was performed with Statistical Package for the Social Sciences (Version 21.0; SPSS.). For the Three-point bending test, the data were analyzed using two-tailed t test. The distribution of data was normal, which was determined by the Kolmogorov-Smirnov test. The data were analyzed using one way analysis of variance (ANOVA) followed by Tukey's post–hoc test. Differences were considered significant at 95% confidence level.

RESULTS

THREE-POINT BENDING TEST

Table 2 presents the three-point bending test results of the one-piece FRC rods. The bidirectional FRC rods showed significantly lower values compared to unidirectional FRC rods.

FRACTURE LOAD TEST

Figure 2 shows the mean load-bearing capacities and standard deviations of the experimental groups. The one-piece implants exhibited the highest fracture load among the FRC groups ($p<0.001$). Fiber orientation had no statistically significant effect on the fracture load of one-piece FRC implants. However, the bidirectional FRC abutment had significantly higher fracture load compared to the unidirectional FRC abutment ($p<0.001$). The FRC abutments, in contrast to one-piece FRC implants, had significantly lower load-bearing capacity than zirconia abutments ($p<0.01$). However, titanium abutments showed higher load-bearing values ($p<0.001$) than any of the FRC abutments or the one-piece FRC implants investigated in this study.

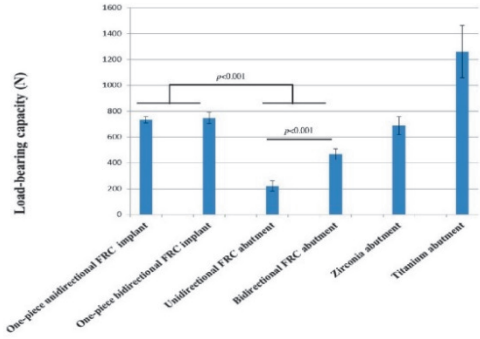

Figure 2: Mean load-bearing capacities and standard deviations of the experimental implants and abutments.

FAILURE MODE

In one-piece FRC implants, the unidirectional implants showed longitudinal delamination while the bidirectional implants showed bending in the neck region *(Figure 3)*. In case of the FRC abutments, catastrophic failure was observed in the unidirectional group, while in the bidirectional group signs of screw bending were noticed. Zirconia abutments failed catastrophically, while titanium abutments demonstrated plasticization of metallic components (implant hexagon- abutment hexagon) and screw bending. Representative fractures are shown in Figure 4.

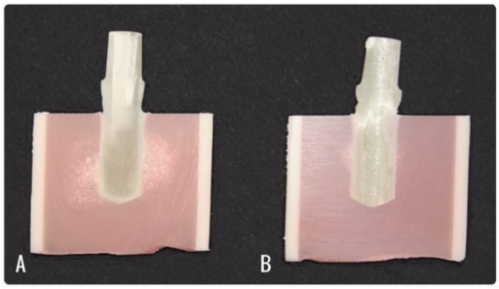

Figure 3: Representative cross-sections of the fracture patterns of one-piece FRC implants: a) unidirectional and b) bidirectional.

Figure 4: Representative fracture patterns of the abutments, left to right: unidirectional FRC; bidirectional FRC; zirconia; and titanium.

SEM IMAGING

Figure 5 shows SEM images of the unidirectionally and bidirectionally reinforced abutments at two different magnifications. Figure 6 presents the precision of fit of FRC abutments in comparison to the control groups at 250× magnification. The mean vertical gap distances and standard deviations in µm were as follows: unidirectional FRC: 0.0 ± 0.0; bidirectional FRC 5.30 ± 0.67; zirconia: 2.14 ± 0.40; and titanium: 4.60 ± 0.38.

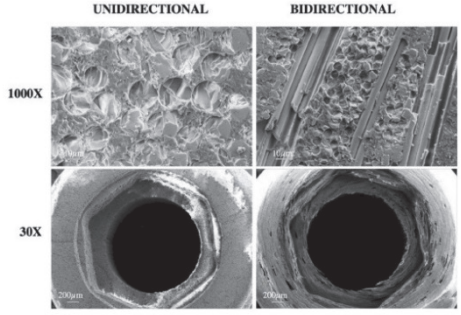

Figure 5: Scanning electron microscopic images of unidirectional reinforced matrix and bidirectional reinforced matrix.

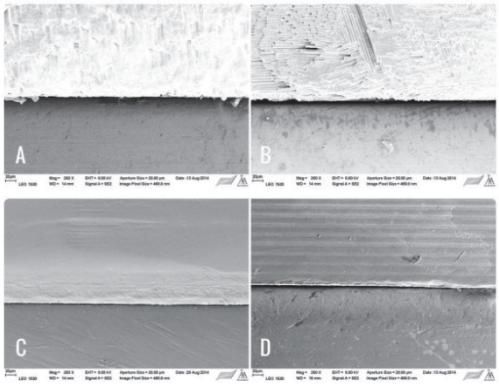

Figure 6: Precision of fit at 250X magnification: a) unidirectional FRC; b) bidirectional FRC; c) zirconia; and d) titanium.

DISCUSSION

This study was performed to assess the load-bearing capacity of novel FRC one-piece implants and abutment prototypes with two different types of fiber structures. Bidirectionally reinforced implants and abutments carry the potential to be used for oral anterior stress-bearing applications. Accordingly they showed higher load-bearing capacity than the expected maximum anterior oral loading force without material failure (delamination). One study evaluated the load-bearing capacity of FRC abutments but only unidirectional fibers were analyzed.[18] The present study is first in reporting the load-bearing capacity of FRC implants and abutments with different types of fiber structure for oral load-bearing applications.

Three-point bending test was used to determine the mechanical properties of FRC where, bidirectional FRC rods, as expected, obtained inferior values compared to unidirectional FRC. It is well documented that bidirectional reinforcement of FRC decreases its strength in comparison with unidirectional reinforcement.[14,25] Nevertheless both groups displayed an elastic modulus similar to cortical bone and dentine and adequate strength that acknowledge them for load-bearing applications.[26,27]

This study revealed that irrespective of the fiber structure, one-piece FRC implants exhibited the highest load-bearing capacities among the experimental FRC groups. Although it is known that the mechanical properties of FRC are influenced by the fiber orientation,[28] this influence was not observed, due to the fact that the high fiber vol.% of the one-piece FRC bulk structure resulted into high resistance to fracture. However, bidirectional fibers showed a greater breakage capacity since they showed bending failure without delamination. This may be explained by the fact that unidirectional fibers transfer the energy longitudinally from the abutment to the implant exhibiting intralaminar matrix fracture leading to stress concentration areas in the resin as illustrated in Figure 3. On the contrary, bidirectional fibers show superior stress bearing

capacity by a more homogenous load distribution enabling bending failure without breakage. One of the main disadvantages of one-piece titanium implants is that they require abutment shaping immediately after the implant insertion, which potentially jeopardize the bone vitality and primary stability through heat transmission.[29] In fact, the controversial results in success rates of titanium one-piece implants are attributable (among other factors) to the heat transfer through underlying tissues during the abutment preparation.[30] Unlike titanium, FRC is easy to grind and modify without heat generation. Furthermore, FRC implants with bioactive glass particles (BAG) have shown osteoinductive properties.[16]

The role of the fiber structure on the load-bearing capacity of FRC orthopedic implants has been previously studied in animal experimentation.[13,14] Moritz *et al.*, observed that the addition of a bidirectional fibers enhanced torsional strength of FRC implants at the expense of flexural strength. However, although showing inferior values on some mechanical properties, they showed similar load bearing performance compared to the unidirectional implants.[14]

In contrast to FRC implants, in FRC abutments fiber structure had a significant impact on the load-bearing capacity. According to this assumption, and similar to the findings of Behr *et al.*, unidirectional fibers did not tolerate compressive loads directed towards the fiber´s axis direction in FRC abutments.[18] In contrast bidirectional fibers provided optimal reinforcement showing fracture loads above the maximum incisal forces. While unidirectional fibers lead to catastrophic failure, the more resilient material achieved by bidirectional reinforcement exhibited screw bending without fiber damage (e.g. delamination). Increasing the stiffness of the bidirectional FRC would provide additional support to the veneering composite in addition to show arrest crack propagation due to enhanced biomechanical matching to the veneering particle filler composite. Recent composite abutments, which showed a comparable modulus of elasticity to the bidirectional FRC, showed a similar damping behavior compared to teeth.[8] Clinically the inclusion of a resilient material helps in transmitting physiologic forces to the peri-implant tissues by mimicking biomechanics of natural dentition better than rigid implant devices do.

In the present study, the load-bearing capacity and failure modes of the control groups (i.e. zirconia and titanium) were comparable to earlier studies.[31,32] Despite the fact that titanium abutments showed the highest load-bearing capacity, such high occlusal loads are rarely encountered in the anterior region.[33]

The accuracy of passive fit has been evaluated by measuring vertical implant abutment distances.[23,34] Interestingly, the unidirectional fibers showed the material's efficacy in gap closure compared to any other abutment materials evaluated in this study. The poor marginal fit reported for titanium abutments is probably because the used implants and abutments were from different manufacturers.[35] Nevertheless, the range of misfit for all experimental groups in the current study is consistent with earlier studies and it can be considered clinically acceptable.[23,34]

Further improvements regarding the design of FRC abutments should be addressed. A higher load-bearing capacity would be expected when testing a solid FRC abutment considering the superior behavior to fracture of the one-piece FRC. Additionally, current advanced metal-resin bonding techniques could greatly improve the adhesion between the metal abutment base and the resin matrix and moreover, adhesive cementation of the abutment into the dental implant could also be considered. Regarding the type of structure, the combination of unidirectional and bidirectional may be required for the mechanical optimization of the abutment and the use of multidirectional fibers should be considered.

In vitro static loading conditions will not address in vivo conditions, but allow to evaluate new designs inexpensively in addition to obtain clinically relevant considerations.[31,32] Some limitations of the study need to be outlined: (1) Cyclic load fatigue tests are believed to be the best technique to evaluate fracture strength and long-term survival of implant abutments,[18,24] nevertheless static load tests are considered to be a basis for fatigue tests (ISO 14801); (2) The screw design could not be standardized due to manufacturer´s recommendations for the zirconia group. In the titanium and FRC abutments the screw head had a tapering design, whereas besides having more threads the zirconia´s abutment screw head had a butt-joint design; (3) This investigation did not include a full veneer crown in the model system and thus higher force failure loads can be expected with crowns (i.e. crowns act as a stress-shielding device allowing a larger load to be applied before failure).

Although the mechanical properties of bidirectional FRC were inferior compared to the unidirectional, were adequate to withstand clinically relevant loads without structural failure. The present work confirmed early studies that the bidirectional reinforcement improves the performance of implant devices.[14] However, further technological development is mandatory before the FRC implants or abutments can be recommended for clinical use.

CONCLUSIONS

Based on the findings of this study, it can be concluded that:

1. Fiber orientation and structure design have a significant influence on the load-bearing capacity of FRC abutments.
2. Bidirectional fiber reinforcement must be considered for use in implant dentistry regarding the different functional loads that are generated in the oral cavity.

ACKNOWLEDGEMENTS

The experimental part of this study was developed in Turku Clinical Biomaterials Centre. The first author was a recipient of a scholarship from Health University of Barcelona Campus.

The authors would like to thank TCBC personnel for their assistance. The authors disclaim any conflict of interest.

MANUFACTURERS' DETAILS

- D 06062, Modell 600, Memmert GmbH + Co.KG, Schwabach, Deutschland
- Elipar S10, 3M Espe, Seefeld, Germany
- Targis Power, Ivoclar, Schann, Liechtenstein
- LR 30K plus, Lloyd, Sussex, UK
- Nexygen, Lloyd Instruments Ltd., Fareham, England
- Zirkonzahn, GmbH, Gais, Italy
- Lance, MIS™,Tel Aviv, Israel
- Teknimplant, Barcelona, Spain
- Vertex™, Vertex-Dental, B.V. Headquarters, The Netherlands
- RelyX™ Ultimate, 3M ESPE Dental, Seefeld, Germany
- Scothbond™ Universal adhesive, 3M, Gmbh, Neuss, Germany
- Roeko, Langenau, Germany
- EverX Posterior™ GC, Japan
- Wild M3Z, Heerbrugg, Switzerland
- Branemark Sytem®, Nobel Biocare, Goteborg, Sweden.
- LEO 1530 Gemini, Helmholtz Centrum, Berlin, Germany
- Version 21.0; SPSS. Inc, Chicago, Illinois

REFERENCES

1. Robling, A.G., Duijvelaar, K.M., Geevers, J.V., Ohashi, N. and Turner, C.H. Modulation of appositional and longitudinal bone growth in the rat ulna by applied static and dynamic force. *Bone*, 2001; **29**:105-113.
2. VanSchoiack, L.R., Wu, J.C., Sheets, C.G. and Earthman, J.C. Effect of bone density on the damping behavior of dental implants: An in vitro method. *Mat. Sci. Eng. C*, 2006; **26**:1307-1311.
3. Hallab, N.J., Jacobs, J.J. and Katz, J.L. Orthopedic applications. In Ratner, B.D., Hoffman, A.S., Schoen, F.J., Lemons, J.E (Eds): Biomaterials Science: an introduction to materials in medicine. San Diego, CA: Elsevier Academic Press, 2004; 526-555.
4. Zembic, A., Kim, S., Zwahlen, M. and Kelly, J.R. Systematic review of the survival rate and incidence of biologic, technical, and esthetic complications of single implant abutments supporting fixed prostheses. *Int. J. Oral Maxillofac. Implants*, 2014; 29 Suppl:99-116.
5. Pjetursson, B.E., Asgeirsson, A.G., Zwahlen, M. and Sailer, I. Improvements in implant dentistry over the last decade: comparison of survival and complication rates in older and newer publications. *Int. J. Oral Maxillofac. Implants*, 2014; 29 Suppl:308-324.
6. Davis, D.M., Rimrott, R. and Zarb, G.A. Studies on frameworks for osseointegrated prostheses: Part 2. The effect of adding acrylic resin or porcelain to form the occlusal superstructure. *Int. J. Oral Maxillofac.* Implants, 1988; **3**:275-280.
7. Gracis, S.E., Nicholls, J., Chalupnik, J.D. and Yuodelis, R.A. Shock-absorbing behavior of five restorative materials used on implants. *Int. J. Prosthodont.*, 1991; **4**:282-291.
8. Magne, P., Silva, M., Oderich, E., Boff, LL. and Enciso, R. Damping behavior of implant-supported restorations. *Clin. Oral Implants Res.*, 2013; **24**:143-148.
9. Boff, LL., Oderich, E., Cardoso, A.C. and Magne, P. Fatigue resistance and failure mode of adhesively restored custom metal-composite resin premolar implant abutments. *Int. J. Oral Maxillofac. Implants*, 2014; **29**:364-373.
10. Abdulmajeed, A.A., Närhi, T.O., Vallittu, P.K. and Lassila, L.V. The effect of high fiber fraction on some mechanical properties of unidirectional glass fiber-reinforced composite. *Dent. Mater.*, 2011; **27**:313-321.
11. van Heumen, C.C., Tanner, J., van Dijken, J.W. *et al.* Five-year survival of 3-unit fiber-reinforced composite fixed partial dentures in the posterior area. *Dent. Mater.*, 2010; **26**:954-960.
12. Aitasalo, K.M., Piitulainen, J.M., Rekola, J. and Vallittu, P.K. Craniofacial bone reconstruction with bioactive fiber-reinforced composite implant. Head Neck, 2014; **36**:722-728.
13. Zhao, D.S., Moritz, N., Laurila, P. *et al.* Development of a multi-component fiber-reinforced composite implant for load-sharing conditions. *Med. Eng. Phys.*, 2009; **31**:461-469.
14. Moritz, N., Strandberg, N., Zhao, D.S. *et al.* Mechanical properties and in vivo performance of load-bearing fiber-reinforced composite intramedullary nails with improved torsional strength. *J. Mech. Behav. Biomed. Mater.*, 2014; 40C:127-139.
15. Abdulmajeed, A.A., Willberg, J., Syrjänen, S., Vallittu, P.K. and Närhi, T.O. In vitro assessment of the soft tissue/implant interface using porcine gingival explants. *J. Mater. Sci. Mater. Med.*, (In press).

Results: Data was analyzed with 1-way ANOVA and Tukey multiple comparison tests ($a = .05$). For the 100 mJ and 200 mJ laser etching groups; 50 μs and 100 μs laser duration resulted in significantly higher surface roughness compared to air-particle abrasion ($p < .05$). The difference between Ra values of 300 μs, 600 μs and air-particle abrasion groups were not statistically significant ($p > .05$). For the 300 mJ laser etching groups; there was no statistically significant difference between the Ra values of 50 μs, 100 μs, 300 μs, 600 μs and air-particle abrasion groups ($p > .05$).

Conclusion: In order to increase surface roughness and promote better bonding to resin luting agents, Er:YAG laser etching may be an alternative to air-particle abrasion for zirconia ceramics. However, high levels of pulse energy and longer pulse length may have an adverse effect on micromechanical locking properties due to decrease in surface roughness.

Keywords: Er:YAG; Zirconia; Adhesion

http://dx.doi.org/10.1016/j.dental.2014.08.003

3

Synthesis and characterization of Y-TZP/TiO_2 composites with different TiO_2 contents

R. Miranda[1], V. Ussui[2], D. Lazar[2], J. Marchi[3], W. Miranda[1], P. Cesar[1,*]

[1] *University of São Paulo, Brazil*
[2] *Institute for Nuclear and Energetic Research, Brazil*
[3] *Federal University of the ABC, Brazil*

Purpose: To synthesize, characterize and sinter a Y-TZP/TiO_2 composite, varying the amount of TiO_2 and the sintering temperature.

Methods and materials: Synthesis of the composite was made using aqueous solutions of precursors (zirconium oxychloride, titanium chloride and yttrium chloride) by means of a co-precipitation route in ammonia medium to produce the following experimental groups (fractions in mol%): Z (100% Y-TZP), ZT10 (90% Y-TZP and 10% TiO_2) and ZT30 (70% Y-TZP and 30% TiO_2). The produced powders were characterized by X-ray diffraction (XRD), particle size analysis (PSA), specific surface area analysis (SBET) and scanning electron microscopy (SEM). Discs (15.0 mm in diameter and 2.5 mm-thick, $n = 10$) were pressed (65 MPa) and sintered at 1400 °C or 1500 °C for 2 h, followed by measurement of the density (D) by the Archimedes method and microstructural analysis by SEM. Student's *t*-test was used to evaluate the effect of temperature on the relative densities of the different material produced.

Results: SEM and PSA showed that the synthesized powders were constituted of agglomerates with average size, in mm, varying as follows: Z (0.5 and 5.4), ZT10 (0.7–17.6) and ZT30 (0.7 and 11.4). SBET values obtained were (m^2/g): Z (47.4), ZT10 (42.3) and ZT30 (58.0). XRD analysis showed peaks of tetragonal and monoclinic zirconia for all groups. All discs showed relative density higher than 94%; and no significant effect of temperature on the relative densities was observed ($p > 0.05$ for all pairwise comparisons, see Table 1).

Table 1

Material	Theoretical density	Relative density (%) as a function of the sintering temperature	
		1400 °C	1500 °C
Z	6.10	98	99
ZT10	5.77	94	94
ZT30	5.34	94	94

SEM indicated that the highest sintering temperature and the presence of TiO_2 favored grain growth in the material microstructure.

Conclusion: The amount of TiO_2 significantly affected the specific surface area and the particle size of the synthesized powders. Although the sintering temperature did not affect the relative density of the specimens, grain growth was higher for samples containing TiO_2 and sintered at the highest temperature.

Keywords: Zirconia; Titania; Synthesis

http://dx.doi.org/10.1016/j.dental.2014.08.004

4

Fracture resistance of fiber reinforced composite implant abutments

M. Etxeberria[1,*], T. Escuin[1], L. Lassila[2], A.A. Abdulmajeed[2], M. Vinyas[1], T.O. Närhi[2]

[1] *University of Barcelona, Department of Prosthetic Dentistry and Department of Pathology and Experimental Therapeutics, Barcelona, Spain*
[2] *University of Turku, Department of Prosthetic Dentistry and Biomaterials Science, Turku, Finland*

Purpose: Stiff implant abutments can transmit overload forces to periimplant bone. Titanium abutments show up to 10 times higher modulus of elasticity compared to natural bone. The use of e-glass fiber-reinforced composites (FRC) may help to overcome the disadvantages of titanium abutments. They have been suggested to act as shock absorber elements due to their low flexural modulus which is close to the natural bone. Moreover FRC have shown high biocompatibility and satisfactory aesthetic properties. The aim of this in vitro study was to test the fracture load and fracture patterns of FRC implant abutments, in an attempt to use FRC as a potential alternative implant abutment.

Materials and methods: Four different groups with a diameter of 4 mm and length of 16 mm of FRC implant abutment systems were manually prepared: (1) one-piece unidirectional FRC; (2) one-piece multidirectional FRC; (3) two-piece unidirectional FRC; (4) two-piece multidirectional FRC. The fracture load was measured using a Universal Testing Machine (LR 30K plus, Lloyd, Sussex, UK, 1 mm/min) according to ISO 14801. The specimens were loaded until failure with static load. Mean load values and fracture patterns of the specimens were analyzed. Statistically significant differences between the groups were analyzed with one-way analysis of variance (ANOVA) followed by Tukey's multiple comparison test.

Results: The mean fracture loads in N were: group 1 (656.1 ± 77.3), group 2 (620.1 ± 116.4), group 3 (311.4 ± 106.7)

and group 4 (333.5 ± 67.2). The one-piece groups (1 and 2) exhibited statistically significant differences compared with the two-pieces groups (3 and 4) ($p < 0.001$). On the other hand, there were not statistically significant differences in terms of fiber direction (multidirectional and unidirectional) ($p = 0.835$).

None of the specimens fractured catastrophically. In one-piece groups longitudinal fracture lines were observed. Whereas in two-piece groups, only a partial delamination of the implant neck region occurred. However debonding failure was noticed in two-pieces groups.

Conclusions: The differently connected FRC abutments exhibited significantly different mean load values. One piece groups' mean load values were higher than the maximum anterior biting forces. However, improvements regarding manufacturing techniques are needed in order to optimize two-piece FRC for clinical trials.

http://dx.doi.org/10.1016/j.dental.2014.08.005

5

Energy requirements for curing light activated cements through CAD/CAM materials

N.E. Goetz, C. Shen, J.-F. Roulet*

University of Florida, Department of Restorative Dental Sciences, Gainesville, FL, USA

Purpose: Develop a method for calculating polymerization time based on properties of CAD/CAM materials, resin cements and light curing units (LCU).

Methods and materials: Part-I: 12 blocks each of e.max CAD (A1, A2, A3) and Enamic (1M1, 2M2, 3M2) were sectioned into 0.5, 1.0, 1.5, 2.0 mm slabs, which were glazed or polished. Using Valo LCU (Ultradent) and MARC-Resin-Calibrator the light absorption was measured. Part-II: One mm thick samples of RelyX Veneer transparent and Variolink Veneer MVO were irradiated for 2.5, 5, 10, 15, 20, 25, 30, 40, 50 and 60 s each through an e.max or Enamic disk to reduce the irradiance. Vickers-micro-hardness (VH) of set cements was measured @ 5 points per sample after 10 minutes and after 10d dark storage at 37 °C to determine energy needed to adequtely cure the cements. Part-III: Using Valo LCU, 1 mm thick samples of the cements used in Part-II were irradiated through 0.5 and 2 mm thick samples of the materials described in Part-I at the irradiation-time needed to deliver the required energy density determined in Part-II. VH was determined after 10 min and 10 d.

Results: Part-I: The thickness significantly reduced the irradiance. For all samples 0.5 mm thickness yielded an average reduction of 50%. The largest reduction was observed with Enamic 3M2-HT. 2 mm thickness reduced the irradiance to 12.5%. Shade did not significantly influence the light transmission. Part-II: Regardless of the incident irradiance, microhardness values reached a plateau of VH 23 for Variolink and VH 26 for RelyX when the energy density of the exiting light at the bottom of the cement exceeded 4.5 J/cm^2. The 10 days VH-values were 43% higher. Part-III: Using the calculated irradiation times almost Identical VH-values to the ones reported in Part II were measured. The data also revealed that darker shade cements yielded higher VH values, and cements cured under Enamic yielded higher VH-values than those cured under e-max. This can be explained with the heat contribution to the curing process: darker shades absorb more energy and Enamic required longer irradiation times.

Conclusion: Within the limitations of this study one can conclude that energy required and curing time of a resin cements based on LCU's and CAD/CAM materials properties can be predicted with relative accuracy utilizing this mathematical model & methodology. By predicting this information clinicians may be able to utilize an evidence based method for resin cement polymerization to achieve a higher degree of conversion with improved mechanical properties, survival and success.

http://dx.doi.org/10.1016/j.dental.2014.08.006

6

Bond strength of Y-TZP zirconia ceramic to different core materials

C.R.G. Torres*, F.C. Frattes, J.B.S. Oliveira, C.R. Pucci, A.B. Borges

Sao Paulo State University – UNESP, Institute of Science and Technology, Department of Restorative Dentistry, Sao Jose Dos Campos, Brazil

Purpose: To evaluate the bond strength of Y-TZP zirconia ceramic to different core materials using a universal self-etching adhesive.

Methods and materials: In order to simulate the crowns bonded over the core materials, zirconia cylinders were obtained from of yttrium oxide stabilized tetragonal zirconia polycrystal (Y-TZP) blocks (IPS e-max ZirCAD, Ivoclair Vivandent) using a diamond trephine mill, followed by sintering in a high temperature furnace. The top of each cylinder was sandblasted and received the tribochemical silica coating. In order to simulate the cores, samples of one of the following materials were prepared: Group 1 – silver alloy (Ag/Sn/Cu, Tecnofix); Group 2 – copper alloy (Cu/Ni/Zn, Goldent LA); Group 3 – dual cured core building composite (Rebilda DC – VOCO); Group 4 – Y-TZP zirconia; Group 5 – enamel; Group 6 – dentin. The core materials were embedded in acrylic resin inside a cylindrical silicone mold. The surfaces were flattened using abrasive #600 SiC paper in order to simulate the texture produced by a diamond bur. The universal self-etching adhesive Futurabond U (Voco) and the dual cure resinous cement Bifix QM (Voco) were applied for bonding and luting. The samples were submitted to shear test using a universal testing machine at a cross speed of 1 mm/min. The obtained data in MPa was analyzed using ANOVA and Tukey's test.

Results: The ANOVA showed a significant difference among the groups ($p = 0.00$). The means of bond strength (±SD) and the results of Tukey's test for the different core materials were: dentin – 12.80 (±3.18)a, enamel – 15.13 (±3.09)ab, composite – 17.20 (±4.67)ab, copper alloy – 18.93 (±4.66)bc, silver alloy – 22.86 (±5.47)c, Zirconia – 23.65 (±3.64)c. The groups followed by the same letters do not present significant differences.